Explorations into the Synthesis and Reactivity of Polynorbornene Frameworks

Victoria K. Kensy

A dissertation

submitted in partial fulfillment of the

requirements for the degree of

Doctor of Philosophy

University of Washington

2019

Reading Committee:

Andrew J. Boydston, Chair

Alshakim Nelson

Julie Kovacs

Program Authorized to Offer Degree:

Chemistry

University of Washington

Abstract

Explorations into the Synthesis and Reactivity of Polynorbornene Frameworks

Victoria K. Kensy

Chair of the Supervisory Committee:
Professor Andrew J. Boydston
Department of Chemistry

Polynorbornenes are a highly versatile polymer that allows for much modification of the side chains and multiple methods for polymerization. Chapter 1 introduces our unique photoredox-mediated ring-opening metathesis polymerization (photo-ROMP) technique for ring-opening metathesis polymerizations (ROMP) that utilizes an organic redox mediator and a vinyl ether initiator, in contrast to metal-based initiators traditionally used in ROMP. The reversibility of the redox-mediated initiation and propagation steps enable spatiotemporal control over the polymerization. In Chapter 2, we explore control over polynorbornene molecular weights using alpha olefins as chain transfer agents, allowing the initiator to be recycled to reduce costs and access low molecular weight oligomers. Molecular weights between 30 kDa and 1 kDa can be targeted simply through altering the stoichiometry of the reaction. Chapter 3 details our work on

the development of a continuous flow reactor for large scale synthesis of photo-ROMP polymers. In Chapter 4, we report the discovery of a mechanochemical method to produce ROMP polynorbornene (ROMP-PNB) from vinyl-addition polynorbornene (VA-PNB). VA-PNBs with three different side chains were found to undergo ring-opening olefination upon sonication in dilute solutions. The sonicated polymers exhibited spectroscopic signatures consistent with conversion of the bicyclic norbornane repeat units into ROMP-PNB. In Chapter 5, we investigated the reversible hetero-Diels–Alder reaction of 1,2-oxazines derived from a peralkylcyclopentadiene and a series of nitrosocarbonyl dienophiles. The nature of the dienophile was found to impart broad tunability to the dynamic character of the oxazine adducts. The reversibility was also observed in polymeric systems of a ROMP-PNB framework. The fidelity of the reaction and tunable sensitivity toward elevated temperature and water signify potential applications in the development of dynamic covalent materials or delivery systems for small molecule payloads.

TABLE OF CONTENTS

LIST OF FIGURES

LIST OF TABLES

LIST OF SCHEMES

ACKNOWLEDGEMENTS

First, I would like to thank my advisor AJ Boydston. AJ was a great advisor and I'm forever grateful for his constant support of my research and the freedom with which he allowed me to choose my own projects. I've learned so many valuable scientific and life lessons from him and he truly inspired me to become a better scientist. He also provided me with so many opportunities to present my work nationally and internationally, allowing me to travel to locations I may have never had the chance to see, and with a truly unique fellowship at the Army Research Labs. With that, I would also like to thank my ARL advisor, Daniel Knorr, for giving me the opportunity to teach other scientists about my research and demonstrating the impact our academic research can have in the real world. It's one thing to give a background in your talk where you speculate the possibilities of your work, but it is another to be a part of applying your work to real projects, in this case for materials for the US Army.

I would like to thank all my Boydston lab members over the years for making the long lab hours more enjoyable and putting up with my musical selections on the speakers. I would like to thank Dr. Adam Goetz for all his help in my first years here; putting up with the constant stream of questions I had (and still have but just send over text), weekly hood mechanisms, and overall amazing mentorship. I would like to thank Johanna Schwartz and Pengtao Lu, we survived five years together! Pengtao, Bo Cao, and I were the remaining Seattle Boydstoners once the group moved to UW-Madison and I am grateful to them for sticking it out with me and pushing each other to the finish. All the graduated members of the lab provided guidance during times which we overlapped here at UW. To the younger lab members, Brock Lynde, Daniel Lee, and the new Wisconsin members, I wish you the best of luck and hope all your syntheses go to 100%.

Additionally, I would like to thank my committee members, Professors Alshakim Nelson, Julie Kovacs, and Duane Storti for encouragement and guidance through the years. The entire UW chemistry department is an amazing group and all the work that goes into the department running so smoothly is truly appreciated.

Outside of lab, my family and friends provided unconditional love and support throughout these five challenging years. Aunt Judy and Uncle Vic let me move in with them for three months during my fellowship at ARL. This was a major factor in my being able to seize this opportunity for personal and professional growth. I cherish those months I got to spend with Justin, even when

we fought over my rooting for “the other team” to always win against his Steelers, and I miss him all the time. In my first two years here, my brother Taylor, sister-in-law Diana, and nephew Caleb lived in Tacoma and it was so amazing to have them out here to celebrate holidays with and visit over weekends. My niece Mila joined the family once they moved to California, and I’ve also loved the chances to go visit your whole family down there as well. All the friends I have made here in Seattle helped me to survive the long grind of five years of graduate school and I can’t thank them enough. Section One Twenty Chad, thank you for all the Sounders games, card nights, brunches, and all other hang outs. Mimi Chelimsky, my best friend, confidant, world travel buddy, has been there for every up and down in my life for the last nine years and I couldn’t have survived it all without our trips and hours long phone calls. Lucas Flagg has been a wonderful source of love, a great shoulder to lean on, and an amazing cat sitter. Last but not least, my two cats, Zeke and Zara that I adopted at the end of my third year here; it is truly a delight to be able to come home to cuddles and love every day.

Finally, I absolutely could not have gotten through this without my parents. You have supported me for all my life in all my choices, even when those choices meant I moved across the world to Australia for 6 months followed by across the country to UW. Knowing that you will always come visit and I always have someone to call when I need to talk has been such a source of comfort and I am eternally grateful to you both. I love you both so much.

DEDICATION

To my parents, for their constant love and support

Chapter 1. Introduction

1.1 Metal-Mediated Ring-Opening Metathesis Polymerizations

Ring-opening metathesis polymerization (ROMP) is a type of chain-growth polymerization, which has emerged as a powerful and broadly applicable technique for synthesizing polymeric materials. The origins of ROMP can be traced back to 1950s when various mixtures of metal salts were recognized for their reactivities toward olefin metathesis, a unique metal-mediated carbon-carbon double bond exchange process.[1] Akin to other forms of olefin metathesis, the resultant polymer conserves all unsaturation associated with the cyclic olefin type monomer. Although there have been numerous reports of various metals used for ROMP, those based on Ru and Mo (**Figure 1.1**) have become most popular due to their excellent functional group tolerance, which has greatly expanded the monomer scope.[2–6] Importantly, careful adjustment of reaction conditions and catalyst choice can be used to achieve living polymerization that, afford polymers with controlled molecular weight, narrow polydispersity and high chain-end fidelity.[7,8]

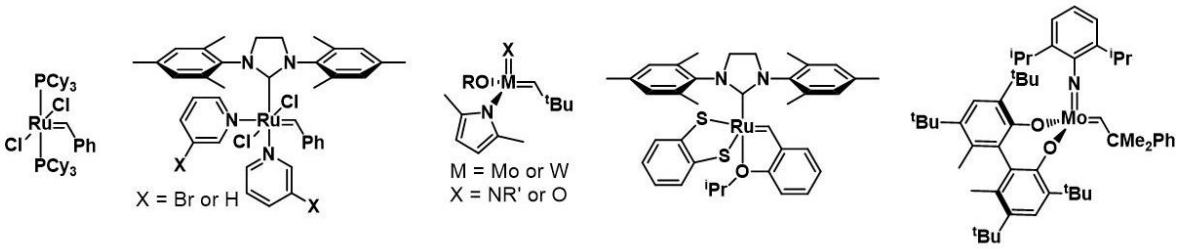

Figure 1.1 Select examples of well-defined metal-based ROMP initiators.

A general mechanism of ROMP based on Chauvin's original proposal is shown in **Scheme 1.1**.[9] Initiation begins with the coordination of a transition-metal alkylidene complex to a cyclic olefin.

A subsequent [2+2] cycloaddition affords a four-membered metallacyclobutane. This highly strained intermediate immediately undergoes a cycloreversion reaction to form a new metal-alkylidene species with exactly the same reactivity, although the resulting complex has increased in size since it now incorporates one monomer unit. Additional monomers undergo this sequence of elementary steps during propagation to ultimately afford a high molecular weight polymer.

Scheme 1.1 Generalized Mechanism of Traditional ROMP using Metal Initiators

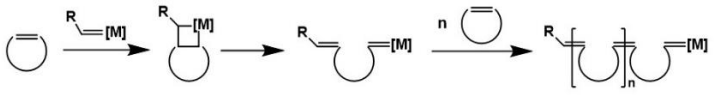

Due to the covalent attachment of metal initiator to the polymer chain, however, ROMP polymers can be very difficult to purify. Living ROMP is commonly quenched through the addition of a specialized chemical reagent, which selectively removes the transition metal from the chain end and deactivates it from further propagation. However, these metallic by-products not only shorten the lifetime of bulk materials, but also limit the application of ROMP polymers in biomedical or microelectronic devices. Although there has been much effort devoted to improving purification procedure, these extra processes dramatically increase the length and cost of polymer production.[10,11]

To address the need for metal-free alternatives to traditional ROMP, as well as add to general community efforts to develop "greener" controlled polymerizations, our group envisioned an organic alternative to traditional metal-mediated ROMP.[12] It is noteworthy about this general interest on deriving organocatalyzed polymerization from traditionally metal-catalyzed controlled polymerization. For example, Hawker group and Miyake group independently initiated the development of metal-free atom-transfer-radical-polymerization (MF-ATRP), which is an organic

counterpart for transition-metal-mediated ATRP.[13,14] For an overview on MF-ATRP and other organocatalyzed polymerizations, we direct the reader to these cited review articles.[15,16] In this account, we overview the evolution of our MF-ROMP methodology, starting with its inception inspired by pioneering electrochemical and photochemical work. We then summarize our recent efforts on the elaboration of this technique, including the expansion of catalyst and monomer scopes, elucidation of plausible mechanism and preparation of diverse block copolymers.

1.2 An Electrochemical Approach to MF-ROMP

Inspired by Chiba's electrochemical approach to intermolecular cross metathesis between vinyl ethers and terminal olefins, we hypothesized that an "all-organic" electrochemical ROMP could also be possible. In Chiba's pioneering experiments, it was demonstrated that oxidation of vinyl ethers leads to the formation of a [2+2] radical cation complex, reminiscent of the metallacyclobutane intermediate in traditional metal-mediated ROMP, that is subsequently reduced to give a cyclobutane (**Scheme 1.2**).[17,18] It is apparent from the ROMP mechanism that the success of traditional ROMP relies on the cycloreversion of the strained metallacyclobutane intermediate to give the propagating species. We postulated that outcompeting the reduction of [2+2] complex by rapid ring-opening of strained cyclic olefin could result in a new ROMP type polymerization with unique mechanism.

Scheme 1.2 Electrochemical Olefin Metathesis and Cyclobutane Formation

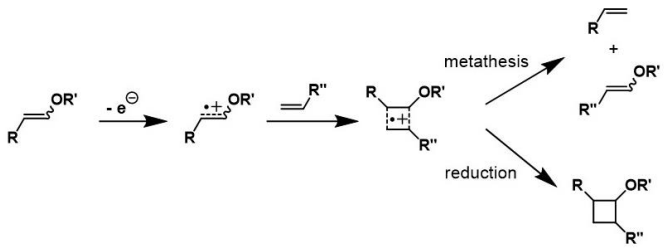

Specifically, we hypothesized that (**Scheme 1.3**), after the single-electron oxidation of vinyl ether (**A**), the reactive radical cation intermediate (**B**) could react with a strained cyclic olefin to form a [2+2] complex (**C**). Rapid ring-opening to release the ring strain would outcompete the reduction of **C**, thereby regenerating a reactive radical cation (**D**) with monomer incorporated. The active chain end would then propagate and ultimately afford ROMP polymer (**E**). Reduction of the radical cation chain end would eventually render a ROMP polymer (**F**) with vinyl ether end group.

Scheme 1.3 Hypothesized Mechanism of Redox-Mediated MF-ROMP

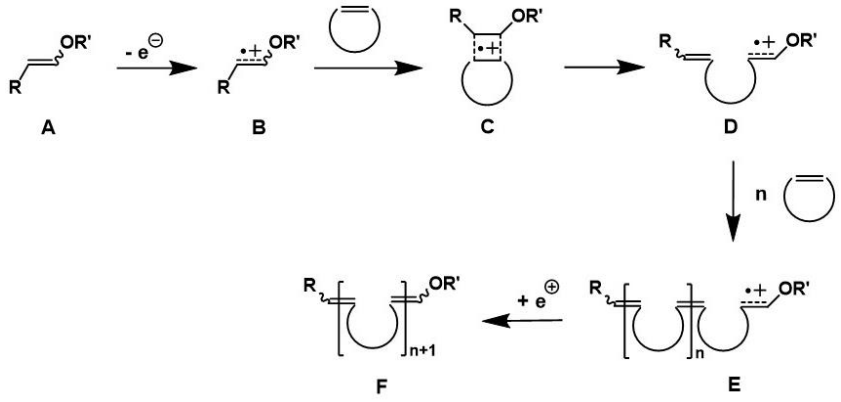

To investigate the direct oxidation of vinyl ethers and propensity for the generated radical cation to initiate ROMP, we conducted bulk electrolysis on solutions of norbornene **1** containing readily available vinyl ether initiators (**2a**, **2b** and **2c**) (**Scheme 1.4**).[12] We focused on using **1** as our initial screening monomer, since this structure possessed relatively high strain (~ 100 kJ/mol) among common ROMP monomers. Initial results were discouraging, as there was no detection of polymer in solution after bulk electrolysis for 3 hours. During the cleaning of the carbon fiber anode, however, we noticed the surface of anode was coated with a white precipitate that was also insoluble in methanol. Characterization of this deposited residue using ^{1}H-NMR spectroscopy revealed signals consistent with polynorbornene (PNB) prepared via traditional ROMP technique. It was also observed that the end group signal is consistent with vinyl ether after removal of any

residual vinyl ether initiator through precipitation. Gel-permeation chromatography (GPC) analysis exhibited a number average molecular weight (M_n) of 11.8 kDa ($Đ$ = 2.2), which confirmed the macromolecular nature of the product. Although the yields were consistently low (only ~ 3%), these initial results confirmed that the anodic oxidation of vinyl ethers could initiate the polymerization of 1**,** likely via a ROMP-type mechanism.

Scheme 1.4 Electro-mediated MF-ROMP and select vinyl ether initiators

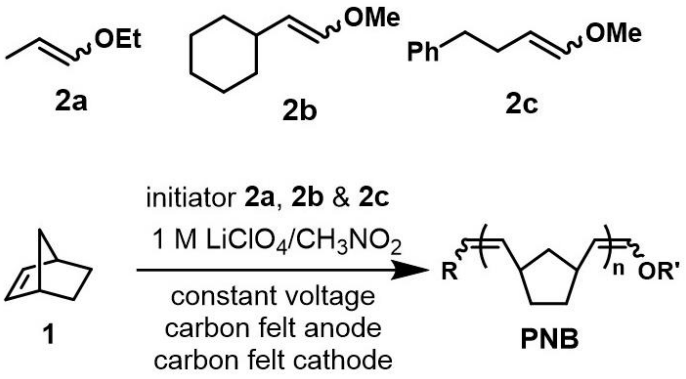

We attributed this low yield to the poor solubility of both **1** and PNB in the bulk electrolysis system that is, based on nitromethane (CH_3NO_2) and lithium perchlorate ($LiClO_4$). During electrolysis, the insolubility of PNB led to the deposition of growing polymer onto the anode surface, which prevented further oxidation of the vinyl ether initiator and resulted in a rapid decrease in current. However, after screening various electrode materials and electrolyte/solvent combination, we realized that carbon fiber electrodes, $LiClO_4$, and $CH3NO_2$ were crucial for the success of electromediated MF-ROMP. Other attempts to increase the yield, including the use of an ultrasonic bath, afforded small improvements (**Table 1.1**).

Table 1.1 Summary of results from the electro-mediated MF-ROMP of monomer **1** and initiators **2a-c**

initiator	$[M]_0/[I]_0$[a]	M_n (kDa)[b]	$Đ$[c]	Yield (%)
2a	28/1	6.2	1.4	12
2b	28/1	4.8	1.5	14
2c	28/1	6.7	1.5	13

[a]Initial molar ratio of monomer and initiator. [b]Determined by GPC using multiangle laser light scattering (MALLS). [c]Dispersities determined by GPC.

1.3 A PHOTOCHEMICAL APPROACH TO MF-ROMP

To circumvent the solubility issues encountered in the electrochemical set up, we questioned whether the vinyl ether radical cation could be accessed by another method. It is well known that the photoredox processes are susceptible to a broader solvent scope and homogeneous oxidation than their electrochemical counterparts. Photo-oxidants such as 2,4,6-tri(4-methoxyphenyl)pyrylium and ruthenium tris(bipyrimidine) have been used by the Nicewicz and Yoon groups respectively, for the photoredox-mediated synthesis of cyclobutanes (**Scheme 1.5**).[19–23] Assuming that a cyclic olefin would outcompete the reduction in favor of ring-opening, we envisioned that a photo-chemical ROMP could be possible.

Scheme 1.5 Photoredox-Mediated Cyclobutane Formation

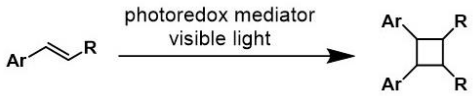

We chose pyrylium salts **3a** as our initial photocatalyst since it has been identified as good candidate for facilitating photooxidation and is completely organic. As the oxidizing power of excited **3a** has been calculated to be 1.89 V vs SCE, this mediator was expected to be good oxidizers for vinyl ether initiators because the oxidation potentials of **2a-c** are in the range of 1.30

V to 1.43 V vs SCE. Our photochemical set up consisted of 3 mol% of catalyst loading relative to initiator, dichloromethane (CH_2Cl_2) as the solvent (monomer concentration ~ 1.9 M), and a 2-watt blue LED bulb (λ_{em} = 450 -480 nm) as the visible light source (**Table 1.2**).

Table 1.2 Summary of results from the photoredox-mediated MF-ROMP of monomer **1**, initiators **2a-c**, and photoredox catalyst **3a** and Picture of Reaction Set-Up

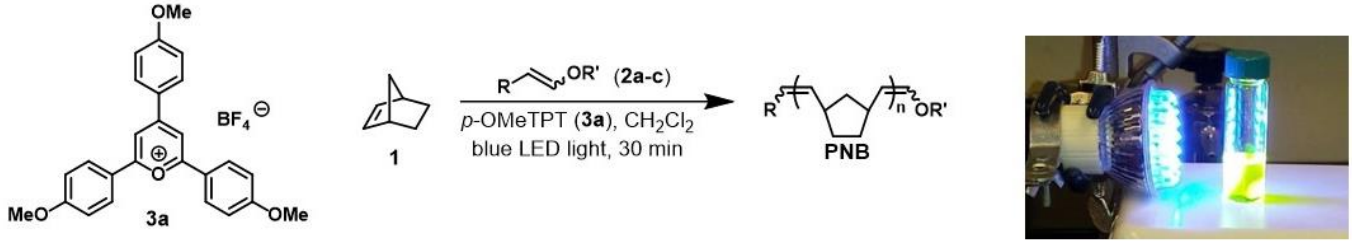

initiator	$[\mathbf{1}]_0 : [\mathbf{2}]_0 : [\mathbf{3}]_0$[a]	$[M]_0$ (M)[b]	conversion[c] (%)	$M_{n,\,theo}$ [kDa]	$M_{n,\,exp}$ [kDa]	Đ
2c	97 : 1 : 0.03	1.9	88 (73)	8.0	15.1	1.7
2b	97 : 1 : 0.03	1.9	92 (80)	8.4	14.9	1.6
2a	106 : 1 : 0.03	2.0	87 (67)	9.0	15.8	1.6
2a	48 : 1 : 0.03	1.8	95 (78)	4.3	8.1	1.4
2a	491 : 1 : 0.03	5.3	51 (25)	23.6	22.2	1.5
2a	494 : 1 : 0.03	1.8	72 (50)	33.4	43.9	1.5
2a	1000 : 1 : 0.03	1.9	61 (47)	57.4	60.2	1.6

[a]Initial molar ration of **1**, **2** and **3**. [b]Initial concentration of **1**. [c]Conversion of **1**, as determined by ^{1}H-NMR analysis; isoalted yields after precipitation given in parentheses. $M_{n,\,theo}$ is theoretical number average molecular weight calculated from initial **1** : **2** ratio and % conversion of **1**. $M_{n,\,exp}$ is experimental number average molecular weight determined by GPC using MALLS. Dispersities ($Đ$) determined by GPC.

Each initiator gave PNB in good yield via the photoredox pathway (**Table 1.2**). Although **2c** provides a distinguishable NMR handle, most of the polymerizations were carried out using **2a** since this vinyl ether initiator is commercially available. Varying the initial monomer to initiator loading provided a certain degree of control over the final M_n with moderate initiator. The dispersities of resultant PNB were found to vary between 1.4 and 1.7 across different experiments.

We also discovered that successful polymerization could be carried out at high monomer concentration (5.3 M). This result suggests that bulk polymerizations using a liquid monomer may be possible in the future. Control experiments confirmed that the initiator, photoredox mediator, and light source were each required for successful polymerization.

During the course of the polymerization, we observed a gradual increase in M_n with increasing conversion of monomer, which is consistent with the chain growth nature of ROMP (**Figure 1.2**). The linearity was not as precise as traditional "living" ROMP, though there was a positive correlation. We attributed this to the relative rates of initiation and propagation in the photoredox method and, any number of early termination events.

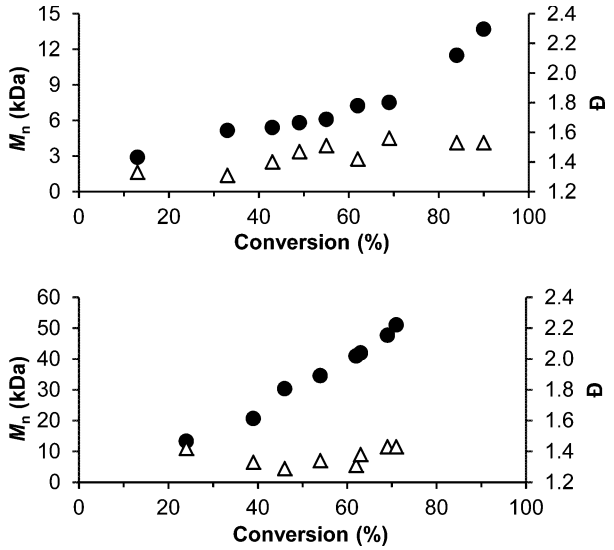

Figure 1.2 Plot of Mn (black dot) and Đ (white triangle) vs % conversion of monomer using initial **1** : **2a** of **(top)** 100 : 1 and **(bottom)** 500 : 1.

We also discovered that light could be used to reversibly activate the vinyl ethers, which allowed a high degree of temporal control over the polymerization. We noticed that there were no significant changes in monomer conversion and molecular weight during the periods in which the light was off (**Figure 1.3**). And each re-exposure to light resulted in increased conversion and

molecular weight. These results were consistent with the deactivation and reactivation of polymer vinyl ether chain ends, rather than photoinitiation of new polymer chains. This level of temporal control is not possible in traditional metal-based ROMP system.

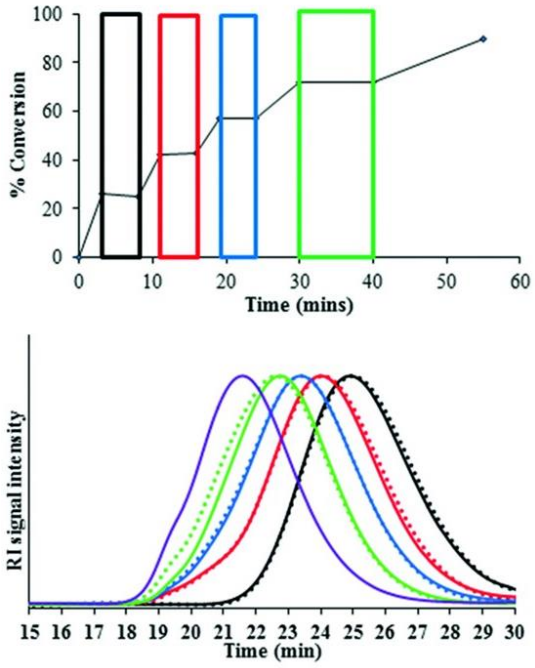

Figure 1.3 (top) Plot of percentage conversion of monomer over time (periods of dark are highlighted by rectangular boxes; **(bottom)** GPC traces for dark/light cycles (the solid lines represent GPC traces following exposure to blue LED light and the dotted lines refer to GPC traces of periods in the dark immediately following a period light; colors are correlated with those in top figure.

1.4 Investigating the Scope of MF-ROMP

1.4.1 *Screening photoredox catalysts*

Mechanistically, we envisioned that the vinyl ether radical cation was generated by oxidation of the vinyl ether via single-electron transfer to the excited pyrylium cation. Based on previous experimental results, we also revealed that the propagating radical chain end likely forms a dynamic redox couple with the reduced pyrylium salts. Therefore, we decided to screen different photooxidants with various pyrylium salts **3a-d** and closely related thiopyrylium salts **4a-d** to

determine any trends between photo-oxidant performance and excited state reduction potential E^*_{red}.[24]

For the series of either pyrylium salts or thiopyrylium salts, we uncovered that increasing the excited reduction potential E^*_{red} resulted in lower monomer conversion. It is possible that photooxidants with higher oxidizing potentials may lead to overoxidation of vinyl ether initiators, even oxidation of norbornene and PNB main-chain olefins. These results suggest that careful choice over the strength of photooxidants is critical for a successful polymerization.

We next examined the catalytic performance of each pyrylium/thiopyrylium pair with identical substituents. Our results showed that thiopyrylium salts gave higher monomer conversion than the similar functionalized pyrylium. For example, **4a** emerged as a promising photooxidants for MF-ROMP and slightly outperformed **3a**, which was used in our initial photoredox experiments. By comparison, **4b** and **4c** also reached higher conversion than **3b** and **3c**, respectively.

The molecular weight and dispersity of isolated PNB were generally consistent across the series of both pyrylium and thiopyrylium salts. These results suggested to us that the relative rates of initiation and propagation are not strongly influenced by the nature of photo-oxidants, since we expect similar oxidation potentials between the initiator and chain end vinyl ethers.

Table 1.3 Results of MF-ROMP using pyrylium and thiopyrylium photo-oxidants

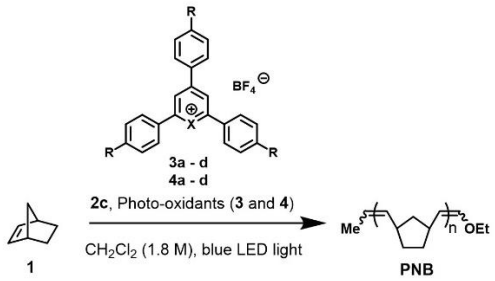

Photo-oxidants	R	X	E^*_{red} (V vs SCE)	conversion[a] (%)	M_w[b] (kDa)	$Đ$[c]
3a	MeO	O	1.89	75 ± 4	20.0	1.5
4a	MeO	S	1.86	84 ± 1	36.3	1.6
3b	Ph	O	2.02	31 ± 1	7.4	1.4
4b	Ph	S	2.02	52 ± 3	13.3	1.4
3c	Me	O	2.23	12 ± 1	5.5	1.2
4c	Me	S	2.20	26 ± 1	7.3	1.5
3d	H	O	2.46	9 ± 1	n.d.	n.d.
4d	H	S	2.41	< 5	n.d.	n.d.

[a]Conversion of **1**, as determined by ^{1}H-NMR analysis [b]weight average molecular weight determined by GPC using MALLS. [c]Dispersities determined by GPC.

To directly compare the performance of two best photooxidants **3a** and **4a** in each series, we monitored the conversion over time for each mediator. Although both photooxidants led to consistently high conversion, it was clear that during the polymerization thiopyrylium **4a** led to higher conversion at the same time intervals in comparison with **3a** (**Figure 1.4**). The ability of **4a** to reach critical conversion at a shorter time may give an advantage in applications requiring gelation or crosslinking.

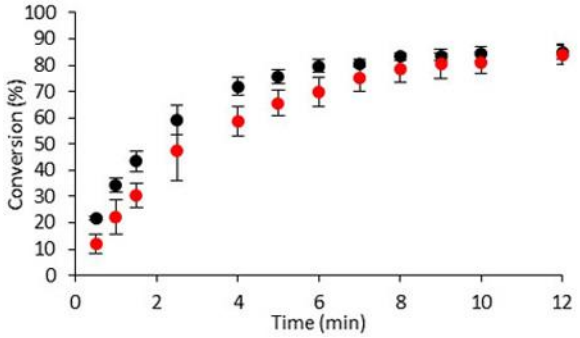

Figure 1.4 Plot of conversion versus time using photo-oxidants **3a** (red) and **4a** (black) in MF-ROMP of norbornene **1**.

1.4.2 *Expanding the scope of monomer*

As stated previously, the development of well-defined metal catalysts has transformed traditional ROMP into an extraordinary polymerization technique with remarkable functional group tolerance and monomer scope. Since our MF-ROMP experiments had thus far only focused on norbornene **1**, we decided to prepare polymers with more complex functionality.[25,26] We started our examination by testing dicyclopentadiene (DCPD) and related monomers. When polymerized within metal-based ROMP catalysts, *endo*-DCPD **5a** affords cross-linked thermoset materials with excellent properties, that can be used in applications such as vehicle body panels and wind turbine blades. However, the nature of the cross-linking process generally traps the metal catalysts inside the bulk material, resulting in limited lifetime from deleterious side reactions. We questioned if our MF-ROMP method could allow for the preparation of cross-linked polyDCPD without metal contamination.

Monomer **5a** was then subjected to our previous reported photoredox MF-ROMP condition. Although there was no sign of cross-linking, we were able to synthesize a linear polyDCPD (M_n = 3.8 kDa; $Đ$ = 1.1) with monomer conversion around 15%. Because of their great solubility and pendant olefin moieties, these linear polyDCPD were subjected to thiol-ene reaction conditions to

afford cross-linked materials under fully metal-free protocols. We attempted to optimize this polymerization to achieve higher monomer conversion (**Table 1.4**), however, the variation of monomer concentration and pyrylium salts loading resulted in no significant change in conversion. Decreasing polymerization temperature and initial ratio of monomer to initiator gave a slight improvement in conversion. ^{1}H-NMR revealed that multiple enol ether species at the polymer chain ends, possibly from deleterious side reactions of the vinyl ether radical cations, thus limiting monomer conversion.

Table 1.4 Attempted optimization on MF-ROMP of *endo*-DCPD **5a**

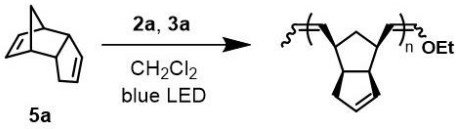

[**5a**]$_0$: [**3a**]$_0$: [**2a**]$_0$[a]	[**5a**]$_0$ (M)[b]	temp (^{o}C)	conversion[c] (%)
100 : 1 : 0.07	2.25	23	13
100 : 1 : 0.07	1.75	23	15
100 : 1 : 0.07	2.80	23	13
102 : 1 : 0.25	1.75	23	15
100 : 1 : 0.07	1.75	4	19
51 : 1 : 0.07	1.76	23	20

[a]Initial molar ration of **5a**, **3a** and **2a**. [b]Initial concentration of **5a**. [c]Conversion of **5a**, as determined by ^{1}H-NMR analysis.

We next investigated whether the presence of monomer **5a** was detrimental to the MF-ROMP of monomer **1**. The copolymerization between **5a** and **1** was set up using feed ratio of monomers (**5a** + **1**) to initiator **2a** of 100 : 1. **Figure 1.5** shows good correlation of *endo*-DCPD **5a** loading to the composition and M_n of the final polymer. We realized that the amount of incorporation of **5a** increases with increasing initial loading, although the amount of *endo*-DCPD content is less than

the theoretical value based on the feed ratio. As we expected, higher initial loading of **5a** led to a significant decrease in both monomer conversion and M_n of final polymer. Since moderate conversion (~ 50 – 60 %) of **5a** was achieved at low loading, we concluded that the decreased reactivity of the monomer was not responsible for low conversions of **5a** during MF-ROMP homopolymerization.

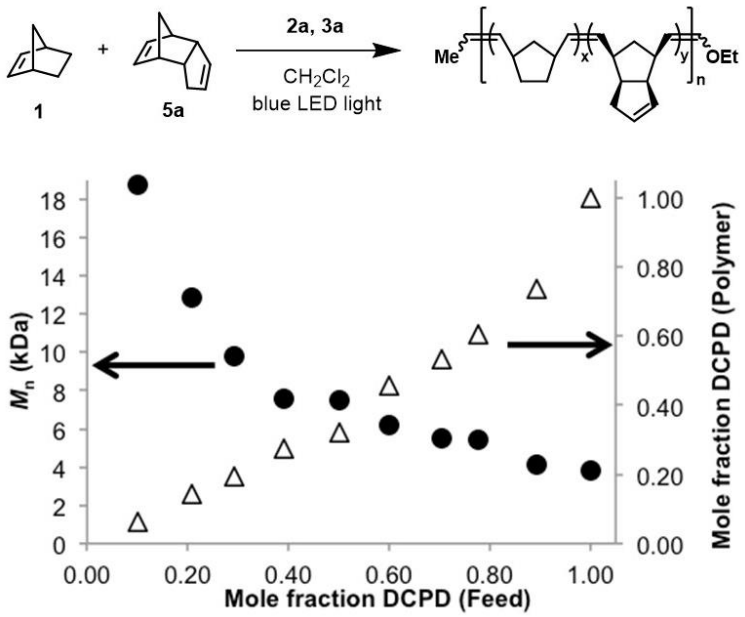

Figure 1.5 Plot of M_n (black dot) and DCPD incorporated into final polymer (white triangle) vs DCPD loaded for DCPD/NB copolymerization.

To better rationalize the low conversion of *endo*-DCPD, we examined two potential explanations. The first scenario hypothesizes that the steric bulk of the additional cyclopentene ring in monomer **5a** might attenuate the rate of new monomer incorporation. The second hypothesis is that, the proximity of the pendant cyclopentene to the propagating radical cation might create problems, since the intramolecular reactivity of neighboring olefins with radical cation intermediates is well-documented. To probe these two possible pathways, we prepared monomers **5b-d** to compare their MF-ROMP performance with **5a**. While monomers **5b** and **5d** avoid the possibility of any

undesired intramolecular reactivity with the extra olefin, monomer **5c** would be expected to perform well if the problem was strictly steric in nature.

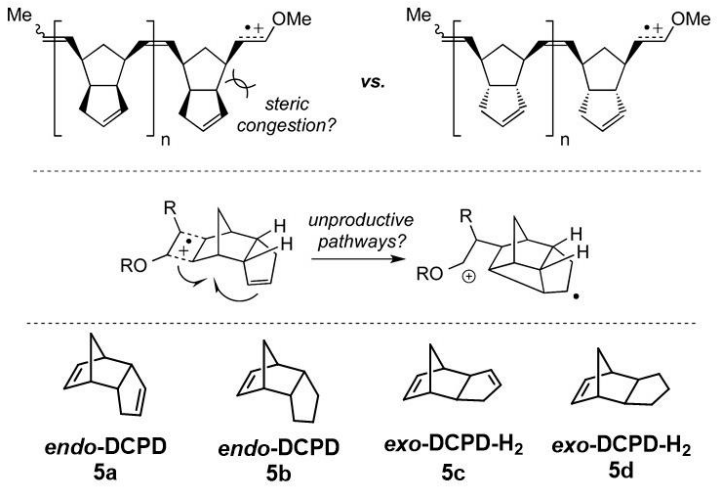

Figure 1.6 Potential reasons for decreased DCPD conversion and scope of monomers studied

Monomers **5a-d** underwent MF-ROMP to varying degrees under our previously reported conditions (**Figure 1.7**). Similar to what was observed for *endo*-DCPD monomer **5a**, *exo*-DCPD monomer **5c** was found to perform poorly with 20% conversion. However, for dihydroDCPD monomers **5b** (55% conversion) and **5d** (>90% conversion), these MF-ROMP reactions performed significantly better. The results from monomer **5d** was comparable to previous MF-ROMP of norbornene **1**. These results suggested to us that the poor performance of monomers **5a** and **5c** most likely arises from the pendant cyclopentene structures, since the steric impedance in monomer **5b** did not diminish its reactivity. To further investigate the poor monomer conversion of DCPD, we performed MF-ROMP of **1** in the presence of cyclopentene, which afforded similar conversion to control experiments with no additives. Also, cyclopentene proved to be unreactive in homopolymerization or in stoichiometric reactions with **2a**. Taken together, these control

experiments confirmed that the intramolecular nature of the side reaction between pendant cyclopentene groups and propagating radical cation chain end is hindering conversion.

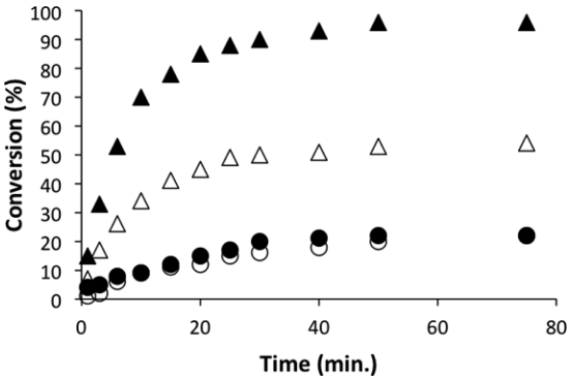

Figure 1.7 Plot of conversion vs time for monomers **5a** (white dot), **5b** (white circle), **5c** (black dot) and **5d** (black triangle).

To further expand the monomer scope of MF-ROMP, we became interested in exploring the functional group tolerance for this new method so that we could identify functionalized monomers compatible with our methodology. For simply testing the functional group compatibility within MF-ROMP, we studied the effect of small molecule additives on the polymerization of monomer **1** using our previously reported photoredox conditions. Feed ratio of these additives was varied from 1 to 100 vs vinyl ether initiator to mimic stoichiometric conditions with initiator and monomer, respectively. Given the high reactivity of radical cation intermediates, we initially were concerned about polar functional groups. However, the results from additive study, as summarized in **Table 1.5**, were quite encouraging. The difference in monomer conversion for the series of added alcohols was ascribed to their relative nucleophilicity, since tert-butanol with the highest steric hindrance resulted in the best MF-ROMP performance. For those less nucleophilic additives, such as electron-deficient hexafluroisopropanol (HFIP) and sterically hindered methyl-tertbutyl-ether (MTBE), there was little impact on norbornene conversion even at 100 equivalents relative to initiator. Moreover, the observed moderate conversion of **1** in the presence of small amounts of

water (1 : 1 with initiator, 310 ppm by wt) encouraged us to explore the MF-ROMP efficiency outside glovebox. The procedure of photoredox mediated MF-ROMP was greatly simplified after we observed excellent conversion from reactions set up under ambient conditions.

Table 1.5 Effect of additives on MF-ROMP of norbornene **1**

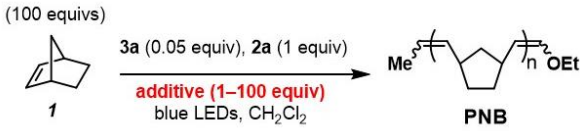

Additive	Equivalents[a]	Conversion[b] (%)
none	-	80
H2O	1	53
MeOH	1	40
i-PrOH	1	68
t-BuOH	1	80
t-BuOH	100	0
HFIP	100	72
MTBE	100	78

[a]Relative to vinyl ether initiator. [b]Conversion of **1**, as determined by ^{1}H-NMR analysis.

After observing tolerance toward alcohols and ethers, we started to investigate monomers with similar functionality (**Table 1.6**). We initially targeted norbornenes **6** and **7** functionalized with unprotected alcohols; however, they unsurprisingly precluded any polymerization. We then prepared a series of norbornene derivatives with protected alcohols (**8a-d**). Among these monomers, only the tertbutyldimethylsilyl (TBS) group, **8d,** resulted in successful homopolymerization with 50% conversion. We also investigated the copolymerization ability of those functional norbornene derivatives when they were loaded in a 1 : 3 feed ratio relative to norbornene. Each monomer underwent successful copolymerization with **1** though conversions

and incorporation varied with **8d** showing the best MF-ROMP compatibility. We also prepared monomers **8e-g** to investigate the tolerance of MF-ROMP toward other functional groups. Neither **8e** nor **8f** showed any homopolymerization but copolymerized with **1** to low conversion and incorporation. **8g** surprisingly homopolymerized but did not inhibit or react in copolymerization with **1,** which was determined to be due to the much more rapid polymerization of **1** compared to **8g**. In addition to demonstrating several new monomers that perform well for MF-ROMP, these investigations also provide insight into mechanistic considerations for future monomer design.

Table 1.6 Results of copolymerization between norbornene and functional monomers

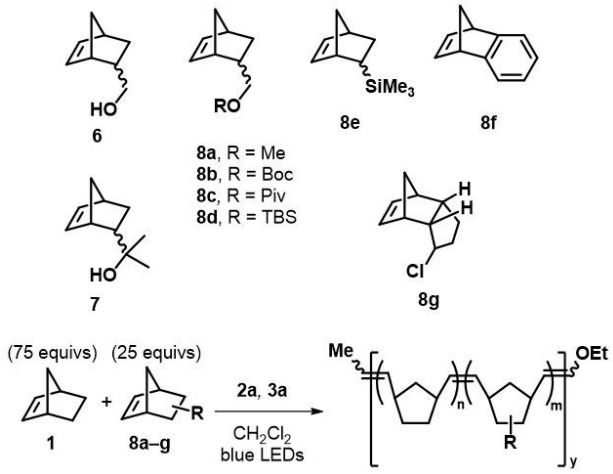

Co-monomer	conversion[a] (%)	1 : 8[b] (polymer)	Mw[c] (kDa)	*Đ*
8a	77 (34)	82 : 18	20.3	1.4
8b	70 (30)	88 : 12	95.0	3.7
8c	74 (55)	89 : 11	37.2	2.2
8d	78 (71)	80 : 20	27.0	1.5
8e	47 (9)	90 : 10	5.3	1.3
8f	34 (19)	74 : 26	7.9	1.2
8g	87 wrt **1**	100 : 0	24.0	1.5

[a]Determined by ^{1}H-NMR analysis of a reaction aliquot. Yield in parentheses after isolation of polymer.[b]Determined by ^{1}H-NMR spectroscopy of isolated polymer. [c]Weight-average molecular weight determined by GPC using MALLS. Dispersities (*Đ*) determined by GPC.

1.4.3 *Synthesizing block copolymer via MF-ROMP*

In addition to the expansion of the monomer scope, we also investigated the feasibility of preparing block copolymer structures via MF-ROMP.[27–29] In a tandem copolymerization, chain end stability is critical for the living characteristics that enable successful chain extension from one block to another. For MF-ROMP, we were concerned about the stability of the reactive radical cation chain ends during sequential monomer addition, so, we sought to determine the parameters that could achieve successful tandem block copolymerization.

Norbornene **1** and exo-dihydroDCPD **5d** were selected as our model monomers due to their exceptional MF-ROMP reactivity. We evaluated chain end stability and relative success of chain extension to the second polymer block by varying the reaction time for the first block copolymer formation (**Figure 1.8**). Specifically, the first block was polymerized in parallel with reaction times of 1, 2, and 3 hours. After that, the second monomer was added, and the polymerization continued for another 2 hours. In 1 hour, the polymerization of **1** reached its maximum conversion, but the M_n of the polymer increased at the 2- and 3-hour marks, suggesting chain coupling was occurring readily. Upon addition of **5d** as the second monomer, block copolymers formed, but the longer reaction times produced larger number of dead chains. Besides shortened reaction time, switching order of polymerization between **1** and **5d** also helped for minimizing the chain-chain coupling, which was ascribed to more sterically hindered repeat units being less susceptible to attack by the vinyl ether chain ends.

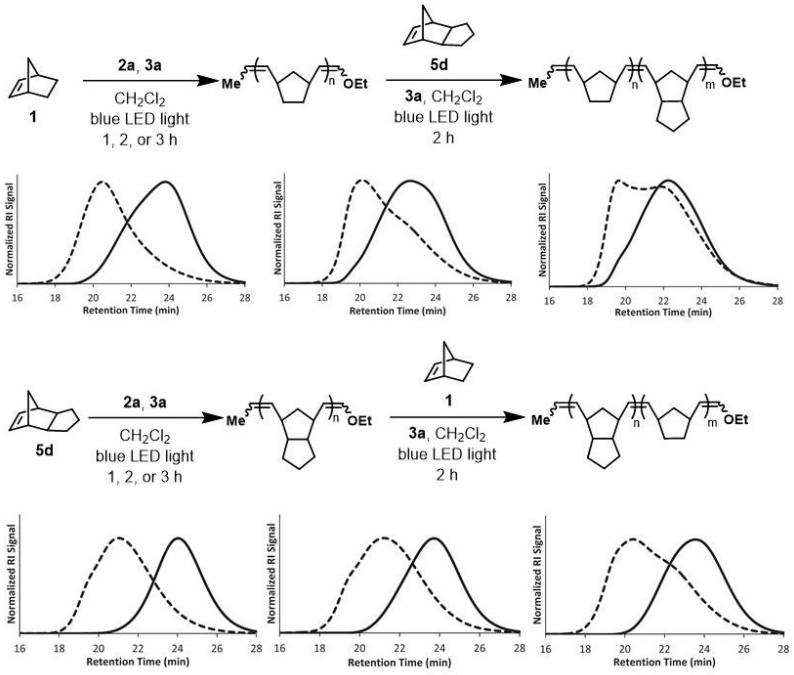

Figure 1.8 GPC traces for block polymer Solid = GPC trace after first block formation, dashed = SEC after diblock formation. **(Top) 1** used for first block, reaction times left to right = 1, 2, 3 h. **5d** then used for second block with reaction time = 2 h. **(Bottom) 5d** used for first block, reaction times left to right = 1, 2, 3 h. **1** then used for second block with reaction time = 2 h.

Since most functionalized monomers suffered low or zero conversion, the diversity of block copolymer preparation through the MF-ROMP mechanism was quite limited. To address this problem, we attempted to prepare block copolymers through polymerizations with different mechanisms. The successful integration of MF-ROMP with other types of polymerizations not only uncovers a new synthetic transformation, but also substantially expands the accessible type of block copolymers.

Two pathways stood out to us to integrate MF-ROMP with other polymerization techniques. The first method is based on the expedient synthesis of corresponding macroinitiators derived from various prepolymers and, easy installation of vinyl ether moieties (**Scheme 1.6**). To test the feasibility of this method, difunctional macroinitiators with vinyl ether chain ends **9** and **10** were

prepared from commercially available polyethylene- and polypropylene glycol using simple organic transformations. Triblock copolymers **12** and **13** were prepared through metal-free ROMP after initiation of both vinyl ether chain ends. Those organic initiators can also be installed as pendent groups on polymer precursors, as shown by the preparation of polystyrenes **11** with pendant vinyl ether groups through conventional controlled radical polymerization. Upon exposure to organic photoredox ROMP condition, graft polystyrene with polynorbornene **14** as side chains could be prepared with moderate to high monomer conversion.

Scheme 1.6 Block copolymer by grafting MF-ROMP from macroinitiators.

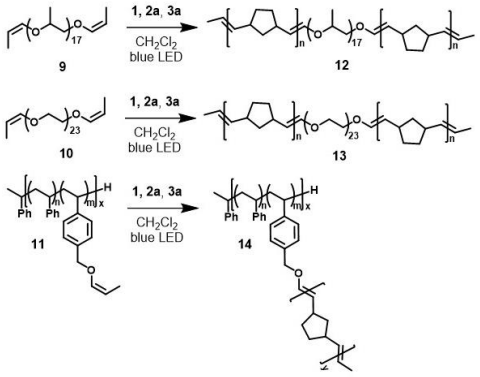

The second method we envisioned incorporated, a mechanism-switch dual polymerization, for those macroinitiators that are difficult to prepare directly from a prepolymer. A bifunctional initiator, with a vinyl ether on one side and distinct initiation site on the other, might be the key to solve this problem. Since it would be interesting to graft MF-ROMP from a biocompatible polymer, we prepared bifunctional initiator **15** which, besides a vinyl ether moiety, also possess a hydroxy group capable of initiating the polymerization of lactide, lactone and cyclic carbonate. Three distinct macroinitiators, polylactide **16**, polycaprolactone **17** and polytrimethylene carbonate **18**, with controlled molecular weight and narrow dispersity, were produced via

organocatalyzed ring-opening polymerization (*o*-ROP) (**Scheme 1.7**). The ^{1}H-NMR analysis confirmed the integrity of the vinyl ether chain ends after *o*-ROP of the assorted cyclic monomers. Exposing those vinyl ether end-capped polymers to MF-ROMP conditions allowed the grafting of ROMP polymer on the original polymer scaffolds with moderate to high conversions.

Scheme 1.7 Block copolymers made from sequential o-ROP and MF-ROMP.

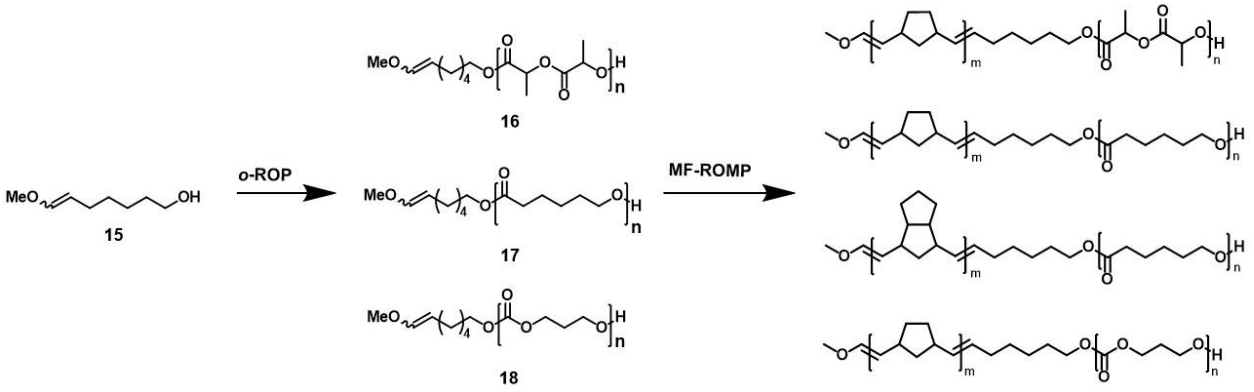

To further elaborated this method, we developed a one-pot methodology by sequential polymerization of *o*-ROP and MF-ROMP. The key of this method is to carry out *o*-ROP first, and the polymerization should be quenched by adding excess pyrylium salts to react with the catalyst, triazabicyclodecene, and photo-catalyze the MF-ROMP reaction after the addition of ROMP monomer.

1.5 NOTES AND REFERENCES FOR CHAPTER 1

(1) Ivin, K. J.; Mol, J. C. *Olefin Metathesis and Metathesis Polymerization*; Academic Press: San Diego, CA, 1997.

(2) Schrock, R. R. Recent Advances in High Oxidation State Mo and W Imido Alkylidene Chemistry. *Chem. Rev.* **2009**, *109*, 3211–3226.

(3) Schrock, R. R. Synthesis of Stereoregular Polymers through Ring-Opening Metathesis Polymerization. *Acc. Chem. Res.* **2014**, *47* (8), 2457–2466.

(4) Trnka, T. M.; Grubbs, R. H. The Development of Olefin Metathesis Catalysts : An Organometallic Success Story. *Acc. Chem. Res.* **2001**, *34*, 18–29.

(5) Vougioukalakis, G. C.; Grubbs, R. H. Ruthenium-Based Heterocyclic Carbene-Coordinated Olefin Metathesis. *Chem. Rev.* **2010**, *110*, 1746–1787.
(6) Samojlowicz, C.; Bieniek, M.; Grela, K. Ruthenium-Based Olefin Metathesis Catalysts Bearing N -Heterocyclic Carbene Ligands. *Chem. Rev.* **2009**, *109*, 3708–3742.
(7) Bielawski, C. W.; Grubbs, R. H. Living Ring-Opening Metathesis Polymerization. *Prog. Polym. Sci.* **2007**, *32*, 1–29.
(8) Choi, T.; Grubbs, R. H. Controlled Living Ring-Opening-Metathesis Polymerization by a Fast-Initiating Ruthenium Catalyst. *Angew. Chem. Int. Ed.* **2003**, *42*, 1743–1746.
(9) Chauvin, Y. Olefin Metathesis: The Early Days (Nobel Lecture). *Angew. Chem. Int. Ed.* **2006**, *45*, 3741–3747.
(10) Mol, J. C. Industrial Applications of Olefin Metathesis. *J. Mol. Catal. A Chem.* **2004**, *213*, 39–45.
(11) Vougioukalakis, G. C. Removing Ruthenium Residues from Olefin Metathesis Reaction Products. *Chem. - A Eur. J.* **2012**, *18*, 8868–8880.
(12) Ogawa, K. A.; Goetz, A. E.; Boydston, A. J. Metal-Free Ring-Opening Metathesis Polymerization. *J. Am. Chem. Soc.* **2015**, *137*, 1400–1403.
(13) Treat, N. J.; Sprafke, H.; Kramer, J. W.; Clark, P. G.; Barton, B. E.; Read De Alaniz, J.; Fors, B. P.; Hawker, C. J. Metal-Free Atom Transfer Radical Polymerization. *J. Am. Chem. Soc.* **2014**, *136*, 16096–16101.
(14) Theriot, J. C.; Mccarthy, B. G.; Lim, C.; Miyake, G. M. Organocatalyzed Atom Transfer Radical Polymerization : Perspectives on Catalyst Design and Performance. *Macromol Rapid Commun* **2017**, *38*, 1700040.
(15) Discekici, E. H.; Anastasaki, A.; Read de Alaniz, J.; Hawker, C. J. Evolution and Future Directions of Metal-Free Atom Transfer Radical Polymerization. *Macromolecules* **2018**, *51*, 7421–7434.
(16) Yilmaz, G.; Yagci, Y. Photoinduced Metal-Free Atom Transfer Radical Polymerizations: State-of-the-Art, Mechanistic Aspects and Applications. *Polym. Chem.* **2018**, *9*, 1757–1762.
(17) Miura, T.; KIm, S.; Kitano, Y.; Tada, M.; Chiba, K. Electrochemical Enol Ether/Olefin Cross- Metathesis in a Lithium Perchlorate/ Nitromethane Electrolyte Solution**. *Angew. Chem. Int. Ed.* **2006**, *45*, 1461–1463.
(18) Chiba, K.; Miura, T.; Kim, S.; Kitano, Y.; Tada, M. Electrocatalytic Intermolecular Olefin Cross-Coupling by Anodically Induced Formal [2+2] Cycloaddition between Enol Ethers and Alkenes. *J. Am. Chem. Soc.* **2001**, *123*, 11314–11315.
(19) Du, J.; Skubi, K. L.; Schultz, D. M.; Yoon, T. P. A Dual-Catalysis Approach to Enantioslective [2+2] Photocycloadditions Using Visible Light. *Science (80-.).* **2014**, *344*, 392–397.
(20) Schultz, D. M.; Yoon, T. P. Solar Synthesis : Prospects in Visible Light Photocatalysis Solar Synthesis. *Science (80-.).* **2014**, No. 1239176.
(21) Romero, N. A.; Nicewicz, D. A. Organic Photoredox Catalysis. *Chem. Rev* **2016**, *116*, 10075–10166.
(22) Riener, M.; Nicewicz, D. A. Synthesis of Cyclobutane Lignans via an Organic Single Electron Oxidant-Electron Relay System. *Chem. Sci.* **2013**, *4*, 2625–2629.
(23) Lu, Z.; Yoon, T. P. Visible Light Photocatalysis of [2+2] Styrene Cycloadditions via Energy Transfer. *Angew. Chem. Int. Ed. Engl.* **2012**, *51*, 10329–10332.
(24) Pascual, L. M. M.; Dunford, D. G.; Goetz, A. E.; Ogawa, K. A.; Boydston, A. J.

Comparison of Pyrylium and Thiopyrylium Photooxidants in Metal-Free Ring-Opening Metathesis Polymerization. *Synlett* **2016**, *27*, 759–762.
(25) Goetz, A. E.; Boydston, A. J. Metal-Free Preparation of Linear and Cross-Linked Polydicyclopentadiene. *J. Am. Chem. Soc.* **2015**, *137*, 7572–7575.
(26) Goetz, A. E.; Pascual, L. M. M.; Dunford, D. G.; Ogawa, K. A.; Knorr, D. B.; Boydston, A. J. Expanded Functionality of Polymers Prepared Using Metal-Free Ring-Opening Metathesis Polymerization. *ACS Macro Lett.* **2016**, *5*, 579–582.
(27) Lu, P.; Alrashdi, N. M.; Boydston, A. J. Bidirectional Metal-Free ROMP from Difunctional Organic Initiators. *J. Polym. Sci. Part A Polym. Chem.* **2017**, *55*, 2977–2982.
(28) Lu, P.; Boydston, A. J. Integration of Metal-Free Ring-Opening Metathesis Polymerization and Organocatalyzed Ring-Opening Polymerization through a Bifunctional Initiator. *Polym. Chem.* **2019**, *10*, 2975–2979.
(29) Pascual, L. M. M.; Goetz, A. E.; Roehrich, A. M.; Boydston, A. J. Investigation of Tacticity and Living Characteristics of Photoredox-Mediated Metal-Free Ring-Opening Metathesis Polymerization. *Macromol Rapid Commun* **2017**, *38*, 1600766.

Chapter 2. Molecular Weight Control via Chain Transfer in Photo-Redox Mediated Ring-Opening Metathesis Polymerization

2.1 INTRODUCTION

Metal-mediated ring-opening metathesis polymerization (ROMP) is a highly established technology in academic[1–4] and industrial[5,6] settings for applications in high-performance plastics, drug delivery,[7] biomaterials,[8] optics, and organic electronics. Traditional ROMP produces polymers with a broad array of functional groups,[9] excellent control of tacticity and dispersity,[10–15] tunable material properties,[14] and well-defined architectures. However, the covalent incorporation of stoichiometric amounts of metal initiator presents limitations with respect to using the products in certain applications, such as pharmaceutical, biomedical, optics, and electronics.[17] While metal contamination is a large problem in metal-mediated ROMP, the transition metal itself is also costly, as one metal initiator produces only a single polymer chain. At ultrahigh-molecular weights or in bulk synthesis cases, this is not a significant burden, but as lower molecular weight polymers and oligomers are targeted, this cost can become astronomical.

To make polymerizations truly catalytic events, the use of chain transfer agents (CTAs) has shown great success in reversible addition-fragmentation chain-transfer polymerizations,[18] ring-opening polymerizations,[19] Ziegler-Natta polymerizations,[20] and coordinative chain-transfer polymerizations.[21] While CTAs have been used extensively to change the chain end of ROMP polymers,[22-67] not much has been done to convert the metal-alkylidene initiator to a truly catalytic agent.

In the late 1980s, the Schrock group investigated a variety of CTAs in the polymerization of norbornene, concluding that using a molybdenum catalyst and 1,3-dienes or styrenes, they could produce low molecular weight polymers with dispersities below 1.1.[68,69] They demonstrated the ability to recycle the catalyst in a pulsed addition method for ten batches. Cramail et al controlled the molecular weight of polynorbornene (pNB) by varying the ratio of unsaturated diesters (CTA in this case) to monomer.[70] Fontanille and coworkers used acyclic olefins and a tungsten catalyst to control the molecular weight and functionalization of oligomeric dicyclopentadiene in 1992.[71] Grubbs and coworkers expanded the use of CTAs in ROMP in 1995 when they used both molybdenum and tungsten catalysts to synthesize end-functionalized polybutadiene of varying molecular weights by employing a difunctional protected allyl alcohol.[72] Ozawa demonstrated that heteroatom-substituted vinylic compounds could be used to end-functionalize pNBs and also produce low molecular weight oligomers in a single addition approach.[73] Perhaps the most developed method was the pulsed addition method using a Symyx robot where, after accounting for catalyst death, a single low dispersity polymer could prepared in ten cycles of intiator.[74] Very recently the Kilbinger group reported catalytic living ROMP through the use of a degenerative reversible chain-transfer mechanism.[75]

Our group recently developed an organic photo-redox mediated ROMP (photo-ROMP) method that utilizes an organic photo-oxidant to do a one-electron oxidation of a vinyl ether to initiate polymerization.[76] The vinyl ether radical cation, once oxidized by a photochemically excited pyrylium salt, is believed to react in a [2+2] cycloaddition with a cyclic alkene. Release of monomer ring strain favors opening of the cyclobutane intermediate to form the metathesis product with a radical cation propagating end group as shown in **Scheme 2.1**, ultimately leading to polymer

production. Photo-ROMP has been developed to include an array of monomers[77,78] and complex architectures[79] making it more widely applicable to polymer synthesis. Removing the problematic metal catalyst eliminates the problems associated with transition metals and is much more cost-effective; however, this method has its own pitfall as cationic polymerization of the vinyl initiator dominates at high initiator loadings.

Scheme 2.1 (top): Proposed mechanism for photo-redox mediated ROMP
Scheme 2.2 (bottom): Chain transfer in photo-redox mediated ROMP

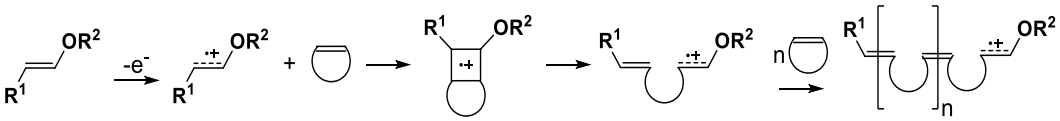

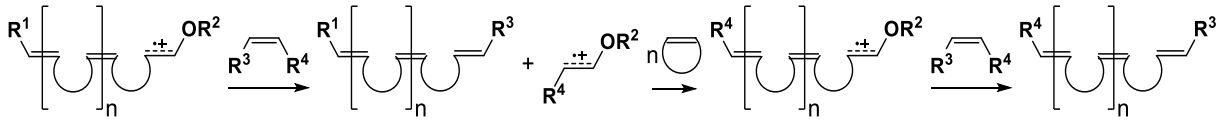

To extend the photo-ROMP method into the low molecular weight regime of polymer synthesis, we wanted to determine if cross metathesis could be used in our system as well. We envisioned a mechanism, much like that of metal-mediated chain transfer, where an acyclic olefin could undergo cross metathesis with the polymer chain end, cleaving the vinyl ether initiator from the polymer and simultaneously creating a new initiator that could undergo subsequent polymerization (**Scheme 2.2**) and the cycle would repeat until all monomer was consumed or the reaction was terminated. We sought to obviate the need for pulsed additions or slow monomer addition, thereby allowing all reagents to be added to the pot before starting the polymerization. Initially, we attempted to use internal olefins, which have been heavily used as CTAs in metal-mediated ROMP, but we saw no cross metathesis occurring. When we moved to terminal olefins, we observed cross metathesis and the ability to control molecular weight by altering the concentration of CTA.

Scheme 2.3: Monomer, initiator, photocatalyst, and chain transfer agents used in this study

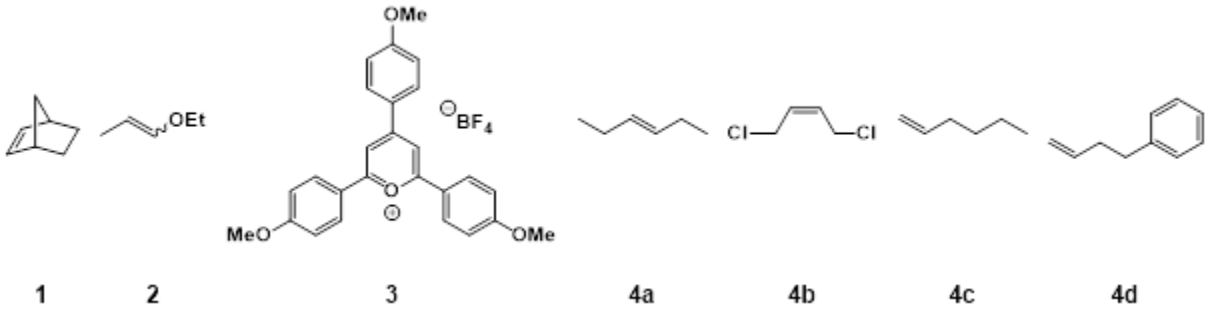

2.2 Results and Discussions

Using our previously reported conditions for photo-ROMP,[76] monomer **1** was polymerized upon exposure to blue light using vinyl ether initiator **2**, photoredox mediator **3**, and varying equivalents of CTAs **4a-d** (**Scheme 2.3**). The internal CTAs (**4a & 4b**) showed no difference in molecular weight from the control experiments, indicating that no cross metathesis was occurring during these polymerizations, which was also confirmed by NMR end group analysis. Moving from internal olefins to the terminal olefins (**4c & 4d**), we saw an initial ability to modulate the molecular weight of the resulting polymer using the chain transfer agent. To investigate this observation further, we increased the monomer to initiator loading of **1** to **2** to 200:1 to increase the molecular weight range, decreased the concentration of the reaction to 0.5M to enhance solubility, and varied the loading of CTA **4c** from 0 to 400 equivalents relative to **2**. Molecular weights ranging from 27 kDa to 4 kDa were observed as shown in **Figure 2.6**. As seen in **Figure 2.1**, a shift to lower retention times, signifying lower molecular weight polymer, is a result of the increase in CTA loading. A wide variety of molecular weights can be targeted by varying the initial loading of CTA. We saw this same effect using monomer **1** with CTA **4d** (**Figure 2.1** bottom). The shoulders in the GPC traces at low loadings of CTA are a result of chain coupling. This was

investigated by tracking the GPC trace over the course of the reaction and the bimodality doesn't begin until over 55% conversion of monomer as can be seen in **Figure 2.2**.

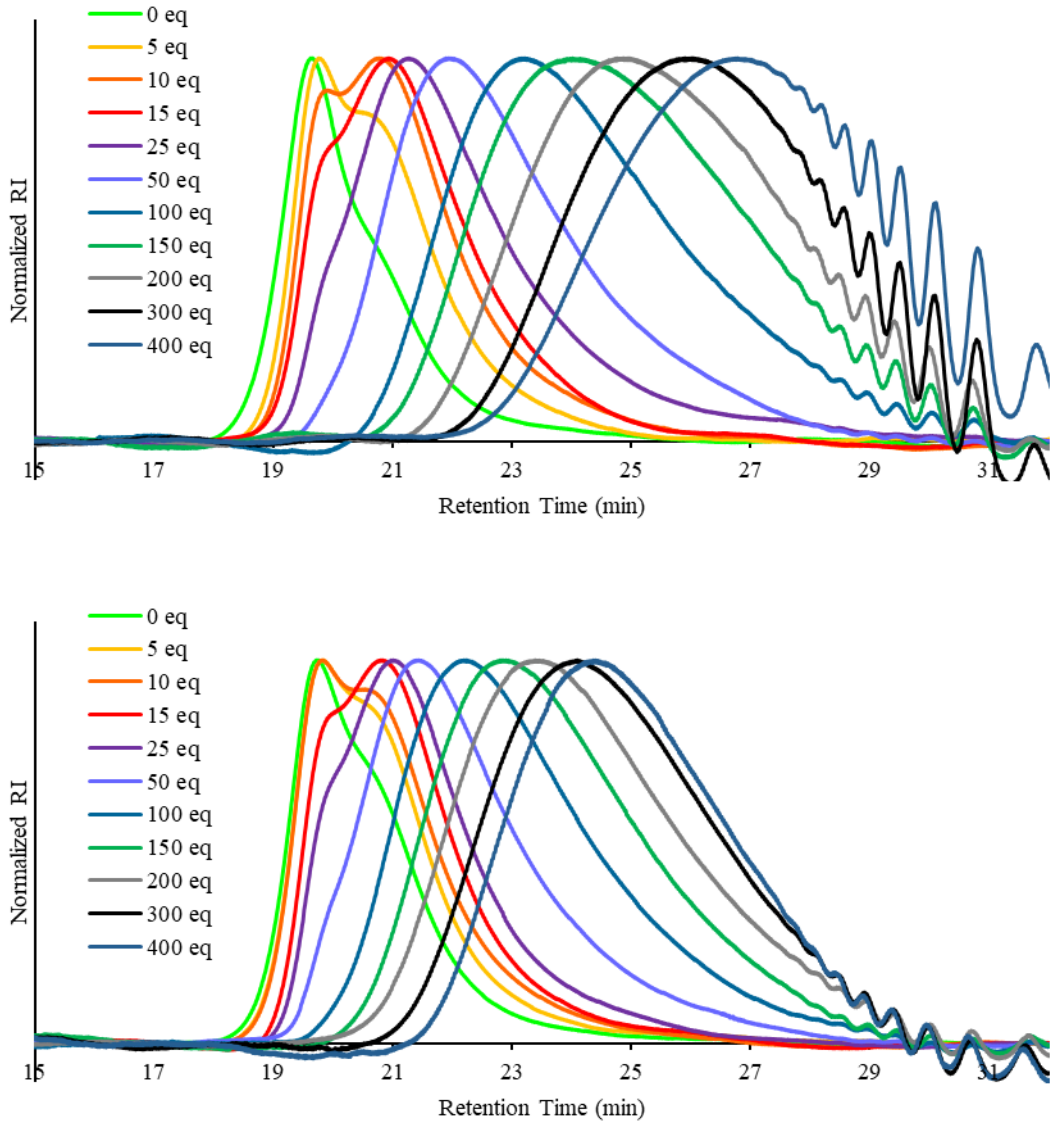

Figure 2.1: Normalized GPC refractive index traces of pNB as a function of equivalents of CTA **4c** (top) and **4d** (bottom) relative to initiator **2** in a polymerization of **1**, using a typical polymerization ratio of 200:1:0.1 **1**:**2**:**3**.

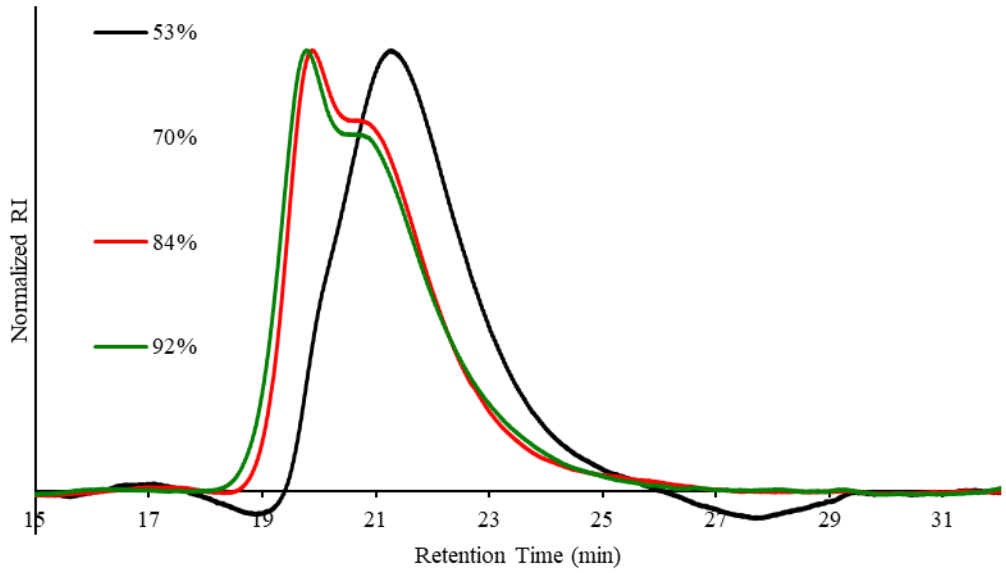

Figure 2.2*:* Normalized GPC refractive index traces of pNB as a function of conversion using CTA **4c** relative to initiator **2** in a polymerization of **1**, using a typical polymerization ratio of 200:1:0.1 **1**:**2**:**3**.

Low molecular weight oligomers are attractive for a variety of applications industrially. They can be used to overcome problems with malodorous monomers by creating less volatile prepolymers that can often be utilized for the same purposes as the original monomer. They can also be used to create resins that can be crosslinked downstream after molding, or to lower or increase the viscosity of polymeric resins for extrusion-based processes. To demonstrate the wide range of viscosities accessible using our cross-metathesis method, we used a rheometer to measure the viscosities of the low molecular weight oligomers. As seen in **Figure 2.3**, the oligomers show shear-thinning behavior that is typical of polymeric materials.

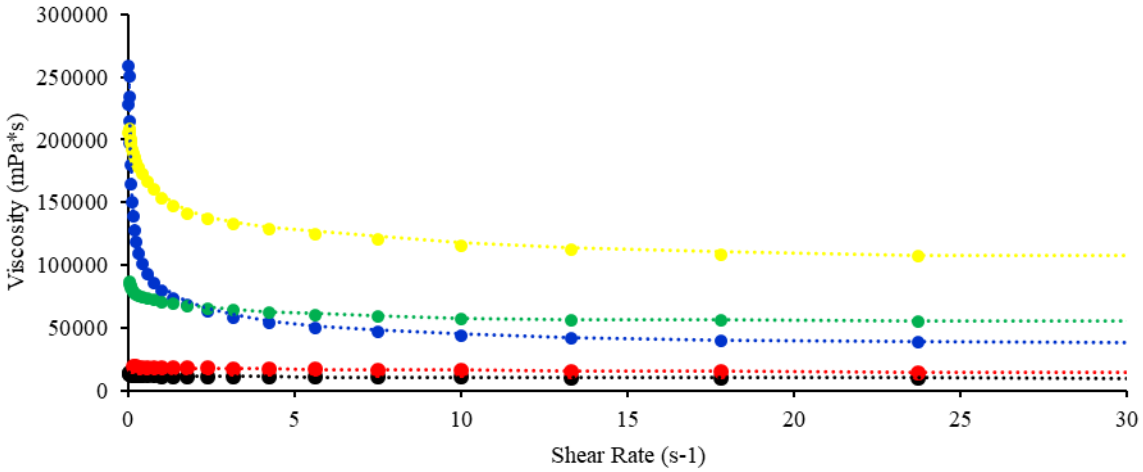

Figure 2.3: Plot of viscosity vs shear rate for polynorbornene samples of varying molecular weight 800 Da (black), 1000 Da (red), 1300 Da (blue), 1800 Da (green), and 3300 Da (yellow). Molecular weights were determined from end group analysis by ^{1}H NMR spectroscopy.

To evaluate the effect of cross metathesis on monomer consumption, we monitored the conversion of **1** to poly(**1**) over time using ^{1}H NMR spectroscopy. As can be seen in **Figure 2.4**, the use of CTAs makes the reaction slower compared to that of monomer alone. Photo-ROMP proceeds via a radical cation mechanism, so to probe whether the slower propagation was due to a decrease in the dielectric constant as well as the, n-hexane ($\varepsilon = 1.89$) was subbed into the reaction to mimic the dielectric constant at 50 equivalents of **4c** ($\varepsilon = 2.05$). As expected, the propagation was also hindered by the decrease in polarity of the reaction solution.

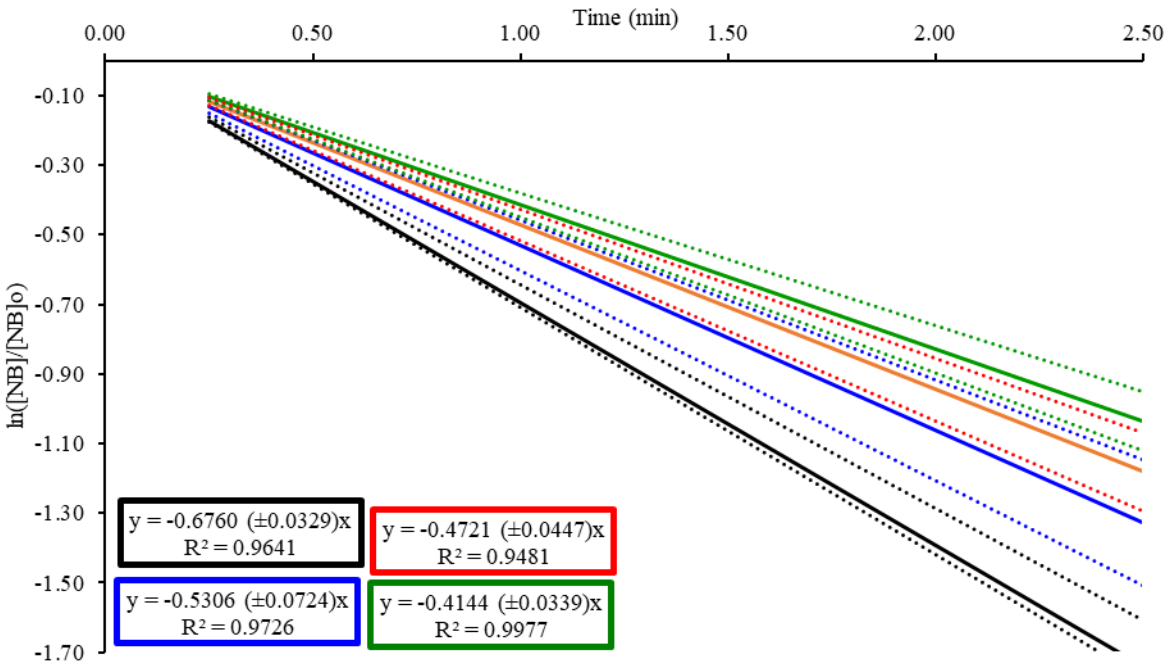

Figure 2.4: Plot of ln([**1**]/[**1**]$_o$) versus time for the photo-ROMP of **1** (CH_2Cl_2, 25 ˚C, [**1**] = 0.5 M) with no additive (black), n-hexane (blue), **4c** as the CTA (red), and **4d** as the CTA (green). Dotted lines are the standard deviation of the slope for triplicate trials.

To determine the mechanism of cross metathesis in our polymerizations, we sought to determine the end groups of the resulting polymers. ^{1}H NMR analysis of purified polymer samples show no vinyl ether end group, typical of our photo-ROMP polymerization method, supporting cross metathesis at the end of the polymer chain. Unfortunately, many proton signals of the CTA, overlap with initiator **2** signals, making it difficult to deconvolute the chain end identities. Matrix-assisted laser-desorption ionization time-of-flight mass spectrometry (MALDI-TOF MS) enables resolution of individual n-mers of the polymer, allowing for determination of the polymer chain end. The MALDI-TOF spectra in **Figure 2.5** shows the n-mers of poly(**1**), using **4c** as a CTA, with a spacing of 94.08 m/z (Theo: 94.15 m/z), the expected repeat unit of poly(**1**). This data shows that the end groups of the polymer chains are the terminal olefin and alkyl units of **4c**.

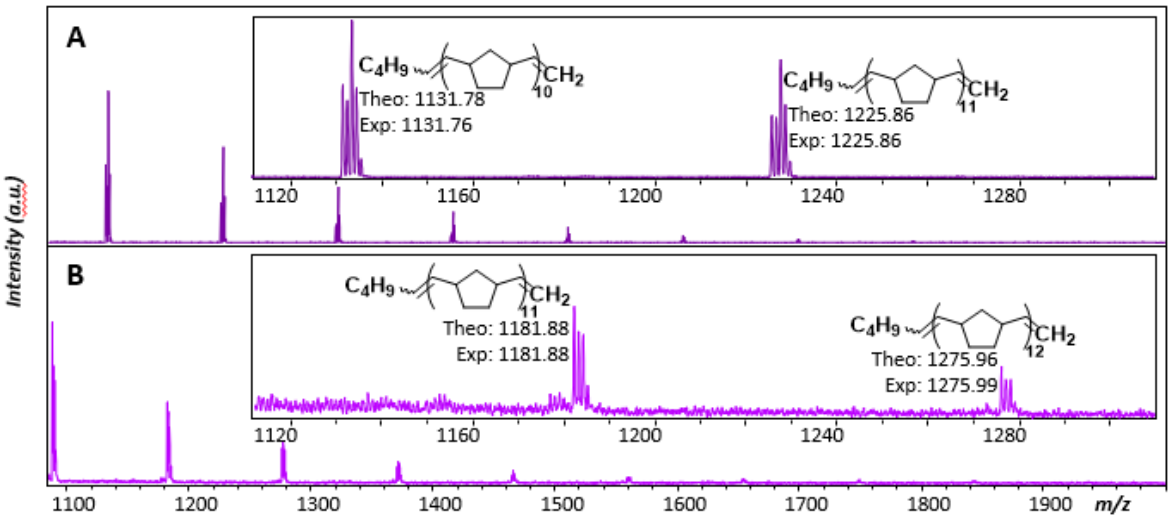

Figure 2.5: MALDI-TOF mass spectra of pNB, initiated with **2** using **4c** as the CTA, ionized with A) Ag^+ and B) Cu^+, with expanded spectra from *m/z* = 1110 to 1310. The spectra were taken in positive reflector mode.

To determine whether the oligomers were being terminated with the terminal olefin and or the longer chain of the CTAs as shown in **Scheme 2.4**, we evaluated the efficiency of ethyl vinyl ether (EVE) as an initiator. Polymerization of norbornene initiated with EVE resulted in low conversion (12%) and had very low initiator efficiency (2.8%). This data indicated that EVE is not responsible for initiating a significant number of new chains following cross metathesis. This is also likely the favored chain transfer product due to steric hinderance in between the CTA and the polyolefin and also produces the most stable radical cation intermediates.

Scheme 2.4: Possible pathways of cross-metathesis

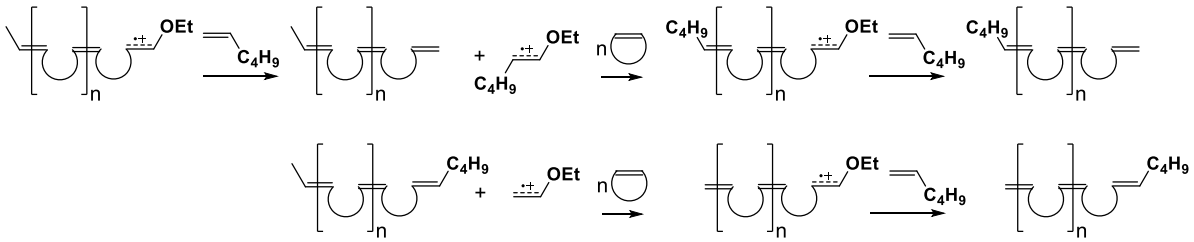

To prove that the cross metathesis was occurring at the chain end and not in the backbone of the polymer, we conducted a control experiment by adding **4c** once monomer **1** had been consumed. ^{1}H NMR analysis of the polymer before and after addition of the CTA showed that the vinyl ether chain end was replaced with the terminal olefin, but the polymer had the same molecular weight by GPC. Cross metathesis predominantly at the chain end is likely due to the higher oxidation potential of the backbone olefins as compared to the vinyl ether chain end.

2.3 CONCLUSIONS

Cross metathesis in photoredox-mediated photo-ROMP can be accomplished using α-olefin CTAs. This method can be used to modulate molecular weight in photo-ROMP, but does decrease the rate of monomer consumption and final conversion. Cross metathesis results in an α-olefin polymer chain end and produces a vinyl ether with internal olefin, which can initiate photo-ROMP following the first metathesis event. Since cross metathesis via photo-ROMP has been successful only with α-olefin CTAs, using CTAs to functionalize chain ends in MF-ROMP remains a challenge.

2.4 EXPERIMENTAL

General Considerations: Dichloromethane (CH_2Cl_2) was dried over 4Å molecular sieves before use. ^{1}H and ^{13}C NMR spectra were recorded on a Bruker AVance 500 MHz spectrometer. Chemical shifts are reported in delta (δ) units, expressed in parts per million (ppm) downfield from tetramethylsilane using residual protio-solvent as an internal standard ($CDCl_3$, ^{1}H : 7.26 ppm and ^{13}C: 77.0 ppm; CD_2Cl_2, ^{1}H: 5.32 ppm and ^{13}C: 53.84 ppm). Data are reported as follows: chemical shift, multiplicity (s = singlet, d = doublet, dd = doublet of doublets, br = broad, m = multiplet), coupling constants,(Hz), and integration. Gel permeation chromatography (GPC) was performed

using a GPC setup consisting of: a Shimadzu pump, 3 in-line columns, and Wyatt light scattering and refractive index detectors with tetrahydrofuran (THF) as the mobile phase. Number-average molecular weights (M_n) and weight-average molecular weights (M_w) were calculated from light scattering. Differential Scanning Calorimetry (DSC) was performed on a Mettler Toledo DSC 3+ calorimeter under nitrogen at a heating rate of 10 °C/min and cooling rate of 5 °C/min. Rheometry was performed on an Anton-Parr MCR302 rheometer at 25 °C. All reactions were carried out in standard borosilicate vials purchased from Fisher Scientific with magnetic stirring unless otherwise noted. Irradiation of photochemical reactions were performed using a 6 W Miracle blue LED indoor gardening bulb purchased from Amazon. The pyrylium tetrafluoroborate salt (**3**) was prepared according to literature procedure.[80] Norbornene (**1**) was sublimed prior to use. CTAs (**4a-d**) were dried over 4Å molecular sieves before use. All other reagents were obtained from commercial sources and used as received.

General Procedure for Chain Transfer Trials

In separate volumetric flasks, stock solutions of **1**, **2**, and **3** were made in CH_2Cl_2. To a 5 mL volumetric flask was added an aliquot of the stock solution of **1** (0.2354 g, 2.5 mmol, 200 equiv.) followed by an aliquot of the stock solution of **3** (0.6 mg, 0.00125 mmol, 0.1 equiv.). 0 to 400 equiv. of CTA were then added and measured gravimetrically. An aliquot of **2** (1.1 mg, 0.0125 mmol, 1 equiv.) was then added to the volumetric flask and the flask was filled to the line with CH_2Cl_2. The solution was transferred to a 2 dram vial with a Teflon cap and a magnetic stir bar. The vial was capped and irradiated with blue LEDs (6 W) 1 cm from bulb for 45 minutes. A small scoop of hydroquinone was added to the vial and an aliquot taken for analysis.

Polymerization Data for **Figure 2.1**

Table 2.1. Results of molecular weight modulation with **4c** as CTA with initial **1**:**2**:**3** of 200 : 1 : 0.1.

		From GPC[b]	
4c (equivs)	Conversion (%)[a]	M_n[c]	$Đ$[d]
400	84	5.2	1.014
300	89	5.1	1.086
200	93	2.5	1.239
150	92	5.0	1.137
100	93	4.6	1.180
50	93	5.5	1.471
25	94	8.5	1.992
15	95	14.4	2.248
10	95	11.6	1.644
5	95	15.8	1.501
0	95	21.0	1.757

[a] % conversion of **1**, determined by ^{1}H NMR spectroscopy. [b] Determined from crude, unprecipitated reaction aliquots: [c] Experimental number-average molecular weight M_n, calculated from experimental weight-average molecular weight determined by GCP using multi-angle laser light scattering (MALLS). [d] Dispersitites ($Đ$) determined by GPC analysis.

Table 2.2. Results of molecular weight modulation with **4c** as CTA with initial **1**:**2**:**3** of 200 : 1 : 0.1.

		From GPC[b]	
4c (equivs)	Conversion (%)[a]	M_n[c]	$Đ$[d]
405	90	5.3	1.051
308	91	6.1	1.118
206	93	4.8	1.028
156	94	5.8	1.045
104	92	6.7	1.109
48	90	5.1	1.485
23	92	8.2	1.454
14	91	13.1	1.289
9	91	12.9	1.473
4	90	15.8	1.471
0	94	26.9	1.371

[a] % conversion of **1**, determined by ^{1}H NMR spectroscopy. [b] Determined from crude, unprecipitated reaction aliquots: [c] Experimental number-average molecular weight M_n, calculated from experimental weight-average molecular weight determined by GCP using multi-angle laser light scattering (MALLS). [d] Dispersitites ($Đ$) determined by GPC analysis.

Table 2.3. Results of molecular weight modulation with **4d** as CTA with initial **1**:**2**:**3** of 200 : 1 : 0.1.

		From GPC[b]	
4c (equivs)	Conversion (%)[a]	M_n[c]	$Đ$[d]
403	73	4.7	1.168
303	81	9.9	1.143
207	86	7.2	1.061
153	90	4.0	1.293
105	89	4.3	1.555
50	88	7.3	1.428
25	89	11.7	1.383
14	89	12.4	1.434
10	90	15.0	1.499
4	88	17.2	1.380
0	87	20.5	1.363

[a] % conversion of **1**, determined by ^{1}H NMR spectroscopy. [b] Determined from crude, unprecipitated reaction aliquots: [c] Experimental number-average molecular weight M_n, calculated from experimental weight-average molecular weight determined by GCP using multi-angle laser light scattering (MALLS). [d] Dispersitites ($Đ$) determined by GPC analysis.

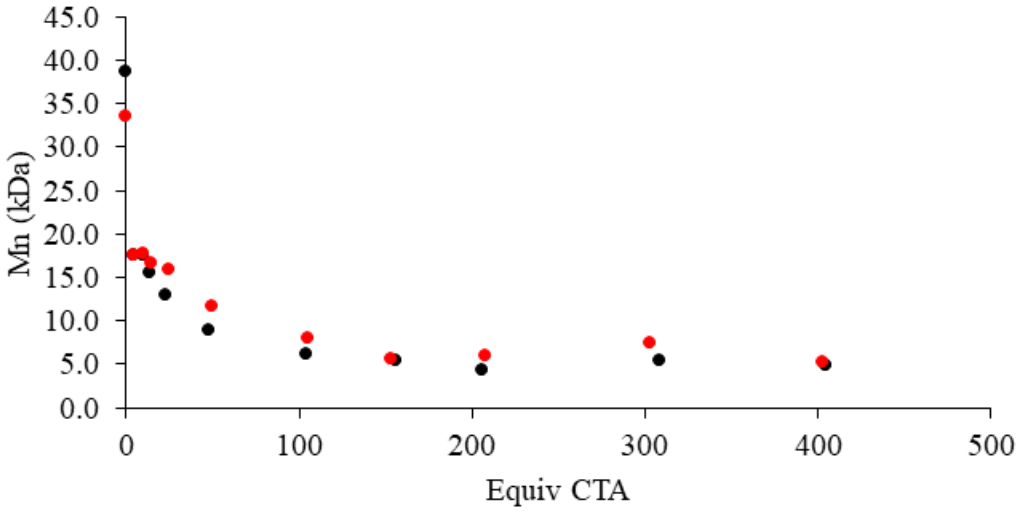

Figure 2.6: Plot of number-average molecular weight M_n (kDa) as a function of equivalents of CTA **4c** (black) and **4d** (red) relative to initiator **2** in a polymerization of **1**, using a typical polymerization ratio of 200:1:0.1 **1**:**2**:**3**. M_n was calculated from weight-average molecular weight M_w, determined by GPC with multi-angle laser light scattering (MALLS), calculated from the peak (peak +/- 30 sec.) of the RI trace.

Procedure for GPC tracking experiment

In separate volumetric flasks, stock solutions of **1**, **2**, **3**, and **4c** were made in CH_2Cl_2. To a 10 mL volumetric flask was added an aliquot of the stock solution of **1** (0.4708 g, 5.0 mmol, 200 equiv.),

an aliquot of the stock solution of **3** (1.2 mg, 0.0025 mmol, 0.1 equiv.), an aliquot of the stock solution of **2** (2.2 mg, 0.025 mmol, 1 equiv.), and an aliquot of the stock solution of **4c** (21.0 mg, 0.25 mmol, 10 equiv.) and the flask was filled to the line with CH_2Cl_2. The solution was transferred to a 20 mL scintillation vial with a Teflon cap and a magnetic stir bar. The vial was capped and irradiated with blue LEDs (6 W) 1 cm from bulb for 45 minutes. At 2, 5, 20, and 45 min, a 0.2 mL aliquot was removed from the reaction. 0.1 ml was diluted with 0.3 mL of $CDCl_3$ for NMR analysis of conversion and 0.1 mL was concentrated and dissolved in THF for GPC analysis.

Table 2.4. Results of molecular weight modulation with **4c** as CTA with initial **1**:**2**:**3** of 200 : 1 : 0.1.

		From GPC[b]	
Time point (min)	Conversion (%)[a]	M_n[c]	$Đ$[d]
2	53	5.3	1.051
5	70	6.1	1.118
20	84	4.8	1.028
45	92	5.8	1.045

[a] % conversion of **1**, determined by ^{1}H NMR spectroscopy. [b] Determined from crude, unprecipitated reaction aliquots: [c] Experimental number-average molecular weight M_n, calculated from experimental weight-average molecular weight determined by GCP using multi-angle laser light scattering (MALLS). [d] Dispersitites ($Đ$) determined by GPC analysis.

General Procedure for Preparation of Polymers for Rheometry

To a 30 mL scintillation vial with Teflon cap containing a magnetic stirbar was added *p*-OMeTPT (3.0 mg, 0.00625 mmol, 0.1 equiv), norbornene (1.1769 g, 12.5 mmol, 200 equiv), 1-hexene (3.10 mL, 25 mmol, 400 equiv), and ethyl propenyl ether (6.9 µL, 0.0625 mmol, 1 equiv). CH_2Cl_2 was added to fill the vial to 25 mL. The vial was capped and irradiated with a blue LED (6 W) 1 cm from bulb for 80 minutes. An aliquot taken for analysis and the remaining reaction mixture was filtered through a plug of neutral alumina, eluting with CH_2Cl_2. The volatiles were removed from

DSC Data

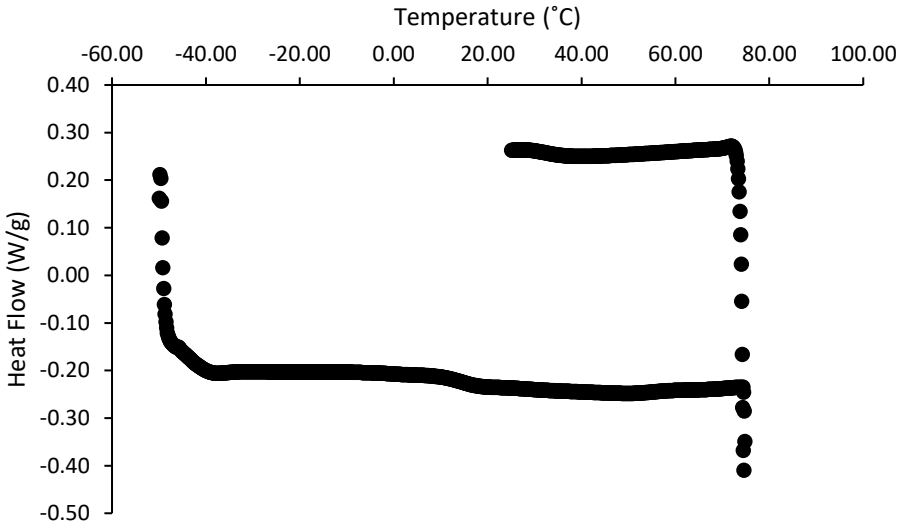

Figure 2.7: Differential scanning calorimetry for 0.8 kDa polynorbornene

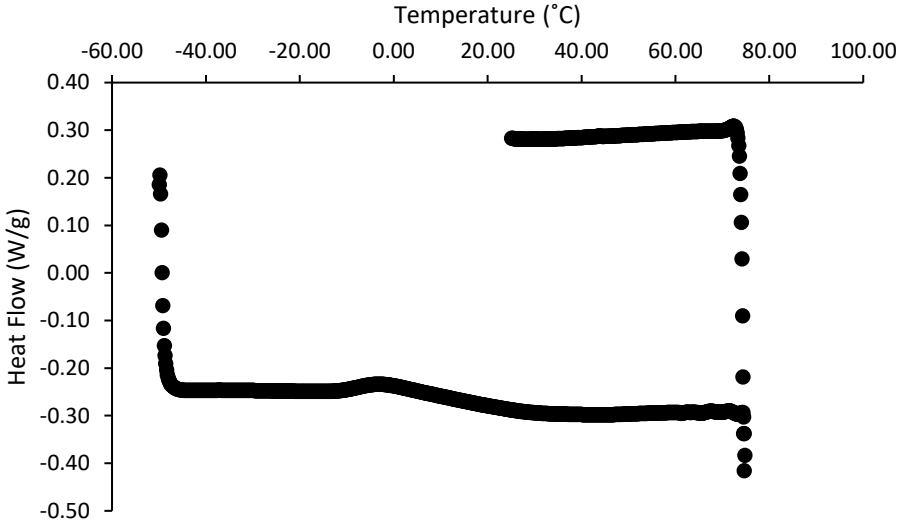

Figure 2.8: Differential scanning calorimetry for 1.0 kDa polynorbornene

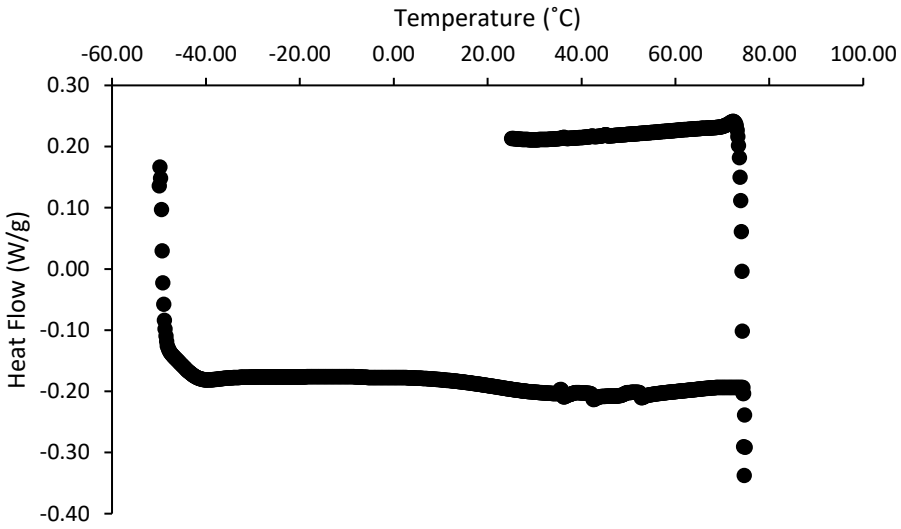

Figure 2.9: Differential scanning calorimetry for 1.3 kDa polynorbornene

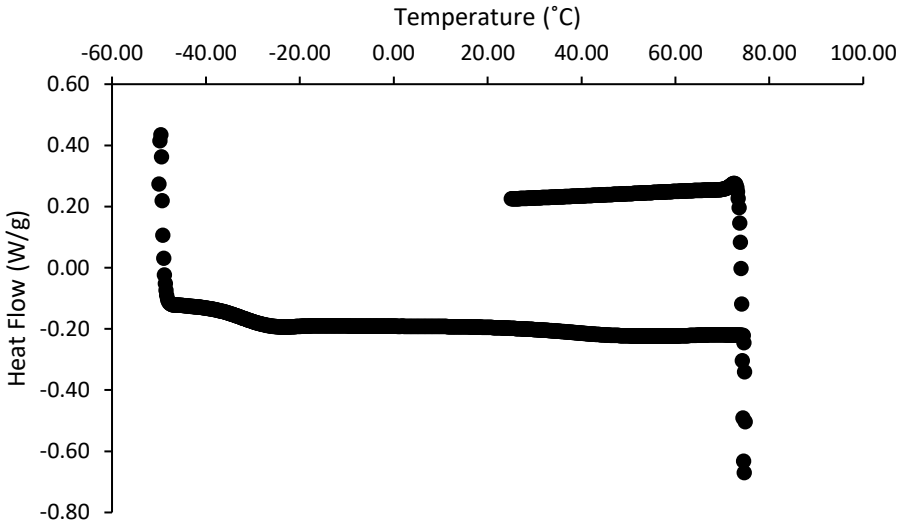

Figure 2.10: Differential scanning calorimetry for 1.8 kDa polynorbornene

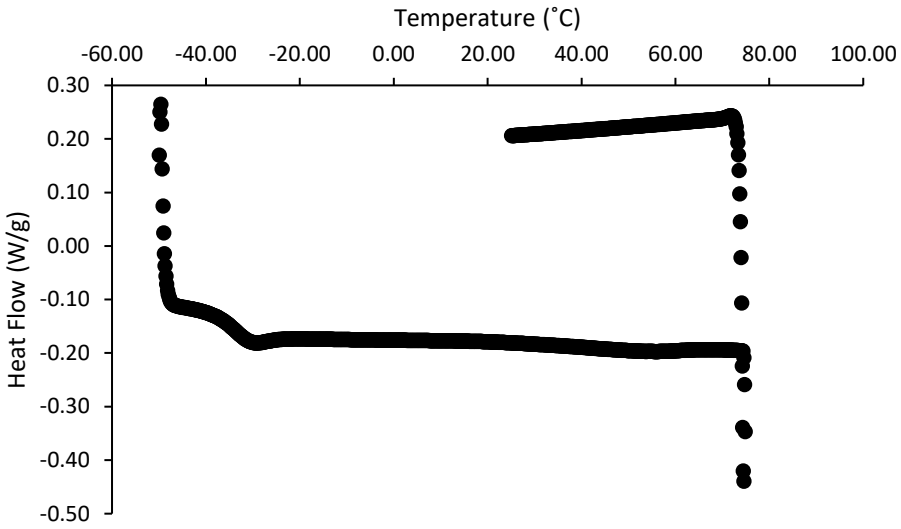

Figure 2.11: Differential scanning calorimetry for 3.3 kDa polynorbornene

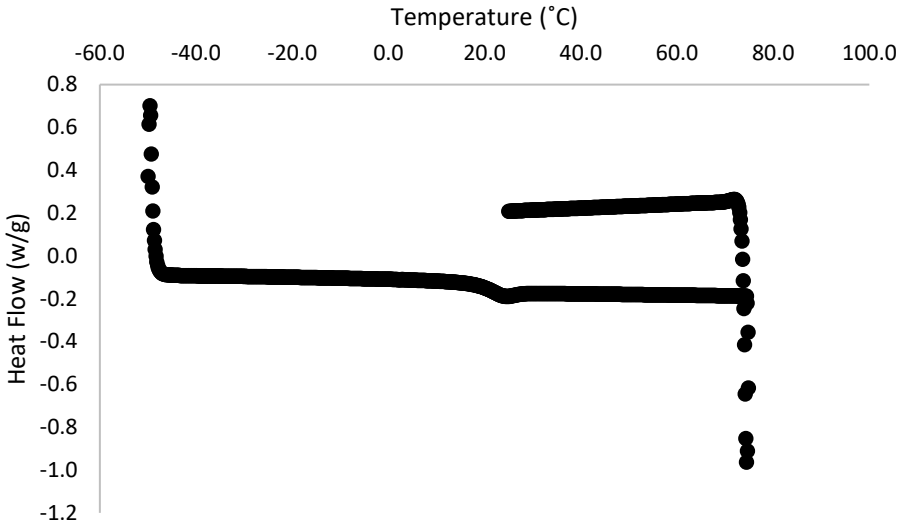

Figure 2.12: Differential scanning calorimetry for 5.8 kDa polynorbornene

General Procedure for Kinetic Experiments

In separate volumetric flasks, stock solutions of **1**, **2**, **3**, and **4c**, **4d**, or n-hexane were made in CD_2Cl_2. To a 1 mL volumetric flask was added an aliquot of the stock solution of **1** (47.1 mg, 0.5 mmol, 200 equiv.), an aliquot of the stock solution of **3** (0.1 mg, $2.5x10^{-4}$ mmol, 0.1 equiv.), an aliquot of the stock solution of **2** (0.2 mg, 0.0025 mmol, 1 equiv.), and an aliquot of the stock solution of **4c** (10.5 mg, 0.125 mmol, 50 equiv.) and the flask was filled to the line with CD_2Cl_2.

The solution was transferred to an NMR tube, which was irradiated with blue LEDs (6 W) 1 cm from bulb, pausing to take ^{1}H NMRs at time intervals indicated in the main text. Reaction mixtures were shaken vigorously at 30 second intervals.

To mimic the dielectric constant of 50 equiv. of 1-hexene (ε = 2.05), 15.3 μL of n-hexane (ε = 1.89) was added to those control experiments.

Procedure for Preparation of Polynorbornene for End Group Analysis by MALDI-TOF

To a 30 mL scintillation vial with Teflon cap containing a magnetic stirbar was added *p*-OMeTPT (10.9 mg, 0.022 mmol, 0.2 equiv) followed by norbornene (1.0639 g, 11.3 mmol, 100 equiv). Dichloromethane (20 mL) was added, followed by 1-hexene (2.79 mL, 22.5 mmol, 200 equiv) and ethyl propenyl ether (12.5 μL, 0.113 mmol, 1 equiv). The vial was capped and irradiated with a blue LED (6 W) 1 cm from bulb for 80 minutes. A small scoop of hydroquinone was added to the vial and an aliquot taken for analysis. The remaining reaction mixture was filtered through a plug of neutral alumina, eluting with CH_2Cl_2. The eluent was concentrated, redissolved in 20 mL CH_2Cl_2 and precipitated into 200 mL of cold, stirring MeOH in a dry ice/acetone bath and the precipitate was collected via filtration and washed with cold MeOH. The precipitation was repeated.

Table 2.5. Molecular weight data for MALDI-TOF polymer samples.

				From GPC		
Monomer	CTA	NB:EPE: *p*-OMeTPT:CTA	Conversion (%)[a]	M_n[b]	M_w[c]	$Đ$[d]
NB	1-hexene	100:1:0.2:200	84	1.1	1.4	1.3

[a] % conversion of norbornene, determined by ^{1}H NMR spectroscopy. [b] Determined from crude, unprecipitated reaction aliquots: Experimental number-average molecular weight M_n calculated from [b] experimental weight-average molecular weight (M_w) determined by GCP using multi-angle laser light scattering (MALLS). [d] Dispersitites ($Đ$) determined by GPC analysis. [e] Number-average molecular weight (M_n) calculated from weight-average molecular weight determined by GPC analysis with MALLS, using central minute of refractive index peak.

MALDI-TOF Methods

Mass spectral data were collected using a Bruker-Daltonics Matrix Assisted Laser Desorption Ionization Time-of-Flight (MALDI-TOF) Autoflex III mass spectrometer in reflector mode with positive ion detection. Typical sample preparation for MALDI-TOF MS data was performed by making stock solutions in THF of matrix (50 mg/ml), polymer analyte (2 mg/ml), and an appropriate cation source (2 mg/ml). The data herein were acquired using trans-2-[3-(4-tert-Butylphenyl)-2-methyl-2-propenylidene]malononitrile (DCTB) as a matrix, and CuBr and AgTFA were used as cation sources. With the Ag^+ cation, the stock solutions were mixed in a 4/2/1 ratio (matrix/analyte/cation). With the Cu^+ cation, the stock solutions were mixed in a 4/2/3 ratio for the 1-hexene initiated pNB. The prepared solutions were vortexed and deposited onto the MALDI target plate and allowed to evaporate via the dried droplet method. MALDI-TOF MS data were calibrated against Poly(ethylene glycol) methyl ether (M_n = 550) from Sigma Aldrich and SpheriCal dendritic calibrants from Polymer Factory (Stockholm, Sweden). M_n and Đ of the resultant spectra were calculated using Polytools software.

For AgTFA: 8/4/2 was always used

For CuBr: 8/4/6 was always used

Ethyl Vinyl Ether Screening

In a 2 dram vial with Teflon cap containing magnetic stir bar, p-OMeTPT (1.1 mg, 2.3 μmol, 0.05 eq), NB (0.4231 g, 4.5 mmol, 100 eq), 2.0 mL CH_2Cl_2, EVE (4.3 μL, 0.045 mmol, 1 eq) were combined. The reaction was stirred and irradiated with a 6 W blue LED bulb for 80 min. A small scoop of hydroquinone was added to the vial and an aliquot taken for analysis by ^1H NMR. The NMR sample was subsequently filtered through a cotton plug and concentrated for GPC analysis.

^{1}H NMR and GPC Data

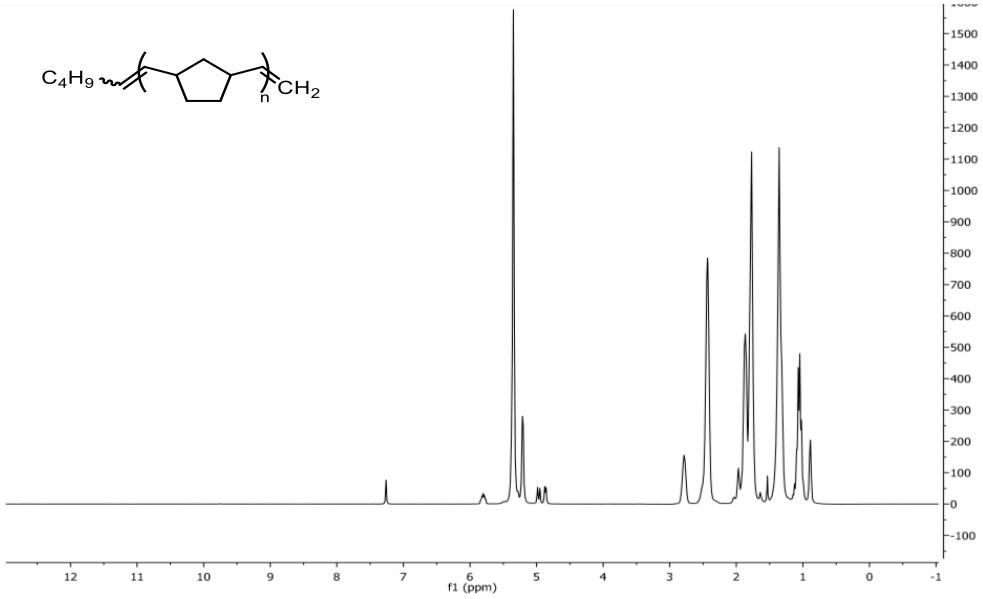

Figure 2.13. ^{1}H NMR spectrum of PNB synthesized via MF-ROMP in the presence of 1-hexene CTA (corresponds to **Table 2.5**) Product determined by MALDI-TOF overlaid.

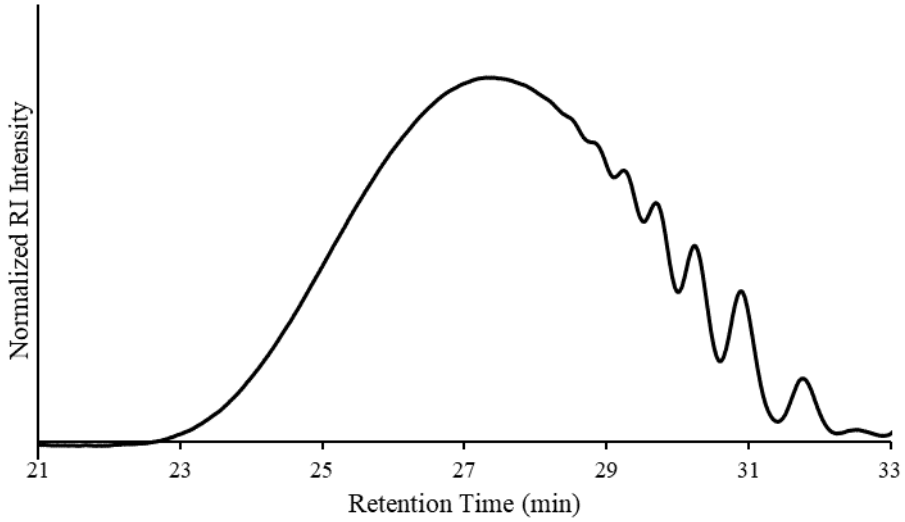

Figure 2.14. GPC refractive index of PNB synthesized via MF-ROMP in the presence of 1-hexene CTA (corresponds to **Table 2.5**).

2.5 NOTES AND REFERENCES FOR CHAPTER 2

(1) Chauvin, Y. Olefin Metathesis: The Early Days (Nobel Lecture). *Angew. Chem. Int. Ed.* **2006**, *45*, 3741–3747.

(2) Grubbs, R. H. Olefin-Metathesis Catalysts for the Preparation of Molecules and Materials (Nobel Lecture). *Angew. Chem. Int. Ed.* **2006**, *45*, 3760–3765.

(3) Bielawski, C. W.; Grubbs, R. H. Living Ring-Opening Metathesis Polymerization. *Prog. Polym. Sci.* **2007**, *32*, 1–29.

(4) Schrock, R. R. Multiple Metal-Carbon Bonds for Catalytic Metathesis Reactions (Nobel Lecture). *Angew. Chemie - Int. Ed.* **2006**, *45*, 3748–3759.

(5) Breslow, D. S. Metathesis Polymerization. *Prog. Polym. Sci.* **1993**, *18*, 1141–1195.

(6) Mol, J. C. Industrial Applications of Olefin Metathesis. *J. Mol. Catal. A Chem.* **2004**, *213*, 39–45.

(7) Hughes, D.; Wheeler, P.; Ene, D. Olefin Metathesis in Drug Discovery and Development - Examples from Recent Patent Literature. *Org. Process Res. Dev.* **2017**, *21*, 1938–1962.

(8) Sutthasupa, S.; Shiotsuki, M.; Sanda, F. Recent Advances in Ring-Opening Metathesis Polymerization, and Application to Synthesis of Functional Materials. *Polym. J.* **2010**, *42*, 905–915.

(9) Slugovc, C. The Ring-Opening Metathesis Polymerisation Toolbox. *Macromol. Rapid Commun.* **2004**, *25*, 1283–1297.

(10) Katz, T. J.; Lee, S. J.; Acton, N. Stereospecific Polymerizations of Cycloalkenes Induced by a Metal-Carbene. *Tetrahedron Lett.* **1976**, *17* (47), 4247–4250.

(11) Rosebrugh, L. E.; Marx, V. M.; Keitz, B. K.; Grubbs, R. H. Synthesis of Highly Cis, Syndiotactic Polymers via Ring-Opening Metathesis Polymerization Using Ruthenium Metathesis Catalysts. *J. Am. Chem. Soc.* **2013**, *135*, 10032–10035.

(12) Jeong, H.; Kozera, D. J.; Schrock, R. R.; Smith, S. J.; Zhang, J.; Ren, N.; Hillmyer, M. A. Z-Selective Ring-Opening Metathesis Polymerization of 3-Substituted Cyclooctenes by Monoaryloxide Pyrrolide Imido Alkylidene (MAP) Catalysts of Molybdenum and Tungsten. *Organometallics* **2013**, *32*, 4843–4850.

(13) Schrock, R. R. Synthesis of Stereoregular Polymers through Ring-Opening Metathesis Polymerization. *Acc. Chem. Res.* **2014**, *47* (8), 2457–2466.

(14) Forrest, W. P.; Axtell, J. C.; Schrock, R. R. Tungsten Oxo Alkylidene Complexes as Initiators for the Stereoregular Polymerization of 2,3-Dicarbomethoxynorbornadiene. *Organometallics* **2014**, *33*, 2313–2325.

(15) Benedikter, M. J.; Frater, G.; Buchmeiser, M. R. Regio- and Stereoselective Ring-Opening Metathesis Polymerization of Enantiomerically Pure Vince Lactam. *Macromolecules* **2018**, *51*, 2276–2282.

(16) Leitgeb, A.; Wappel, J.; Slugovc, C. The ROMP Toolbox Upgraded. *Polymer (Guildf).* **2010**, *51*, 2927–2946.

(17) Vougioukalakis, G. C. Removing Ruthenium Residues from Olefin Metathesis Reaction Products. *Chem. - A Eur. J.* **2012**, *18*, 8868–8880.

(18) Chiefari, J.; Chong, Y. K.; Ercole, F.; Krstina, J.; Jeffery, J.; Le, T. P. T.; Mayadunne, R. T. A.; Meijs, G. F.; Moad, C. L.; Moad, G.; et al. Living Free-Radical Polymerization by Reversible Addition-Fragmentation Chain Transfer: The RAFT Process. *Macromolecules* **1998**, *31*, 5559–5562.

(19) Ajellal, N.; Carpentier, J. F.; Guillaume, C.; Guillaume, S. M.; Helou, M.; Poirier, V.;

Sarazin, Y.; Trifonov, A. Metal-Catalyzed Immortal Ring-Opening Polymerization of Lactones, Lactides and Cyclic Carbonates. *Dalt. Trans.* **2010**, *39*, 8363–8376.
(20) Zhang, Y.; Keaton, R. J.; Sita, L. R. Degenerative Transfer Living Ziegler-Natta Polymerization: Application to the Synthesis of Monomodal Stereoblock Polyolefins of Narrow Polydispersity and Tunable Block Length. *J. Am. Chem. Soc.* **2003**, *125* (30), 9062–9069.
(21) Kempe, R. How to Polymerize Ethylene in a Highly Controlled Fashion? *Chem. - A Eur. J.* **2007**, *13* (10), 2764–2773.
(22) Reyx, D.; Campistron, I.; Hamza, M. Distribution of the Dienic and Trienic α,ω-Difunctionalized Oligomers in the Cross-Metathesis between Cyclopentene and Dimethyl Hex-3-Enedioate. *J. Mol. Catal.* **1986**, *36*, 101–105.
(23) Annunziata, L.; Fouquay, S.; Michaud, G.; Simon, F.; Guillaume, S. M.; Carpentier, J.-F. Mono- and Di-Cyclocarbonate Telechelic Polyolefins Synthesized from ROMP Using Glycerol Carbonate Derivatives as Chain-Transfer Agents. *Polym. Chem.* **2013**, *4*, 1313–1316.
(24) Diallo, A. K.; Annunziata, L.; Fouquay, S.; Michaud, G.; Simon, F.; Brusson, J. M.; Guillaume, S. M.; Carpentier, J. F. Ring-Opening Metathesis Polymerization of Cyclooctene Derivatives with Chain Transfer Agents Derived from Glycerol Carbonate. *Polym. Chem.* **2014**, *5* (7), 2583–2591.
(25) Chung, T. C.; Chasmawala, M. Synthesis of Telechelic 1,4-Polybutadiene by Metathesis Reactions and Borane Monomers. *Macromolecules* **1992**, *25*, 5137–5144.
(26) Sill, K.; Emrick, T. Bis-Dendritic Polyethylene Prepared by Ring-Opening Metathesis Polymerization in the Presence of Bis-Dendritic Chain Transfer Agents. *J. Polym. Sci. Part A Polym. Chem.* **2005**, *43* (22), 5429–5439.
(27) Scherman, O. A.; Rutenberg, I. M.; Grubbs, R. H. Direct Synthesis of Soluble, End-Functionalized Polyenes and Polyacetylene Block Copolymers. *J. Am. Chem. Soc.* **2003**, *125*, 8515–8522.
(28) Clark, P. G.; Guidry, E. N.; Chan, W. Y.; Steinmetz, W.; Grubbs, R. H. Synthesis of a Molecular Charm Bracelet via Click Cyclization and Olefin Metathesis Clipping. *J. Am. Chem. Soc.* **2010**, *132*, 3405–3412.
(29) Hillmyer, M. A.; Grubbs, R. H. Preparation of Hydroxytelechelic Poly(Butadiene) via Ring-Opening Metathesis Polymerization Employing a Well-Defined Metathesis Catalyst. *Macromolecules* **1993**, *26*, 872–874.
(30) Fraser, C.; Hillmyer, M. A.; Gutierrez, E.; Grubbs, R. H. Degradable Cyclooctadiene/Acetal Copolymers: Versatile Precursors to 1,4-Hydroxytelechelic Polybutadiene and Hydroxytelechelic Polyethylene. *Macromolecules* **1995**, *28*, 7256–7261.
(31) Hillmyer, M. A.; Nguyen, S. B. T.; Grubbs, R. H. Utility of a Ruthenium Metathesis Catalyst for the Preparation of End-Functionalized Polybutadiene. *Macromolecules* **1997**, *30* (4), 718–721.
(32) Bielawski, C. W.; Morita, T.; Grubbs, R. H. Synthesis of ABA Triblock Copolymers via a Tandem Ring-Opening Metathesis Polymerization: Atom Transfer Radical Polymerization Approach. *Macromolecules* **2000**, *33*, 678–680.
(33) Maughon, B. R.; Morita, T.; Bielawski, C. W.; Grubbs, R. H. Synthesis of Cross-Linkable Telechelic Poly(Butenylene)s Derived from Ring-Opening Metathesis Polymerization. *Macromolecules* **2000**, *33*, 1929–1935.

(34) Morita, T.; Maughon, B. R.; Bielawski, C. W.; Grubbs, R. H. A Ring-Opening Metathesis Polymerization (ROMP) Approach to Carboxyl- and Amino-Terminated Telechelic Poly(Butadiene)S. *Macromolecules* **2000**, *33*, 6621–6623.
(35) Bielawski, C. W.; Benitez, D.; Morita, T.; Grubbs, R. H. Synthesis of End-Functionalized Poly(Norbornene)s via Ring-Opening Methathesis Polymerization. *Macromolecules* **2001**, *34*, 8610–8618.
(36) Matson, J. B.; Grubbs, R. H. ROMP-ATRP Block Copolymers Prepared from Monotelechelic Poly(Oxa)Norbornenes Using a Difunctional Terminating Agent. *Macromolecules* **2008**, *41*, 5626–5631.
(37) Matson, J. B.; Grubbs, R. H. Monotelechelic Poly(Oxa)Norbornenes by Ring-Opening Metathesis Polymerization Using Direct End-Capping and Cross-Metathesis. *Macromolecules* **2010**, *43*, 213–221.
(38) Thomas, R. M.; Grubbs, R. H. Synthesis of Telechelic Polyisoprene via Ring-Opening Metathesis Polymerization in the Presence of Chain Transfer Agent. *Macromolecules* **2010**, *43*, 3705–3709.
(39) Michel, X.; Fouquay, S.; Michaud, G.; Simon, F.; Brusson, J. M.; Carpentier, J. F.; Guillaume, S. M. Simple Access to Alkoxysilyl Telechelic Polyolefins from Ruthenium-Catalyzed Cross-Metathesis Depolymerization of Polydienes. *Eur. Polym. J.* **2017**, *96* (May), 403–413.
(40) Diallo, A. K.; Michel, X.; Fouquay, S.; Michaud, G.; Simon, F.; Brusson, J. M.; Carpentier, J. F.; Guillaume, S. M. α-Trialkoxysilyl Functionalized Polycyclooctenes Synthesized by Chain-Transfer Ring-Opening Metathesis Polymerization. *Macromolecules* **2015**, *48* (20), 7453–7465.
(41) Vanbiervliet, E.; Fouquay, S.; Michaud, G.; Simon, F.; Carpentier, J. F.; Guillaume, S. M. From Epoxide to Cyclodithiocarbonate Telechelic Polycyclooctene through Chain-Transfer Ring-Opening Metathesis Polymerization (ROMP): Precursors to Non-Isocyanate Polyurethanes (NIPUS). *Macromolecules* **2017**, *50*, 69–82.
(42) Michel, X.; Fouquay, S.; Michaud, G.; Simon, F.; Brusson, J. M.; Carpentier, J. F.; Guillaume, S. M. α,ω-Bis(Trialkoxysilyl) Difunctionalized Polycyclooctenes from Ruthenium-Catalyzed Chain-Transfer Ring-Opening Metathesis Polymerization. *Polym. Chem.* **2016**, *7*, 4810–4823.
(43) Michel, X.; Fouquay, S.; Michaud, G.; Simon, F.; Brusson, J. M.; Roquefort, P.; Aubry, T.; Carpentier, J. F.; Guillaume, S. M. Tuning the Properties of α,ω-Bis(Trialkoxysilyl) Telechelic Copolyolefins from Ruthenium-Catalyzed Chain-Transfer Ring-Opening Metathesis Polymerization (ROMP). *Polym. Chem.* **2017**, *8*, 1177–1187.
(44) Mahanthappa, M. K.; Bates, F. S.; Hillmyer, M. A. Synthesis of ABA Triblock Copolymers by a Tandem ROMP-RAFT Strategy. *Macromolecules* **2005**, *38* (19), 7890–7894.
(45) Pitet, L. M.; Hillmyer, M. a. Combining Ring-Opening Metathesis Polymerization and Cyclic Ester Ring-Opening Polymerization To Form ABA Triblock Copolymers from 1,5-Cyclooctadiene and <scp>d,L</Scp> -Lactide. *Macromolecules* **2009**, *42* (11), 3674–3680.
(46) Theryo, G.; Jing, F.; Pitet, L. M.; Hillmyer, M. A. Tough Polylactide Graft Copolymers. *Macromolecules* **2010**, *43*, 7394–7397.
(47) Pitet, L. M.; Chamberlain, B. M.; Hauser, A. W.; Hillmyer, M. A. Synthesis of Linear, H-Shaped, and Arachnearm Block Copolymers by Tandem Ring-Opening Polymerizations.

Macromolecules **2010**, *43* (19), 8018–8025.
(48) Pitet, L. M.; Hillmyer, M. A. Carboxy-Telechelic Polyolefins by ROMP Using Maleic Acid as a Chain Transfer Agent. *Macromolecules* **2011**, *44*, 2378–2381.
(49) Amendt, M. A.; Pitet, L. M.; Moench, S.; Hillmyer, M. A. Reactive Triblock Polymers from Tandem Ring-Opening Polymerization for Nanostructured Vinyl Thermosets. *Polym. Chem.* **2012**, *3*, 1827–1837.
(50) Radlauer, M. R.; Matta, M. E.; Hillmyer, M. A. Regioselective Cross Metathesis for Block and Heterotelechelic Polymer Synthesis. *Polym. Chem.* **2016**, *7*, 6269–6278.
(51) Nomura, K.; Hou, X. Cis-Specific Chain Transfer Ring-Opening Metathesis Polymerization Using a Vanadium(V) Alkylidene Catalyst for Efficient Synthesis of End-Functionalized Polymers. *Organometallics* **2017**, *36*, 4103–4106.
(52) Liu, P.; Yasir, M.; Ruggi, A.; Kilbinger, A. F. M. Heterotelechelic Polymers by Ring-Opening Metathesis and Regioselective Chain Transfer. *Angew. Chemie - Int. Ed.* **2018**, *57*, 914–917.
(53) Hilf, S.; Berger-Nicoletti, E.; Grubbs, R. H.; Kilbinger, A. F. M. Monofunctional Metathesis Polymers via Sacrificial Diblock Copolymers. *Angew. Chemie - Int. Ed.* **2006**, *45* (47), 8045–8048.
(54) Hanik, N.; Kilbinger, A. F. M. Narrowly Distributed Homotelechelic Polymers in 30 Minutes: Using Fast In Situ Pre-Functionalized ROMP Initiators. *J. Polym. Sci. Part A Polym. Chem.* **2013**, *51*, 4183–4190.
(55) Hilf, S.; Kilbinger, A. F. M. Heterotelechelic Ring-Opening Metathesis Polymers. *Macromolecules* **2010**, *43*, 208–212.
(56) Xia, Y.; Verduzco, R.; Grubbs, R. H.; Kornfield, J. A. Well-Defined Liquid Crystal Gels from Telechelic Polymers. *J. Am. Chem. Soc.* **2008**, *130* (5), 1735–1740.
(57) Ji, S.; Hoye, T. R.; Macosko, C. W. Controlled Synthesis of High Molecular Weight Telechelic Polybutadienes by Ring-Opening Metathesis Polymerization. *Macromolecules* **2004**, *37*, 5485–5489.
(58) Banik, S. M.; Monnot, B. L.; Weber, R. L.; Mahanthappa, M. K. ROMP-CT/NMP Synthesis of Multiblock Copolymers Containing Linear Poly(Ethylene) Segments. *Macromolecules* **2011**, *44* (18), 7141–7148.
(59) Gibson, V. C.; Okada, T. Synthesis of End-Functionalized Polynorbornenes and Polynorbornanes via Metathesis: Novel Macromonomers for Polycondensation Reactions. *Macromolecules* **2000**, *33*, 655–656.
(60) Katayama, H.; Fukuse, Y.; Nobuto, Y.; Akamatsu, K.; Ozawa, F. Ring-Opening Metathesis Polymerization Using Alkenyl Sulfides as Chain-Transfer Agents: Efficient Route to Unsymmetrical Poly(Norbornene)-Based Macroinitiators Bearing a Terminal Hydroxy Group. *Macromolecules* **2003**, *36*, 7020–7026.
(61) Öztürk, B. Ö.; Çalışgan, G.; Özer, H.; Şehitoğlu, S. K. Imidazole End-Functionalized Polycyclooctenes from Chain-Transfer Ring-Opening Metathesis Polymerization and Aminolysis Reactions. *React. Funct. Polym.* **2018**, *126*, 63–73.
(62) Scherman, O. A.; Ligthart, G. B. W. L.; Ohkawa, H.; Sijbesma, R. P.; Meijer, E. W. Olefin Metathesis and Quadruple Hydrogen Bonding: A Powerful Combination in Multistep Supramolecular Synthesis. *Proc. Natl. Acad. Sci.* **2006**, *103*, 11850–11855.
(63) Ding, L.; Xie, M.; Yang, D.; Song, C. Efficient Synthesis of Long-Chain Highly Branched Polymers via One-Pot Tandem Ring-Opening Metathesis Polymerization and Acyclic Diene Metathesis Polymerization. *Macromolecules* **2010**, *43*, 10336–10342.

(64) Higley, M. N.; Pollino, J. M.; Hollembeak, E.; Weck, M. A Modular Approach toward Block Copolymers. *Chem. - A Eur. J.* **2005**, *11* (10), 2946–2953.
(65) Yang, S. K.; Ambade, A. V; Weck, M. Supramolecular ABC Triblock Copolymers via 1-Pot, Orthogonal Self-Assembly. **2010**, *132* (5), 1637–1645.
(66) Pinazzi, C. P.; Campistron, I.; Croissandeau, M. C.; Reyx, D. Application of Metathesis Reactions to the Syntehsis of a,w-Functional Prepolymers. *J. Mol. Catal.* **1980**, *8*, 325–328.
(67) Pinazzi, C. P.; Guilmet, I.; Reyx, D. Metathese Entre Le Methyl-4-Octene et Le Cyclooctadiene-1,5. *Tetrahedron Lett.* **1976**, No. 13, 989–992.
(68) Schrock, R. R.; Yap, K. B.; Yang, D. C.; Sitzmann, H.; Sita, L. R.; Bazan, G. C. Evaluation of Cyclopentene-Based Chain-Transfer Agents for Living Ring-Opening Metathesis Polymerization. *Macromolecules* **1989**, *22*, 3191–3200.
(69) Crowe, W. E.; Mitchell, J. P.; Gibson, V. C.; Schrock, R. R. Chain-Transfer Agents for Living ROMP [Ring-Opening Metathesis Polymerization] Reactions of Norbornene. *Macromolecules* **1990**, *23*, 3534–3536.
(70) Cramail, H.; Fontanille, M.; Soum, A. Functional Oligomers of Norbornene. Part 1. Oligomerization by Ring-Opening Metathesis Polymerization in the Presence of Unsaturated Diesters. *J. Mol. Catal.* **1991**, *65*, 193–203.
(71) Heroguez, V.; Soum, A.; Fontanille, M. Functional Oligomerization of Dicyclopentadiene. *Polymer (Guildf).* **1992**, *33* (15), 3302–3304.
(72) Hillmyer, M. A.; Grubbs, R. H. Chain Transfer in the Ring-Opening Metathesis Polymerization of Cyclooctadiene Using Discrete Metal Alkylidenes. *Macromolecules* **1995**, *28*, 8662–8667.
(73) Katayama, H.; Urushima, H.; Ozawa, F. Ring-Opening Metathesis Polymerization of Norbornene in the Presence of Heteroatom-Substituted Vinylic Compounds: Highly Selective Synthesis of End Functionalized Poly(Norbornene)S. *Chemistry Letters*. 1999, pp 369–370.
(74) Matson, J. B.; Virgil, S. C.; Grubbs, R. H. Pulsed-Addition Ring-Opening Metathesis Polymerization: Catalyst-Economical Syntheses of Homopolymers and Block Copolymers. *J. Am. Chem. Soc.* **2009**, *131*, 3355–3362.
(75) Yasir, M.; Liu, P.; Tennie, I. K.; Kilbinger, A. F. M. Catalytic Living Ring-Opening Metathesis Polymerization with Grubbs' Second- and Thrid-Generation Cataylsts. *Nat. Chem.* **2019**, *11*, 488–494.
(76) Ogawa, K. A.; Goetz, A. E.; Boydston, A. J. Metal-Free Ring-Opening Metathesis Polymerization. *J. Am. Chem. Soc.* **2015**, *137*, 1400–1403.
(77) Goetz, A. E.; Pascual, L. M. M.; Dunford, D. G.; Ogawa, K. A.; Knorr, D. B.; Boydston, A. J. Expanded Functionality of Polymers Prepared Using Metal-Free Ring-Opening Metathesis Polymerization. *ACS Macro Lett.* **2016**, *5*, 579–582.
(78) Goetz, A. E.; Boydston, A. J. Metal-Free Preparation of Linear and Cross-Linked Polydicyclopentadiene. *J. Am. Chem. Soc.* **2015**, *137*, 7572–7575.
(79) Lu, P.; Alrashdi, N. M.; Boydston, A. J. Bidirectional Metal-Free ROMP from Difunctional Organic Initiators. *J. Polym. Sci. Part A Polym. Chem.* **2017**, *55*, 2977–2982.
(80) Martiny, M.; Steckhan, E.; Esch, T. Cycloaddition Reactions Initiated by Photochemically Excited Pyrylium Salts. *Chem. Ber.* **1993**, *126*, 1671–1682.

Chapter 3. Photo-Redox Mediated Ring-Opening Metathesis Polymerization Using a Continuous Flow Reactor

3.1 INTRODUCTION

Organic photochemistry is a highly researched field today due to a call for more sustainable and environmentally friendly techniques. The photon is considered "a green reagent that is absorbed without leaving a residue" allowing for waste reduction from other reagents.[1] Using light to initiate polymerizations has at least three distinct advantages over the metal-mediated counterparts; access to higher energy transformations, temporal control over the process, and spatial control over the reaction.[2] Due to these unique advantages, photo catalysis has begun seeing great progress in organic and polymer synthesis.[3] Despite the benefits and advances in the field, organic photochemistry has not been adopted widely among industry due to limitations in scale up. Major hazard concerns associated with the scale up of photochemistry include: the use of chemically inert, transparent but hazardous solvents, low quantum yields, significant energy demands for high energy light sources, and high dilutions needs for light penentration.[4]

Continuous flow techniques are a way to mediate the drawbacks associated with large batch reactors for photochemical reactions. Small channels holding reaction solution allow for easy light penetration and enhanced reaction speeds. The enhanced rates prevent unwanted side reactions due to overexposure to light sources. They also prevent the buildup of heat in the reaction mixture as a typical batch reactor would have. Processing of the products can be done simultaneously with the reaction which prevents accumulation of large quantities of flammable

solvent mixtures as well. Many polymerization methods and their photo- counterparts have been adapted for continuous flow techniques including free radical polymerizations, reversible addition-fragmentation chain transfer polymerizations, atom transfer radical polymerizations, ring-opening polymerizations, and Grignard metathesis polymerizations, but ring-opening metathesis polymerizations have yet to be expanded into this field.[87-97]

This account is the first example of ring-opening metathesis polymerization in continuous flow conditions. Typical metal-mediated ROMP has not been adapted to continuous flow conditions, as it would require either in-line mixing of the metal initiator and monomer or the production of a flow chamber with an anchored catalyst. Two different flow reactors were designed to test and optimize photo-ROMP in flow.

3.2 Results and Discussion

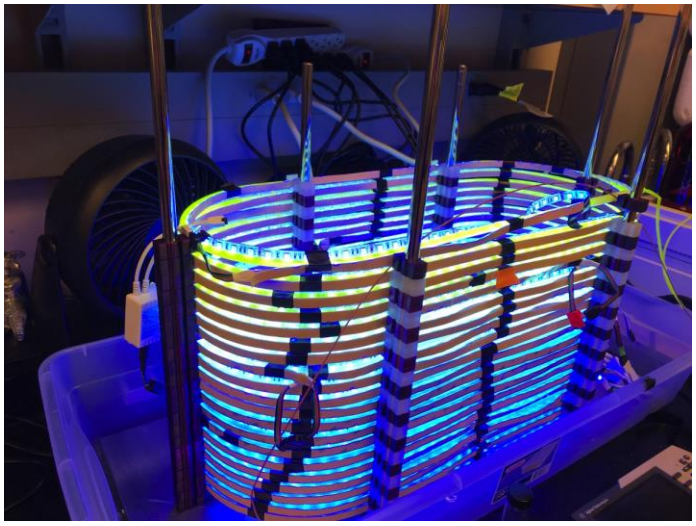

Figure 3.1 : First generation glass flow reactor

To make photo-ROMP more industrially relevant, we investigated methods to increase production from single batch experiments. Continuous-flow microreactors have been developed

for laboratory scale reactions, but industrially scale photo-chemical reactors are not commonplace. We first developed a glass flow reactor with a 589 mL capacity using blue LED light strips (**Figure 3.1**) and an Agilent 1100 isocratic pump. This flow reactor was designed using 30 meters of glass tubing, inner diameter 5 mm, wound into a continuous oval coil. After some trial and error, it was determined that a parking ramp style configuration was best for continuous flow that precluded the formation of air bubbles. To securely house the glass reactor, I designed a metal support base with metal rods and then designed and 3D printed support brackets that would hold the glass tubing in place. LED strips (purchased from Amazon) were attached directly to the glass tubing with electrical tape to maximize light penetration into the glass tubing. As optimization runs continued, I determined that the HPLC pump needed to be altered internally to allow for the reaction mixture to pass completely through without any clogging. The augmented design allowed for a production of 77 grams of oligomeric norbornene per hour and was used to produce 1 kilogram of oligomer for a collaboration with the Army Research Labs. This reactor is currently in use at Boydston Chemical Innovations.

The second-generation flow reactor (**Figure 3.2**) was designed to overcome the limitations of the first reactor, namely the fragility of the glass tubing, the corrosion and easily clogged internal features of the HPLC pump, and the inability to test the reaction as it was running. This reactor uses light-transparent, solvent-resistant PFA tubing (inner diameter of ½ inch) that can easily be replaced if broken, contaminated, or worn. The tubing is connected to a standard peg board using plastic zip ties to allow for easy replacement. An LED light panel was constructed by winding the LED strips around a center wooden panel. These LED strips allow for control over the light intensity and a range of wavelengths of light to allow for the use of other photocatalysts, as they are developed. These three panels were connected in a wooden frame with hinges that gives access

to the tubing for repairs while still allowing the tubing to be as close to the light panel as possible for increased light penetration. Another addition to this reactor is a series of Kynar ports (**Figure 3.3**) with silicone septa that enable process stream sampling and injections. With these ports, the reaction can be sampled at different retention times to determine the extent of the reaction, which allows for quicker adjustment of the flow rate to enhance conversions. They also allow for the potential to create block-copolymers through the addition of a new monomer while still in flow. This flow reactor is equipped with a peristaltic pump with PTFE tubing, which precludes the reaction mixture from being in contact with any of the internal pump fixtures, thus preventing corrosion and clogs. The pump also increases the maximum flow rate from 10 mL/min of the HPLC pump to over 1000 mL/min if needed. The second generation is much larger than the previous one with 1130 mL capacities per side and each side can be used in parallel to increase through-put, or in series to increase residence time.

Figure 3.2 : Second generation flow reactor including myself (5’ 5”) for scale.

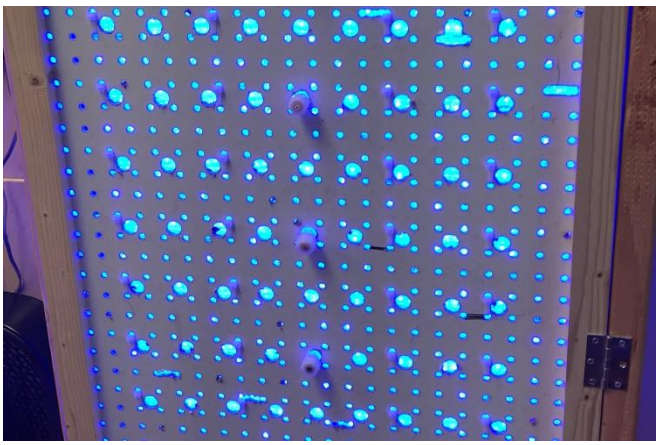

Figure 3.3: Close up of the Kynar sampling ports

Optimization of this flow reactor has so far increased the production yield to 2.6 kg of crude polymer per day. The first optimization to be investigated was the concentration of reaction mixture (**Table 3.1**). Our typical photo-ROMP polymerizations are run at 2.0 M, which results in a very thick viscous mixture once conversions have reached about 80%. We were concerned that this concentration would prevent sufficient mixing and diffusion within the reactor and limit the conversion, but we also wanted to balance the maximum amount of product with the minimum amount of other reagents. Studies showed that conversion stopped at 41% for the 2.0 M solution. Lowering the concentration to 0.5 and 1 M allowed for average conversion and 1 M will be used to move forward with more optimizations.

Table 3.1: Concentration optimization studies for continuous flow

NB : EPE : TPT	Flow Rate (mL/min)	Conc. (M)	Conversion (%)[a]	M_n (kDa)[b]
100 : 1 : 0.05	10	0.5	71	8.7
100 : 1 : 0.05	10	1	78	8.7
100 : 1 : 0.05	10	2	41	5.2

[a] % conversion of norbornene, determined by ^{1}H NMR spectroscopy. [b] Determined from crude, unprecipitated reaction aliquots: Number-average molecular weight (M_n) calculated from weight-average molecular weight determined by GPC analysis with MALLS.

3.3 EXPERIMENTAL

General Considerations: Dichloromethane (CH_2Cl_2) was dried over 4Å molecular sieves before use. ^1H and ^{13}C NMR spectra were recorded on a Bruker AVance 500 MHz spectrometer. Chemical shifts are reported in delta (δ) units, expressed in parts per million (ppm) downfield from tetramethylsilane using residual protio-solvent as an internal standard ($CDCl_3$, ^1H : 7.26 ppm and ^{13}C: 77.0 ppm; CD_2Cl_2, ^1H: 5.32 ppm and ^{13}C: 53.84 ppm). Data are reported as follows: chemical shift, multiplicity (s = singlet, d = doublet, dd = doublet of doublets, br = broad, m = multiplet), coupling constants,(Hz), and integration. Gel permeation chromatography (GPC) was performed using a GPC setup consisting of: a Shimadzu pump, 3 in-line columns, and Wyatt light scattering and refractive index detectors with tetrahydrofuran (THF) as the mobile phase. Number-average molecular weights (M_n) and weight-average molecular weights (M_w) were calculated from light scattering. The pyrylium tetrafluoroborate salt (**3**) was prepared according to literature procedure.[16] Norbornene (**1**) was vacuum-sublimed prior to use. All other reagents were obtained from commercial sources and used as received. The flow reactor was created using ½" ID x 9/16" OD x 1/32" Wall Versilon PFA tubing purchased from US Plastic Corp. The housing was constructed using pine 2x4s, composite pegboard, and hardware purchased from Home Depot. The LED panel was built using iHomy Flexible LED Strips (16.4 feet, 300 RGB LEDs with 5050 SMD chips) purchased from Amazon. The flow reactor stored full of clean, dried dichloromethane between runs. All polymerizations were run in a cold room at 4 ˚C.

General Procedure for Flow Reactor Trials

To a 2 L amber bottle was added **3** (0.4863 g, 0.001 mol, 0.05 equiv), **1** (188.3 g, 2 mol, 100 equiv), 2 L of CH_2Cl_2, and a magnetic stir bar. The solution was stirred for 1 hour to dissolve **3**. After 1

hour, **2** (2.21 mL, 0.02 mol, 1 equiv) was added. The bottle was taken to the cold room, stirred, and the pump tube was inserted into the bottle. The reaction mixture was pumped into the reactor with a flow rate of 10 mL/min. Samples were taken at each of the ports to monitor conversion using a syringe. After exiting the reactor, the solution was collected in a 4 L amber bottle. ^{1}H NMR matched previously reported data.[17]

3.4 Notes and References For Chapter 3

(1) Politano, F.; Oksdath-Mansilla, G. Light on the Horizon: Current Research and Future Perspectives in Flow Photochemistry. *Org. Process Res. Dev.* **2018**, *22*, 1045–1062.

(2) Chatani, S.; Kloxin, C. J.; Bowman, C. N. The Power of Light in Polymer Science : Photochemical Processes to Manipulate Polymer Formation, Structure, and Properties. *Polym. Chem.* **2014**, *5*, 2187–2201.

(3) Corrigan, N.; Shanmugam, S.; Xu, J.; Boyer, C. Photocatalysis in Organic and Polymer Synthesis. *Chem. Soc. Rev.* **2016**, *45*, 6165–6212.

(4) Oelgemöller, M. Green Photochemical Processes and Technologies for Research & Development, Scale-up and Chemical Production. *J. Chin. Chem. Soc.* **2014**, *61*, 743–748.

(5) Ye, P.; Cao, P. F.; Su, Z.; Advincula, R. Highly Efficient Reversible Addition–Fragmentation Chain-Transfer Polymerization in Ethanol/Water via Flow Chemistry. *Polym. Int.* **2017**, *66*, 1252–1258.

(6) Brocken, L.; Price, P. D.; Whittaker, J.; Baxendale, I. R. Continuous Flow Synthesis of Poly(Acrylic Acid) via Free Radical Polymerisation. *React. Chem. Eng.* **2017**, *2*, 662–668.

(7) Nyrop, J. L.; Soheili, A.; Xiang, R.; Meng, F.; Waldman, J. H.; Jia, X.; Parmar, R. G.; Thuronyi, B. W.; Williams, J. M.; Dimichele, L.; et al. Comparison of Flow and Batch Polymerization Processes for Production of Vinyl Ether Terpolymers for Use in the Delivery of SiRNA. *J. Polym. Sci. Part A Polym. Chem.* **2014**, *52*, 1119–1129.

(8) Wu, T.; Mei, Y.; Cabral, J. T.; Xu, C.; Beers, K. L. A New Synthetic Method for Controlled Polymerization Using a Microfluidic System. *J. Am. Chem. Soc.* **2004**, *126* (32), 9880–9881.

(9) Parida, D.; Serra, C. A.; Gómez, R. I.; Garg, D. K.; Hoarau, Y.; Bouquey, M.; Muller, R. Atom Transfer Radical Polymerization in Continuous Microflow: Effect of Process Parameters. *J. Flow Chem.* **2014**, *4*, 92–96.

(10) Parida, D.; Serra, C. A.; Garg, D. K.; Hoarau, Y.; Bally, F.; Muller, R.; Bouquey, M. Coil Flow Inversion as a Route to Control Polymerization in Microreactors. *Macromolecules* **2014**, *47*, 3282–3287.

(11) Parida, D.; Serra, C. A.; Garg, D. K.; Hoarau, Y.; Muller, R.; Bouquey, M. Flow Inversion: An Effective Means to Scale-up Controlled Radical Polymerization Tubular Microreactors. *Macromol. React. Eng.* **2014**, *8* (8), 597–603.

(12) Hornung, C. H.; Postma, A.; Saubern, S.; Chiefari, J. Sequential Flow Process for the Controlled Polymerisation and Thermolysis of RAFT-Synthesised Polymers. *Polymer*

(Guildf). **2014**, *55*, 1427–1435.
(13) Mahadevan, M.; Lee, S.; Dessiatoun, S. V.; Ohadi, M.; Al Hajri, E.; Choi, K. Y. Heterogeneous Catalytic Polymerization of Ethylene in Microtubular Reactor Systems. *Chem. Eng. Technol.* **2016**, *39*, 293–300.
(14) Kadhirvel, P.; Machado, C.; Freitas, A.; Oliveira, T.; Dias, R. C.; Costa, M. R. Molecular Imprinting in Hydrogels Using Reversible Addition-Fragmentation Chain Transfer Polymerization and Continuous Flow Micro-Reactor. *J. Chem. Technol. Biotechnol.* **2015**, *90*, 1552–1564.
(15) Natalello, A.; Morsbach, J.; Friedel, A.; Alkan, A.; Tonhauser, C.; Muller, A. H. E.; Frey, H. Living Anionic Polymerization in Continuous Flow: Facilitated Synthesis of High-Molecular Weight Poly(2-Vinylpyridine) and Polystyrene. *Org. Process Res. Dev.* **2014**, *18*, 1408–1412.
(16) Martiny, M.; Steckhan, E.; Esch, T. Cycloaddition Reactions Initiated by Photochemically Excited Pyrylium Salts. *Chem. Ber.* **1993**, *126*, 1671–1682.
(17) Ogawa, K. A.; Goetz, A. E.; Boydston, A. J. Metal-Free Ring-Opening Metathesis Polymerization. *J. Am. Chem. Soc.* **2015**, *137*, 1400–1403.

Chapter 4. The intrinsic mechanochemical reactivity of vinyl-addition polynorbornene[1]

4.1 INTRODUCTION

Mechanoresponsive polymers that undergo chemical transformations in response to mechanical stress have been explored in many applications including force sensing,[1,2] small molecule release,[3] catalyst activation,[4] self-reinforcing materials,[5] and autonomously healable systems.[6] Macromolecular scaffolds allow for efficient transduction of tensile forces into particular molecular-scale geometric strain that can guide mechanophore activation.[7–11] In most cases, a single mechanophore is incorporated into the center region of the polymer main chain, and the tensile load on the polymer backbone changes the potential energy surface of the mechanophore. Mechanical manipulation of the mechanophore potential energy surface is useful for analytical and physical organic studies to elucidate novel reactions that proceed via unique pathways inaccessible by, or impractical for, thermal or photochemical input. Mechanophore activation can also be used as a synthetic strategy to lower the thermal or photochemical energy input required for known reaction pathways such as ring-opening isomerization. However, due to the low concentration of mechanophores per polymer chain, activation can be difficult to quantify and large changes in bulk material properties are typically not observed. Additionally, small deviations in mechanophore location, relative to the center of the polymer chain, may also affect activation efficiency.[12]

[1] Reproduced with permission from Lee, D. C.; Kensy, V. K.; Maroon, C. R.; Long, B.K.; Boydston, A. J. "The intrinsic mechanochemical reactivity of vinyl-addition polynorbornene" *Angew. Chem. Int. Ed.*, **2019**, 58, 1-5. Copyright 2019 Angewandte Chemie International Edition.

The incorporation of multiple mechanophores along a single polymer chain overcomes these limitations and offers significant advantages with regard to effecting large changes in physicochemical properties. The increased concentration of mechanophores in the polymer chain can facilitate quantification of mechanophore activation, induce large changes in bulk material properties, and eliminate the need to precisely place a single mechanophore at the center of the polymer chain for activation. Examples of these custom designed multi-mechanophore polymers include those containing strained rings along the polymer backbone, such as cyclopropanes[5,13–15] and cyclobutanes[16], which have been shown to exhibit high mechanochemical activity.

Inspired by these polymechanophores, we hypothesized that simple, commercially available cyclopolymers containing inherently strained rings might also function as intrinsic polymechanophores. We were particularly interested in polynorbornenes made by vinyl-addition polymerization (VA-PNBs), which contain norbornane repeat units having an estimated strain energy of 73.4 kJ/mol.[17] In general, VA-PNBs are easy to synthesize, offer a wide variety of side chain functionality, and display desirable mechanical and chemical properties that have thus motivated their widespread application and industrial production.[18–22] To our knowledge, the mechanochemical reactivity of VA-PNBs has not been reported. Herein, we report our initial investigations into the intrinsic mechanochemical reactivity of VA-PNBs bearing trimethylsilyl (VA-TMS), triethoxysilyl (VA-TES), and hexyl (VA-Hex) side chains, as depicted in **Scheme 4.1**. We hypothesized that the mechanism of ring-opening olefination would be similar to that of other cyclopolymers containing strained rings,[23] and would proceed via homolytic bond scission within the norbornane rings to produce a diradical intermediate that could then propagate bidirectionally to form ROMP-type repeat units.

Scheme 4.1. Schematic representation of the mechanochemical ring-opening olefination of VA-PNB to produce ROMP-PNB units.

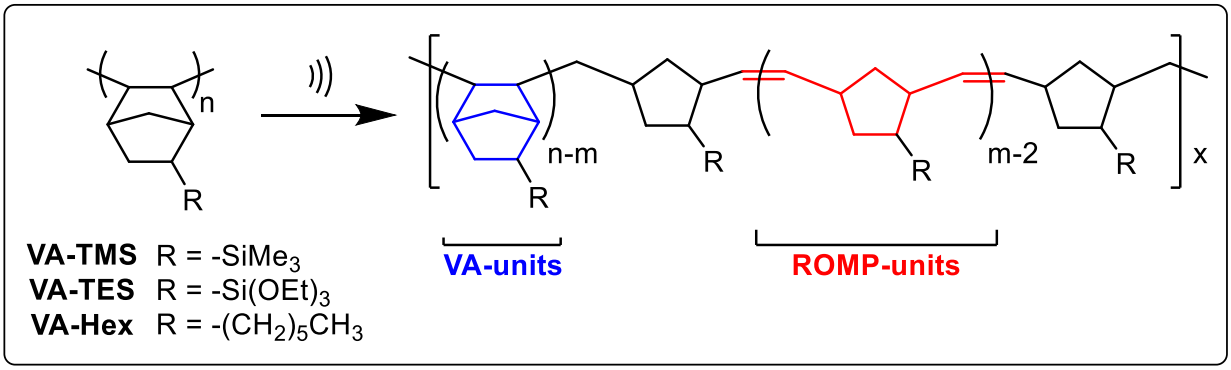

4.2 Results and Discussion

High molecular weight VA-PNBs were prepared using the catalyst, *trans*-[Ni(C_6F_5)$_2$($SbPh_3$)$_2$]. This catalyst has been shown to be highly active and applicable to a broad range of norbornyl-based monomers, including some with polar functionalities.[21] Gel permeation chromatography (GPC) analyses revealed number average molecular weight (M_n) values of 83.3, 219.7, and 185.0 kDa for the VA-TMS, VA-TES, and VA-Hex, respectively. To induce the mechanochemical activation of these polymers, sonication was conducted at 4-6 °C (monitored internally) with a calculated power density of 8.5 W/cm^2 in tetrahydrofuran (THF).

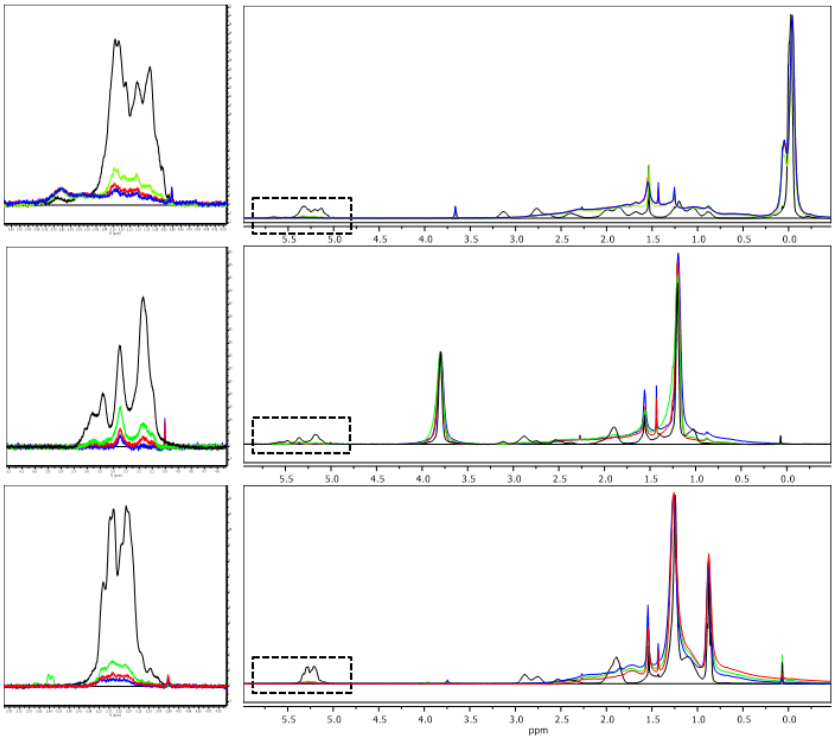

Figure 4.1 NMR spectra of VA-TMS **(top)**, VA-TES **(middle)**, VA-Hex **(bottom)** as a function of sonication time. t = 15 (blue), 30 (red), 240 (green) min of sonication are shown. ^{1}H NMR spectra of authentic ROMP-PNB prepared using Grubbs 2nd generation catalyst (black) is overlaid in each plot. Signal intensity of polymer side chain peaks are aligned for visual aid.

To quantify the mechanochemical activation of the VA-PNBs, aliquots were taken during sonication experiments and analyzed by ^{1}H NMR spectroscopy and GPC equipped with multi-angle laser light scattering detection. The vinylic protons arising from the ring-opening olefination (δ = 5 – 5.8 ppm) were integrated against protons on the polymer side chain, as well as against an internal standard. In all cases, the values were in good agreement and averaged to determine the percentage of repeat units having undergone ring-opening olefination (**Table 4.2**). Representative ^{1}H NMR spectra after sonication of each VA-PNB are shown in **Figure 4.1**. As an example, following the sonication of VA-TES, we observed ^{1}H NMR signals that were consistent with ring-opened PNB segments, and peak integrations indicating that ca. 25% of the repeat units were converted from the VA- to ROMP-type repeating units.

Each polymer displayed steadily increasing olefin content as a function of increasing sonication time, up to 60 min of sonication. Analysis of ^{1}H NMR spectra showed that up to 25% of the VA-TMS and VA-TES repeat units converted to ROMP-type repeat units within the first 60 min of sonication, while VA-Hex only achieved 10% olefination during the same sonication time (**Figure 4.2**). These differences may be due to the large impact that side chains substituents have on each polymer's solution-state conformation, relaxation dynamics, and possibly even on the mechanism for termination after ring opening. VA-TMS and VA-TES were used for further experiments due to their greater extent of olefination. To confirm that the mechanism of activation was mechanochemical and not thermal, VA-PNBs with lower molecular weights were synthesized and sonicated as negative controls (**Figure 4.5-Figure 4.8**). Sonication of the low molecular weight control VA-TES polymers did not result in any observable olefination or chain scission, which was expected as they are below the required degree of polymerization for sonication-induced cleavage.[24]

The NMR and GPC data suggest that ring-opening olefination via sonication was concurrent with chain scission, as is expected from sonication of macromolecules.[25] A representative series of GPC traces taken during sonication of VA-TES are shown in **Figure 4.3 (top)**. In general, we observed that M_n decreased with increasing sonication time and that molecular weight distributions remained monomodal, at least to the same qualitative extent as the pristine samples prior to sonication (**Table 4.5-Table 4.7**). This decrease in molecular weight as a function of sonication time is plotted in **Figure 4.3 (bottom)** for VA-TES (black) and VA-TMS (blue).

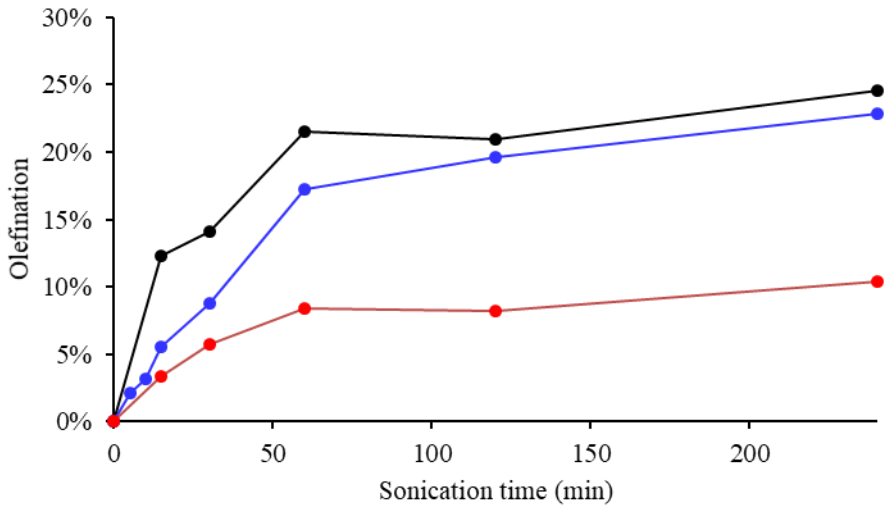

Figure 4.2 Olefination of VA-TMS (black), VA-TES (blue), VA-Hex (red) as determined by ^{1}H NMR analysis.

To better understand the competition between ring-opening olefination and secondary chain scission, the relative efficiencies of olefination compared to chain scission and the absolute rate constants for chain scission were determined. The relative efficiencies of olefination compared to chain scission were evaluated by calculating the number of olefination events achieved before the polymer M_n was halved (i.e., extent of olefination in one scission cycle). Scission cycle (φ) was plotted against olefination and the slope was determined using linear regression. The slope of this plot (φ_1) is a useful metric to characterize the efficiency of mechanochemical activation relative to chain scission because it normalizes olefination per scission cycle to compare across polymers with different side chains and experimental conditions with indeterminant variations.[15,26] Scission cycle (φ) was calculated using the equation $\varphi = \frac{\ln(M_{n,0}) - \ln(M_{n,t})}{\ln 2}$ in which $M_{n,0}$ is the M_n at t = 0 and $M_{n,t}$ is the M_n after a given time (t) of sonication (**Figure 4.4**). VA-TMS exhibits φ_1 = 1.0 olefination per scission cycle and VA-TES exhibits φ_1 = 0.56. For VA-TMS, with an initial degree of polymerization (DP_0) of 500 ($M_{n,0}$ = 83.3 kDa), φ_1 = 1.0 equates to olefination of 5 repeat units

per chain scission event. VA-TES, with DP_0 of 856 ($M_{n,0}$ 219.7 kDa), φ_1 = 0.56–equates to olefination of 4.8 repeat units per chain scission. That the two numbers are similar suggests that the two side chains play similar, or perhaps generally minimal, roles in the olefination of VA-PNBs under mechanochemical activation.

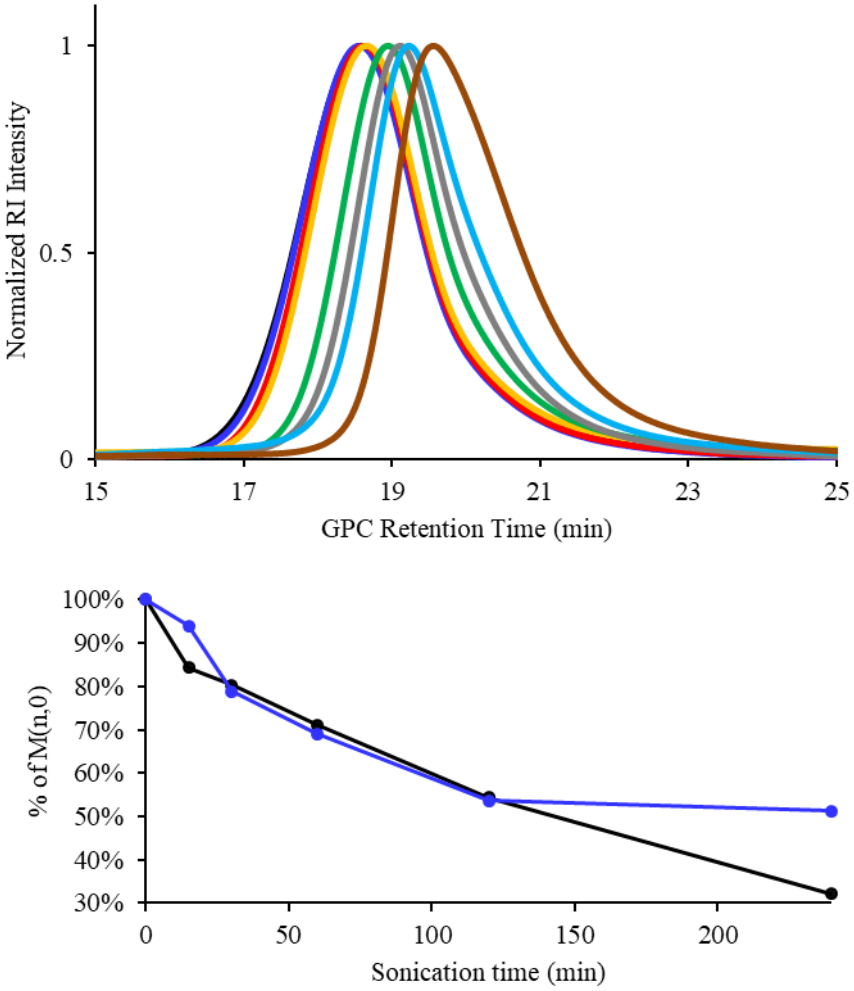

Figure 4.3 (top) GPC traces of VA-TES with increasing sonication time. GPC traces shift to lower retention times with longer sonication. Samples taken at 15, 30, 60, 120, 240 minutes of sonication on-time. **(bottom)** Percent of starting molecular weight ($M_{(n,0)}$) with increasing sonication time determined by GPC (VA-TES, black; VA-TMS, blue).

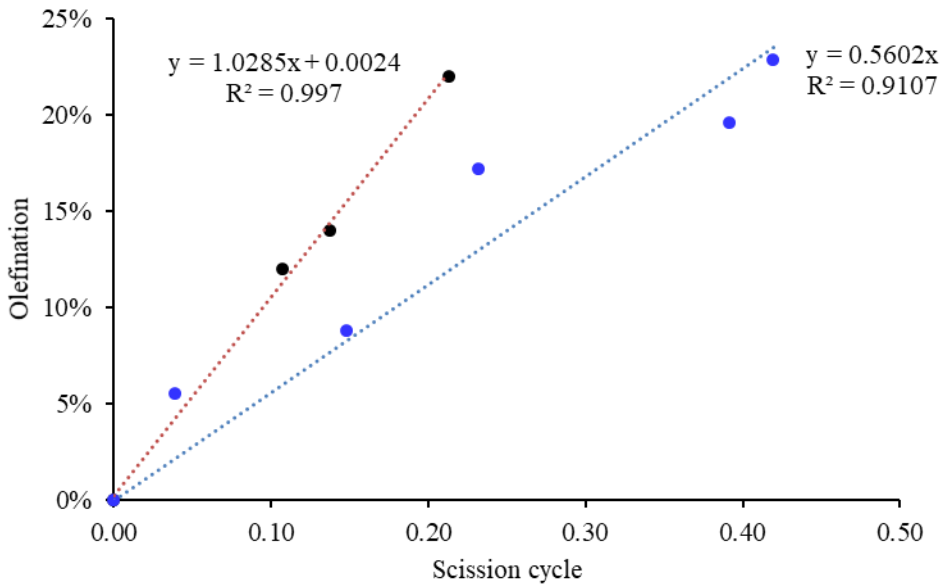

Figure 4.4 Olefination of VA-TMS (black), VA-TES (blue) plotted against scission cycle. Linear fit for olefination vs. scission cycle.

As a representative comparison, rate constants of chain scission ($k_{scission}$) for VA-TMS and authentic ROMP-TMS were determined using the method developed by Malholtra and used by Striegel (**Table 4.1**, **Figure 4.9**, **Figure 4.10**).[27–29] As a note, authentic ROMP-TES synthesized using Grubbs 2nd Generation catalyst could not be used due to its poor solubility in THF, which was used for sonication and GPC analysis. The data showed that VA-TMS has a higher $k_{scission}$ than ROMP-TMS, despite VA-TMS having two pertinent mechanisms by which mechanical loading can be compensated for (ring-opening and chain scission). We hypothesize that mechanochemical ring opening via bond homolysis has the highest rate constant (not determined here), followed by C_{sp3}-C_{sp3} bond scission between VA-TMS repeat units, and then C_{sp3}-C_{sp2} bond scission between VA-ROMP repeat units.

Table 4.1 Rate constants for chain scission during sonication.

Polymer	$k_{scission}$ ($*10^{-6}$ min^{-1})
VA-TMS	1.23
ROMP-TMS	0.726

As discussed earlier, a distinguishing feature of polymechanophores is their ability to induce large changes in bulk material properties in response to mechanical force. Even at low to moderate conversions, the quantity of mechanochemical transformations far exceeds the quantity of transformations achieved by high conversions of polymers containing only a single mechanophore. As a proof of concept, differential scanning calorimetry was used to determine changes in thermal properties of the sonicated VA-PNBs (**Figure 4.11-Figure 4.18**). Therein, sonicated VA-TES (26% olefination, M_n = 54.5 kDa) exhibited a T_g of 111 ºC, whereas pristine VA-TES (M_n = 219.7 kDa) did not exhibit any detectable T_g up to 350 ºC. For comparison, ROMP-TES made by Grubbs 2_{nd} Generation catalyst (M_n = 142.6 kDa) exhibits a T_g of 11 ºC. We initially hypothesized that the norbornane units close to the center of the chain would activate first and propagate outward, resulting in an ABA triblock structure consisting of VA-ROMP-VA repeat units before secondary scission. Assuming all olefination occurred in adjacent repeat units, the short homogenous ROMP blocks should show T_g values of ≤11 ºC according to Flory-Fox relationships of T_g and M_n.[30] The observed higher T_g of 111 ºC instead suggests that the mechanochemically activated regions close to the center of the polymer, where ring-opening olefination is most probable, is closer to a statistical copolymer of VA- and ROMP- type repeat units rather than a homogenous ROMP block, thus giving a T_g dominated by the VA-TES structure but reduced by sequence breaks. It is possible that termination or chain transfer events prevent the formation of homogenous blocks and the mechanism of these termination events merits future study.

4.3 CONCLUSION

In summary, we have demonstrated the intrinsic mechanochemical reactivity of VA-PNBs with conversions to ROMP-PNBs of up to 25% of the repeat units. More generally, the mechanochemical activation of polymers containing strained ring repeat units is a unique method to reconfigure the molecular structure of cyclopolymers. Due to their relative ease of synthesis, high mechanophore content, and their ability to undergo changes in thermal properties and chemical group functionality upon mechanochemical activation, we envision that VA-PNBs have significant potential as functional polymechanophores.

4.4 EXPERIMENTAL

General Considerations: All polymerizations were conducted using standard air-free Schlenk techniques or under an inert atmosphere using an MBraun glovebox unless otherwise noted. Monomers were degassed via freeze-pump-thaw (×3) and stored over 3 Å molecular sieves in a glovebox prior to use. Tetrahydrofuran (THF), toluene, and dichloromethane (DCM) were obtained from a solvent purification system. The catalyst *trans*-$[Ni(C_6F_5)_2(SbPh_3)_2]$ was synthesized according to literature and stored in the glovebox prior to use.[21,22] The catalyst $[Pd(allyl)Cl]_2$ and $AgSbf_6$ activator were purchased from Strem Chemical and used as received. The monomers 5-trimethylsilyl-2-norbornene, 5-triethoxysilyl-2-norbornene, and 5-hexyl-2-norbornene were prepared as previously reported.[21,22,31] All other reagents were obtained from commercial sources and used as received. ^{1}H NMR spectra were recorded on Bruker AVance 300 MHz or Varian 500 MHz spectrometers. Chemical shifts are reported in delta (δ) expressed as parts per million (ppm) downfield from tetramethylsilane using the residual protio-solvent as an internal standard ($CDCl_3$, ^{1}H: 7.26 ppm). Gel permeation chromatography (GPC) was

performed using an Agilent pump, 3 in-line columns, and Wyatt multiangle laser light scattering and refractive index detectors with THF as the mobile phase. Number average molecular weight (M_n) and weight average molecular weight (M_w) were calculated from refractive index data and light scattering using Astra software from Wyatt Technology Corp. Thermogravimetric analysis was performed on a TA TGA Q50 under nitrogen from room temperature to 600 °C at 10 °C/min. Differential Scanning Calorimetry (DSC) was performed on a TA DSC Q250 calorimeter or a Mettler Toledo DSC 3+ calorimeter under nitrogen at a heating rate of 10 °C/min and cooling rate of 5 °C/min. DSC measurements were taken up to 98% of the decomposition temperature as determined by TGA.

Synthetic procedures:

Synthesis of VA-TMS

In a 20 mL scintillation vial with stir bar, *trans*-[$Ni(C_6F_5)_2(SbPh_3)_2$] (5.5 mg, 5 μmol) was added to a solution of 5-trimethylsilyl-2-norbornene (0.83 g, 5 mmol) in DCM (2 mL) and stirred for 24 h. The reaction mixture was then diluted with additional DCM (8 mL) and added dropwise to stirred methanol (250 mL) causing precipitation of the polymer. The polymer was isolated via vacuum filtration, and then dried *in-vacuo* to constant weight to provide 0.30 g (37% yield) of the desired product. Lower molecular weight polymers used for sonochemical control experiments were made similarly but used the catalyst $[Pd(allyl)Cl]_2$ (1 equiv.) and activated with $AgSbF_6$ (2.1 equiv.) following literature procedures.[21]

Synthesis of VA-TES

In a 20 mL scintillation vial with stir bar, *trans*-[$Ni(C_6F_5)_2(SbPh_3)_2$] (5.5 mg, 5 μmol) was added to a solution of 5-triethoxysilyl-2-norbornene (1.28 g, 5 mmol) in DCM (2 mL) and stirred for 24 h. The reaction mixture was then diluted with additional DCM (8 mL) and added dropwise to

stirred methanol (250 mL) causing precipitation of the polymer. The polymer was isolated via vacuum filtration, and then dried *in-vacuo* to constant weight to provide 0.91 g (71% yield) of the desired product.

Synthesis of VA-Hex

In a 20 mL scintillation vial with stir bar, *trans*-[$Ni(C_6F_5)_2(SbPh_3)_2$] (5.5 mg, 5 µmol) was added to a solution of 5-hexyl-2-norbornene (0.89 g, 5 mmol) in DCM (2 mL) and stirred for 24 h. The reaction mixture was then diluted with additional DCM (8 mL) and added dropwise to stirred methanol (250 mL) causing precipitation of the polymer. The polymer was isolated via vacuum filtration, and then dried *in-vacuo* to constant weight to provide 0.20 g (22% yield) of the desired product.

Synthesis of ROMP-TMS

In a 20 mL scintillation vial with stir bar, Grubbs II catalyst (7.8 mg, 0.009 mmol) was dissolved in THF (12 mL). A solution of monomer (1.005 g, 6.01 mmol) in THF (1.1 mL) was added to the solution of Grubbs II. The solution was then stirred at room temperature for 1.5 h. Conversion was monitored by ^1H NMR spectroscopy of reaction aliquots and determined by comparison of peak areas corresponding to polymeric olefin signals versus those of monomer. After 1.5 h, the polymerization was terminated by addition of ca. 1 mL of ethyl vinyl ether, followed by stirring for 5 min. The reaction volume was then reduced under vacuum and the remaining solution was added dropwise into an excess of ethanol, causing precipitation of the product polymer. The polymer was collected via vacuum filtration and then dried under vacuum to provide 864 mg (86% yield) of the desired product.

Synthesis of ROMP-TES

To a flame dried round bottom flask were added a stir bar and Grubbs II catalyst (3.0 mg, 0.004 mmol). The flask was then sealed with a rubber septum and purged with N_2 for 10 min. Then, dry, air-free toluene (4 mL) was added via syringe. A solution of monomer (69.11 μL, 0.27 mmol) in toluene (1 mL) was prepared in a dry, N_2-purged vial fitted with a rubber septum. The monomer solution was then added to the round bottom flask containing the solution of Grubbs II via syringe. The solution was stirred at room temperature for 20 min. Conversions were determined by ^{1}H NMR analysis. The polymerization was terminated by addition of ca. 1 mL of ethyl vinyl ether, followed by stirring for 5 min. The reaction volume was then reduced under vacuum and the remaining solution was added dropwise into an excess of ethanol, causing precipitation of the product polymer. The polymer was collected via vacuum filtration and then dried under vacuum to provide 47.1 mg (68% yield) of the desired product.

Synthesis of ROMP-Hex

In a 20 mL scintillation vial with stir bar, Grubbs II catalyst (3.4 mg, 0.004 mmol) was dissolved in THF (5.7 mL). A solution of monomer (504.7 mg, 2.84 mmol) in THF (0.5 mL) was added to the solution of Grubbs II via syringe. The solution was stirred at room temperature for 3 h. Conversion was monitored by ^{1}H NMR spectroscopy of reaction aliquots and determined by comparison of peak areas corresponding to polymeric olefin signals versus those of monomer. The polymerization was terminated by addition of ca. 1 mL of ethyl vinyl ether, followed by stirring for 5 min. The reaction volume was then reduced under vacuum and the remaining solution was added dropwise into an excess of methanol, causing precipitation of the product polymer. The polymer was collected via vacuum filtration and then dried under vacuum to provide 379 mg (75% yield) of the desired product.

Determination of dn/dc of ROMP-TES due to solubility issues.

A small amount of ROMP-TES was dissolved in THF for at least 8 h. The solution was filtered twice through a 45 μm filter into a tared vial to remove undissolved polymer. A small amount of the filtered solution was used for GPC. The residual solution was used to determine the concentration of the GPC sample by the following. The mass of the resulting polymer solution was determined by subtracting the vial tare weight. The solvent was removed in vacuo and the residual mass was assumed to be polymer mass. The polymer weight was then subtracted from the weight of the residual solution to determine the amount of THF. The concentration of the GPC sample (mg/mL) was determined by dividing the polymer mass by the THF volume.

Sonication Calibration

Calorimetry was used to calibrate the ultrasonic intensity produced by the probe according to literature procedures.[32] A small Dewar flask was filled with exactly 250 mL of Millipore water and the ultrasound probe was submerged approximately 1.25 cm into the water. The exact height was marked for reproducibility. A thermocouple was then introduced into the water. The amplitude on the processor was set to 20%, the initial temperature was recorded, and sonication was started. The temperature of the water was recorded every 15 s for 3 min, and these values were plotted against time to determine $\Delta T/\Delta t$ by the slope of the line. This procedure was repeated for amplitudes of 30, 40, 50, 60, 70, and 80%. The heat due to ultrasonication in J/s, or W, was determined from the following equation: $q = c \cdot m \cdot \Delta temp/\Delta time$, where c = specific heat ($Jg^{-1}°C^{-1}$), m = mass (g), and $\Delta temp/\Delta time$ has units °C/s. The values used were c= specific heat of water = 4.179 $Jg^{-1}°C^{-1}$, mass of water = 250 g, and $\Delta T/\Delta t$ = the slope of the line. The resulting value, q, was divided by the surface area of the horn tip (1.27 cm^2) to find the W/cm^2.

Finally, the power produced was plotted against the percentage of amplitude to generate the calibration curves.

Sonication Procedure

A Suslick flask was oven dried and then attached to the sonicator probe. The arms of the flask were sealed with rubber septa and then the flask was purged with dry N_2. VA-PNB (50 mg) was added under N_2 atmosphere and the sample cell was flushed for 20 min with N_2. Dry THF (10 mL) was then added via syringe. The Suslick flask was then fitted with a balloon filled with N_2 to maintain positive nitrogen pressure. The polymer solution was left for 30 min to facilitate dissolution of the polymer. The polymer solution was then moved to a cold room maintained at 4-6 ℃ and stood for 30 min to allow for temperature equilibration. Polymers were sonicated at 8.5 W/cm^2 with a duty cycles of 1 s on, 9 s off, for a total of 240 min of sonication on-time.

Quantifying conversion of VA repeat units to ROMP repeat units by ^{1}H NMR analysis

Aliquots were taken at 5, 10, 15, 30, 60, 120, 240 min time intervals. At each time point, an aliquot (0.5 mL of polymer solution) was taken with a needle that was oven dried and N_2 purged. The 0.5 mL solution was put under high vacuum for 16 h to remove solvent.

Conversion from VA- to ROMP-type repeat units was determined by two methods and the values averaged. First, the olefin signals in the polymer were integrated against unique proton signals in the polymer side chain as they were assumed to be unaffected by the sonication. For VA-TMS, the olefin peaks were integrated against the protons in the trimethylsilyl group (-Si-***CH$_3$***, δ = -0.2 – 0.2 ppm); for VA-TES, against the triethoxysilyl group (-Si-O-***CH$_2$***-CH_3, δ = 3.6 – 4 ppm); for VA-Hex, against the end of the hexyl group (-***CH$_3$***, δ = 0.75 –1 ppm).

For the second method, a stock solution of 1,4-dicyanobenzene in $CDCl_3$ (106.9 mg in 100 mL) was used for ^1H NMR spectroscopy. A known mass of sonicated polymer was dissolved in this stock solution for NMR analysis. The vinyl proton signals ($\delta = 5 – 5.8$ ppm) were integrated against the 1,4-dicyanobenzene peak ($\delta = 7.8$ ppm) to determine conversion to ROMP polymer. The same mass of VA-PNB and ROMP-PNB were dissolved in the stock solution to determine 0% olefination and 100% olefination, respectively.

Table 4.2 Olefination of VA-TMS

	Sonication time (min)	Olefination determined by: Side chain	Internal standard	Average
VA-TMS	15	11.0%	13.5%	12.3%
	30	12.7%	15.6%	14.2%
	60	17.8%	25.3%	21.5%
	120	18.0%	23.9%	21.0%
	240	19.3%	29.8%	24.5%

Table 4.3 Olefination of VA-TES

	Sonication time (min)	Olefination determined by: Side chain	Internal Standard	Average
VA-TES	5	1.6%	2.7%	2.1%
	10	3.2%	3.2%	3.2%
	15	6.5%	4.6%	5.5%
	30	8.7%	8.9%	8.8%
	60	18.0%	16.4%	17.2%
	120	20.4%	18.8%	19.6%
	240	24.5%	21.2%	22.8%

Table 4.4 Olefination of VA-Hex

	Sonication time (min)	Olefination determined by: Side chain	Internal Standard	Average
VA-Hex	15	2.7%	4.1%	3.4%
	30	4.6%	6.9%	5.7%
	60	6.7%	10.1%	8.4%
	120	6.4%	9.9%	8.2%
	240	8.3%	12.5%	10.4%

Sonication and analysis of low molecular weight control VA-TES

Lower molecular weight VA-TES was sonicated as a negative control to determine that the mechanism of activation was mechanochemical and not thermal. Sonication of 11 kDa VA-TES and 51 kDa VA-TES showed no olefination and no chain scission.

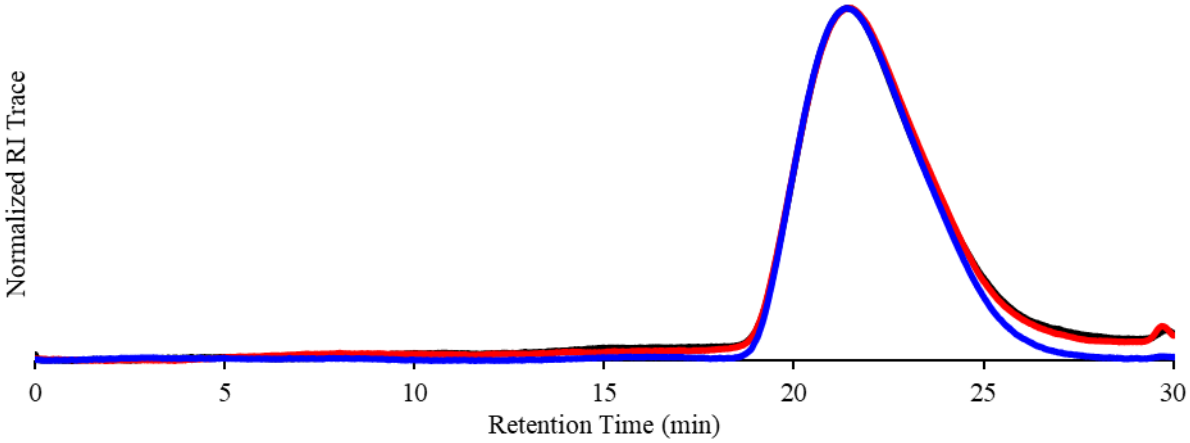

Figure 4.5 Stacked GPC traces of pristine 11 kDA VA-TES (black), VA-TES sonicated for 2 h (red), and VA-TES sonicated for 4 h (blue).

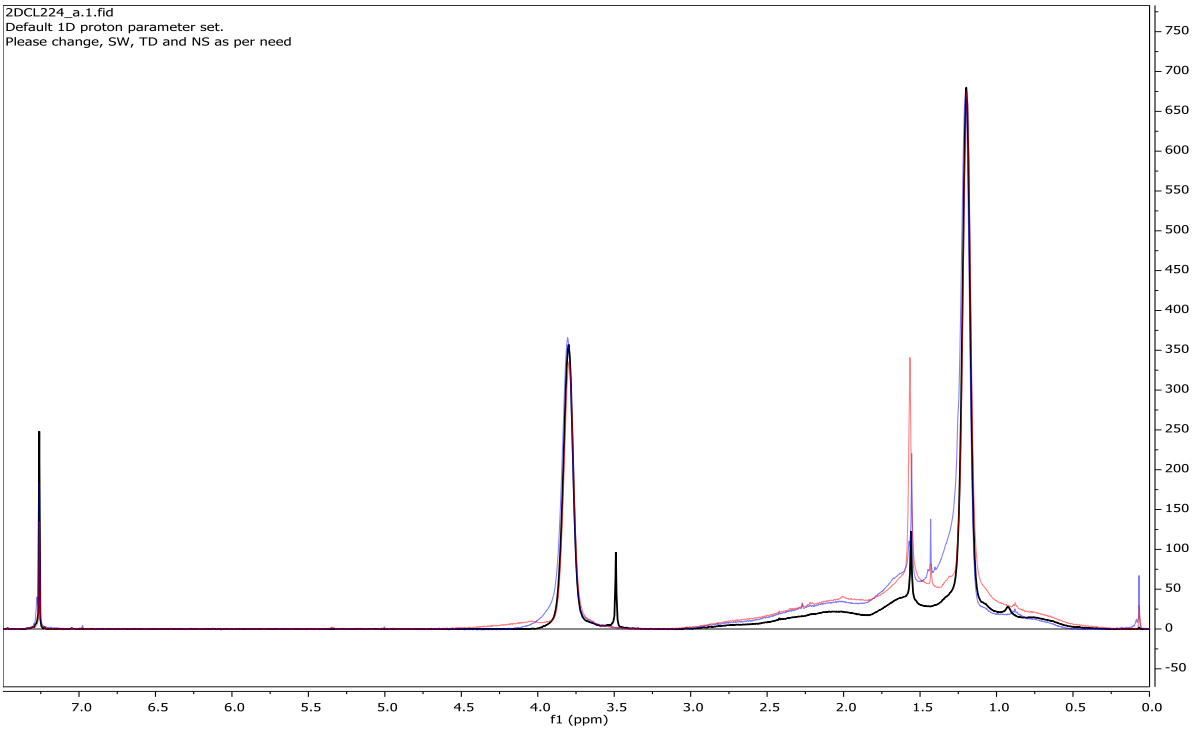

Figure 4.6 Stacked ^{1}H NMR spectra of pristine 11 kDA VA-TES (black), VA-TES sonicated for 2 h (red), and VA-TES sonicated for 4 h (blue).

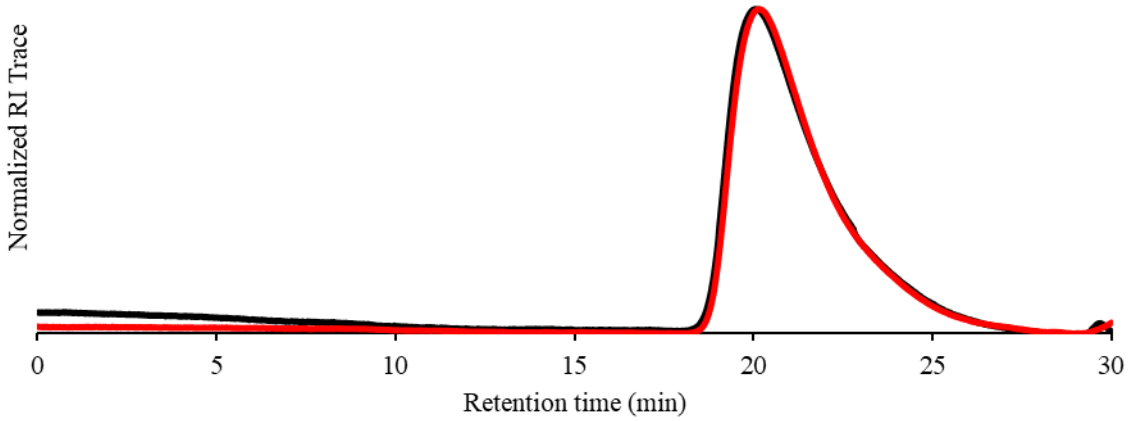

Figure 4.7 Stacked GPC traces spectra of pristine 51 kDA VA-TES (black) and VA-TES sonicated for 4 h (red).

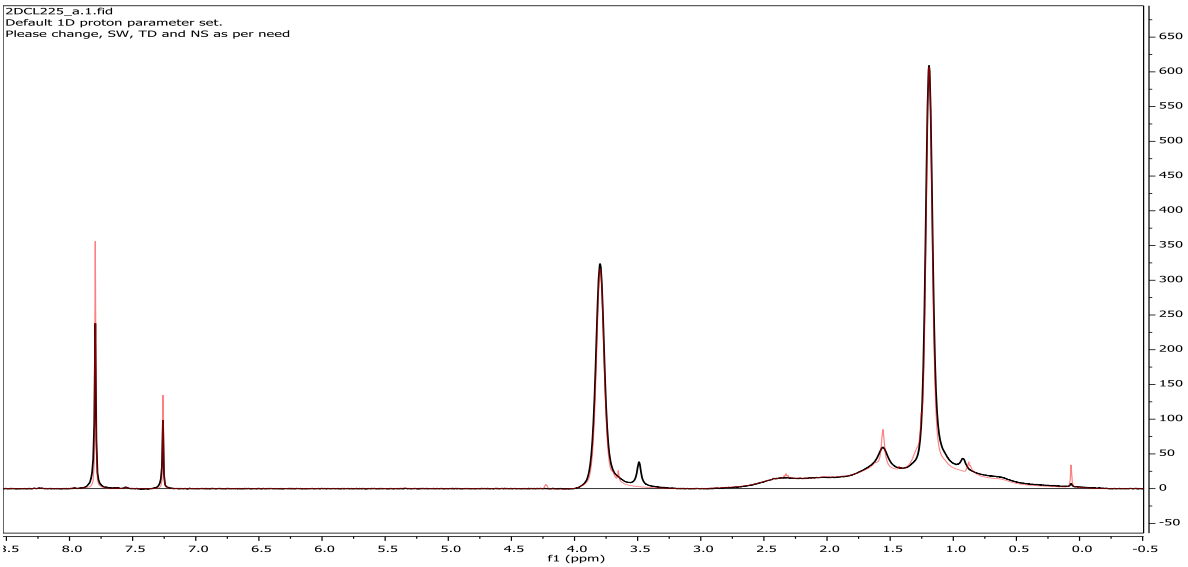

Figure 4.8 Stacked ^{1}H NMR spectra of pristine 51 kDA VA-TES (black) and VA-TES sonicated for 4 h (red).

Changes in molecular weight during sonication

Table 4.5 Molecular weight of VA-TMS

	Sonication time (min)	M_w (kDa)	M_n (kDa)	*Đ*
VA-TMS	0	123	83.3	1.6
	15	97.3	70.2	1.4
	30	87.8	66.9	1.3
	60	73.4	59.3	1.2
	120	57.8	45.3	1.3
	240	44.0	26.8	1.6

Table 4.6 Molecular weight of ROMP-TMS

	Sonication time (min)	M_w (kDa)	M_n (kDa)	*Đ*
ROMP-TMS	0	420.0	185.0	2.3
	15	130.1	87.4	1.3
	30	86.2	62.3	1.3
	60	65.5	48.6	1.3
	120	49.3	40.1	1.3
	240	32.1	24.4	1.3

Table 4.7 Molecular weight of VA-TES

	Sonication time (min)	M_w (kDa)	M_n (kDa)	*Đ*
VA-TES	0	319	219.7	1.5
	15	278.1	206.5	1.3
	30	221.1	173.4	1.3
	60	202.6	151.8	1.3
	120	149.8	117.7	1.3
	240	142.4	112.5	1.3

Determining $k_{scission}$

Table 4.8 Determination of $k_{scission}$ for VA-TMS

	Sonication time (min)	M_n (kDa)	$1/M_n$
VA-TMS	0	83.3	0.012004802
	15	70.2	0.014245014
	30	66.9	0.014947683
	60	59.3	0.016863406
	120	45.3	0.022075055
	240	26.8	0.037313433

Table 4.9 Determination of $k_{scission}$ for VA-TMS

Slope of line	$k_{scission}$ = slope/starting M_n
0.0001026	1.23169E-06

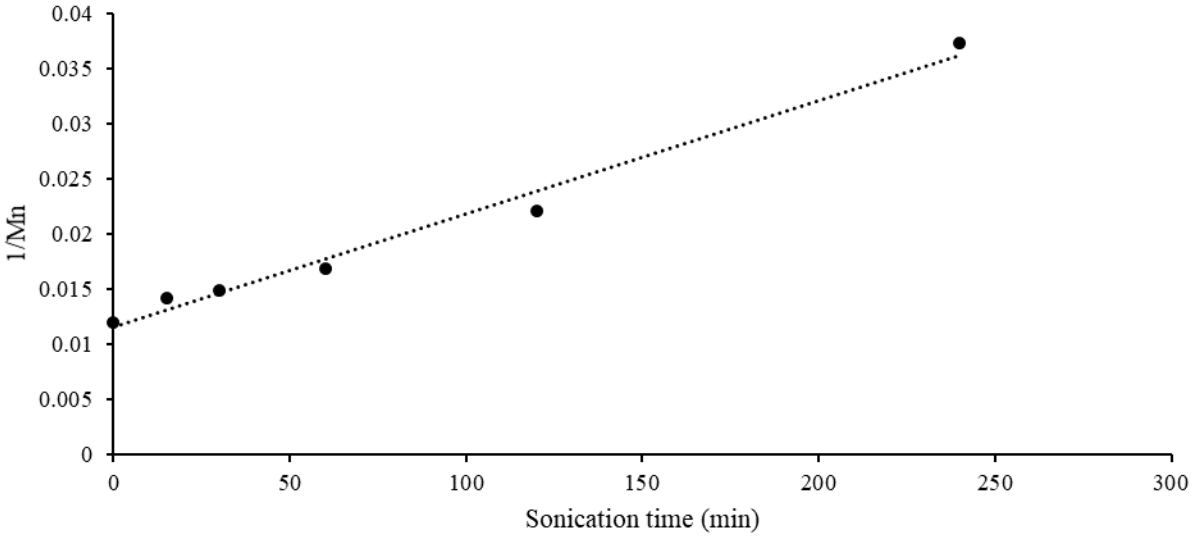

Figure 4.9 Plot of $1/M_n$ vs sonication time to determine the chain scission constant for VA-TMS.

Table 4.10 Determination of $k_{scission}$ for ROMP-TMS

	Sonication time (min)	M_n (kDa)	$1/M_n$
ROMP-TMS	0	185	0.005405405
	15	87.4	0.011441648
	30	62.3	0.016051364
	60	48.6	0.020576132
	120	40.1	0.024937656
	240	24.4	0.040983607

Table 4.11 Determination of $k_{scission}$ for ROMP-TMS

Slope of line	$k_{scission}$ = slope/starting M_n
0.0001229	7.25946E-07

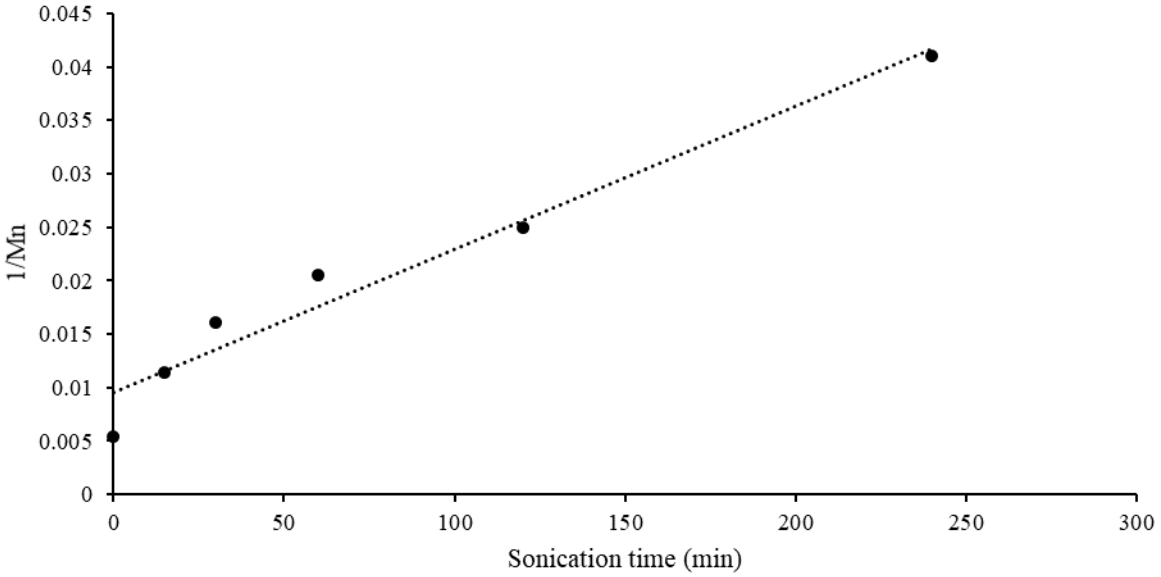

Figure 4.10 Plot of $1/M_n$ vs sonication time to determine the chain scission constant for ROMP-TMS.

Thermal data

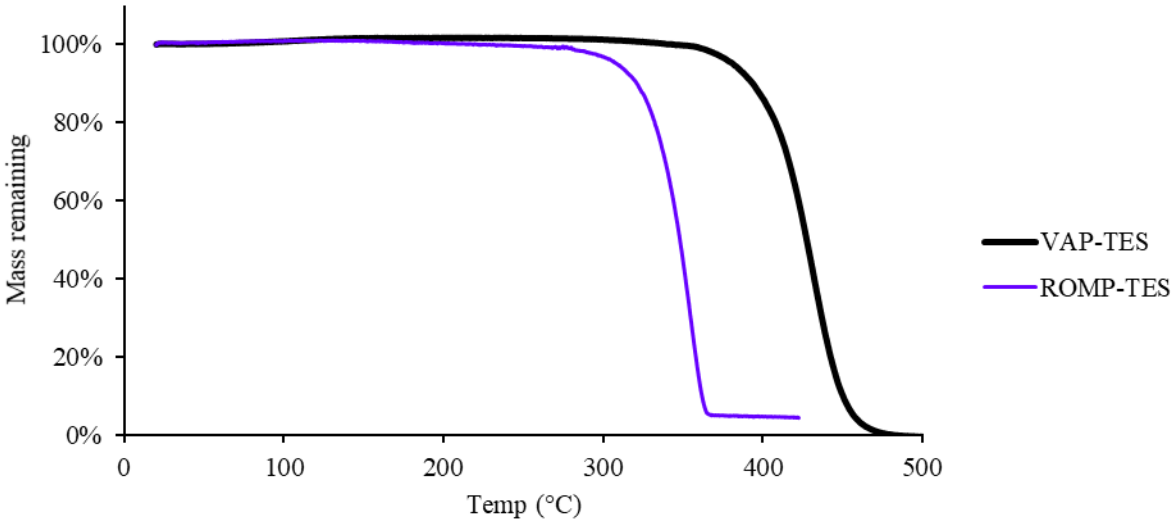

Figure 4.11 Thermogravimetric analysis for VA-TES and ROMP -TES.

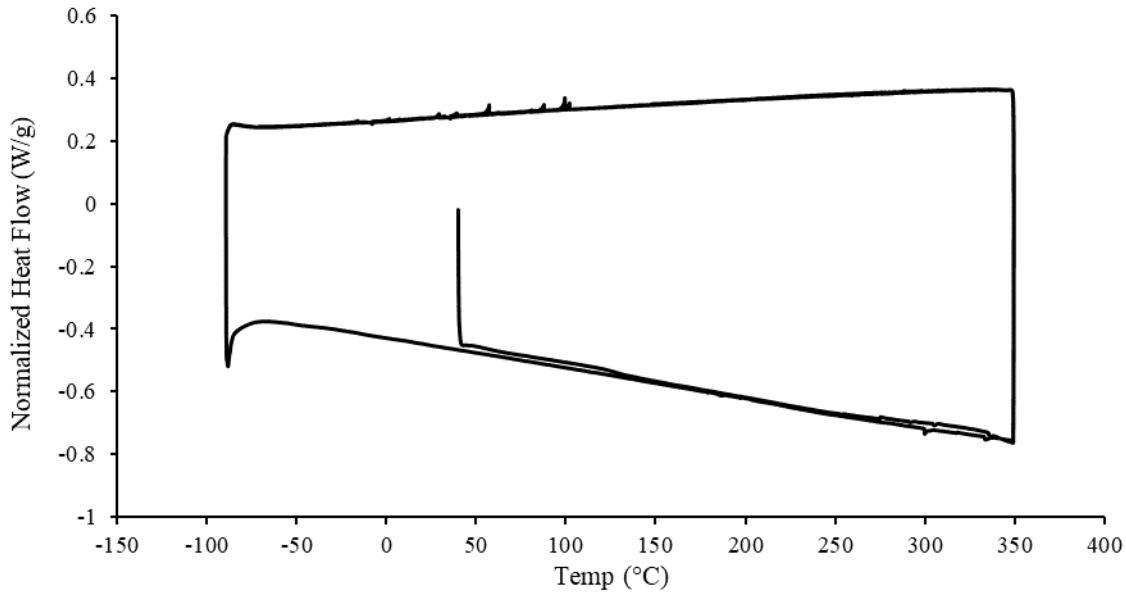

Figure 4.12 Differential scanning calorimetry for pristine VA-TES.

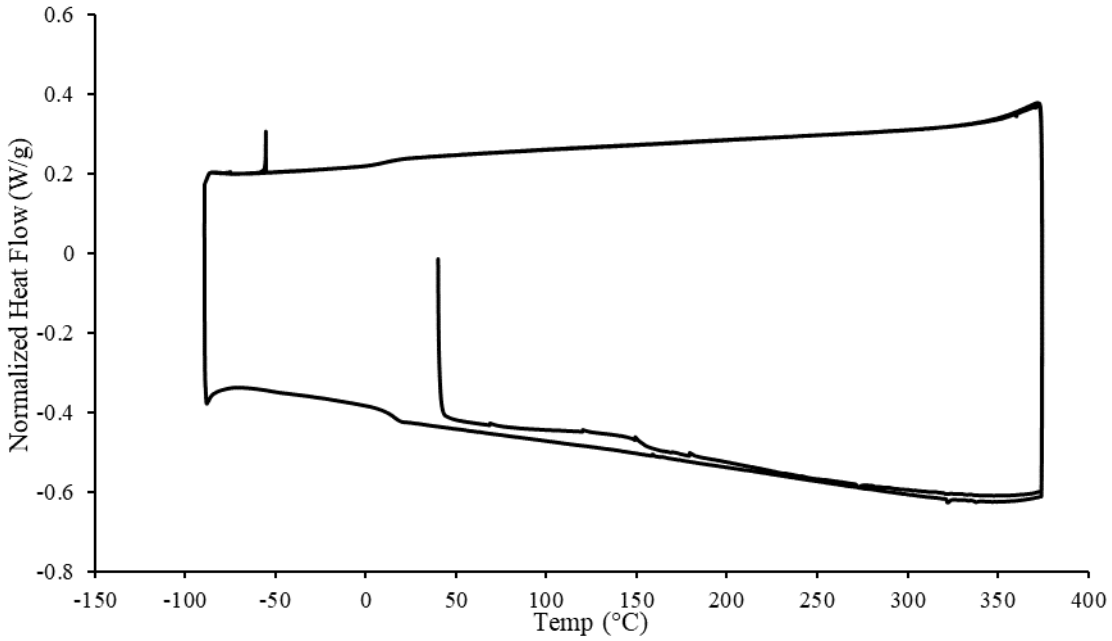

Figure 4.13 Differential scanning calorimetry for ROMP-TES.

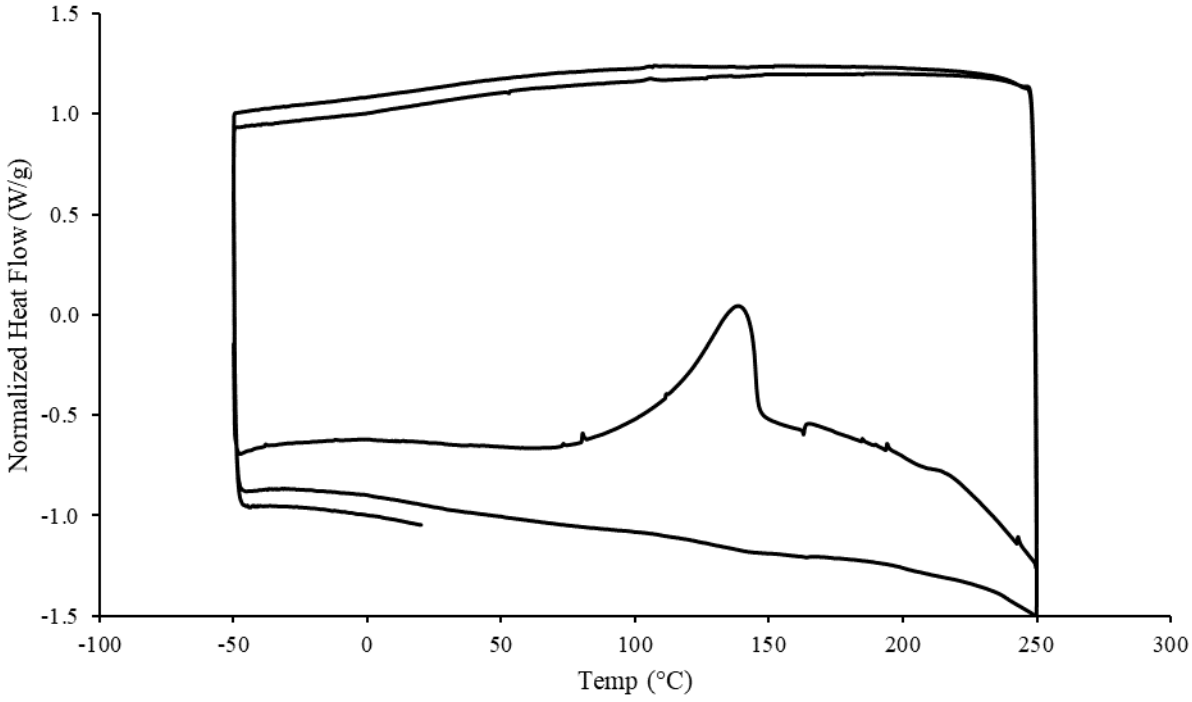

Figure 4.14 Differential scanning calorimetry for sonicated VA-TES.

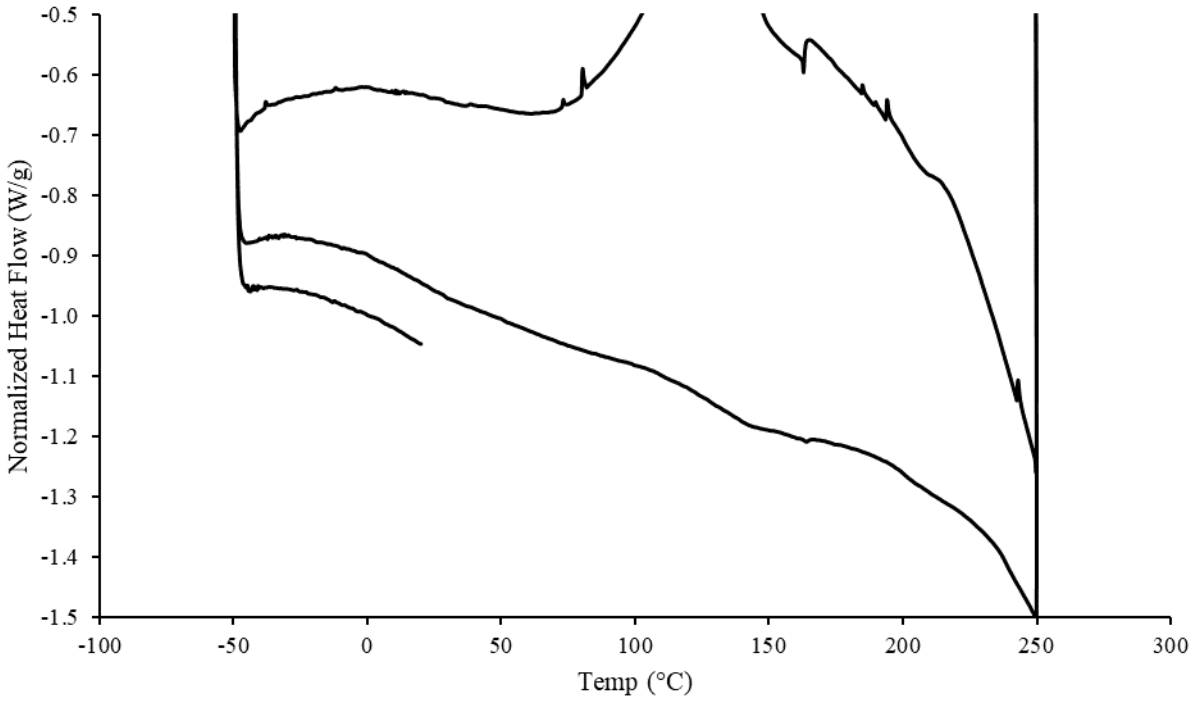

Figure 4.15 Differential scanning calorimetry for sonicated VA-TES zoomed in to display T_g.

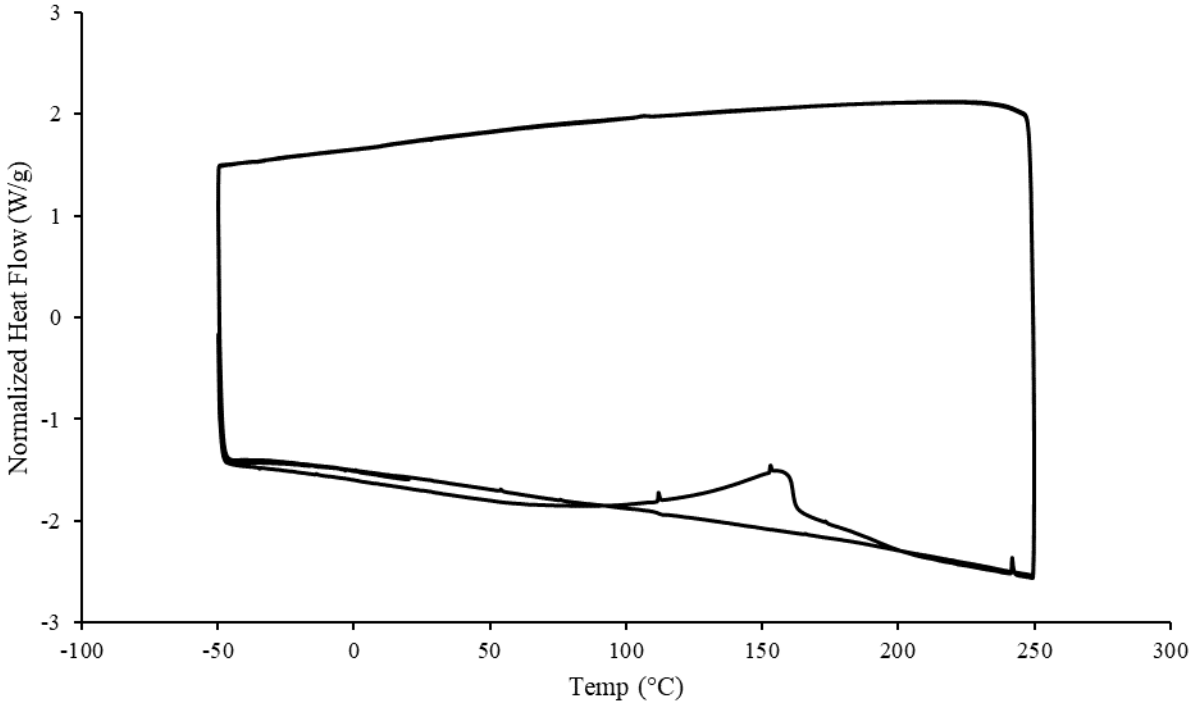

Figure 4.16 Second differential scanning calorimetry for sonicated VA-TES.

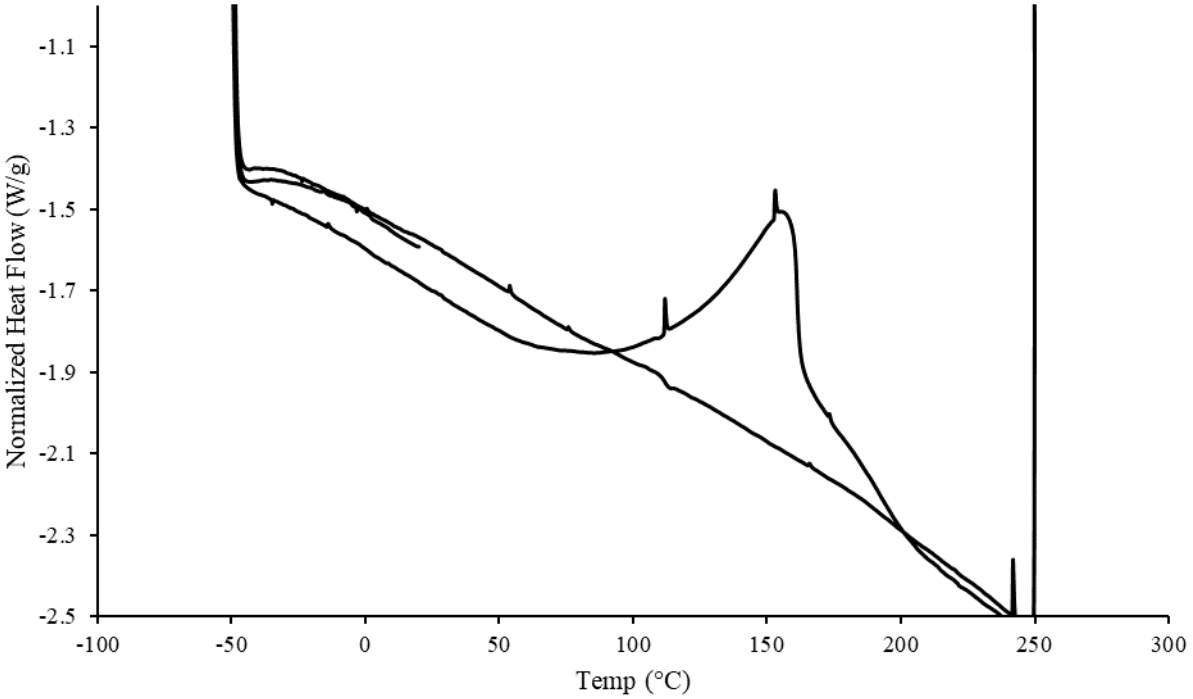

Figure 4.17 Second differential scanning calorimetry for sonicated VA-TES zoomed in to display T_g.

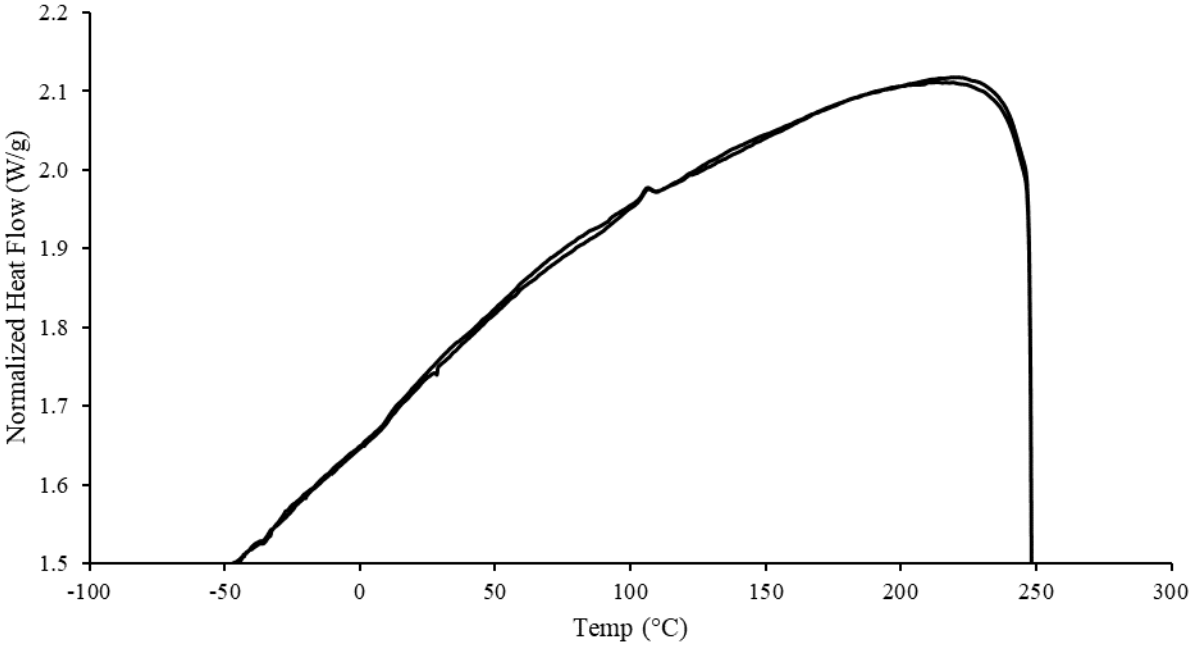

Figure 4.18 Second differential scanning calorimetry for sonicated VA-TES zoomed in to display T_g.

4.5 NOTES AND REFERENCES FOR CHAPTER 4

(1) Gossweiler, G. R.; Hewage, G. B.; Soriano, G.; Wang, Q.; Welshofer, G. W.; Zhao, X.; Craig, S. L. Mechanochemical Activation of Covalent Bonds in Polymers with Full and Repeatable Macroscopic Shape Recovery. *ACS Macro Lett.* **2014**, *3*, 216–219.

(2) Chen, Y.; Spiering, a. J. H.; Karthikeyan, S.; Peters, G. W. M.; Meijer, E. W.; Sijbesma, R. P. Mechanically Induced Chemiluminescence from Polymers Incorporating a 1,2-Dioxetane Unit in the Main Chain. *Nat. Chem.* **2012**, *4*, 559–562.

(3) Cao, B.; Boechler, N.; Boydston, A. J. Additive Manufacturing with a Flex Activated Mechanophore for Nondestructive Assessment of Mechanochemical Reactivity in Complex Object Geometries. *Polymer (Guildf).* **2018**, *152*, 4–8.

(4) Piermattei, A.; Karthikeyan, S.; Sijbesma, R. P. Activating Catalysts with Mechanical Force. *Nat Chem* **2009**, *1* (2), 133–137.

(5) Ramirez, A. L. B.; Kean, Z. S.; Orlicki, J. A.; Champhekar, M.; Elsakr, S. M.; Krause, W. E.; Craig, S. L. Mechanochemical Strengthening of a Synthetic Polymer in Response to Typically Destructive Shear Forces. *Nat. Chem.* **2013**, *5* (9), 757–761.

(6) Balkenende, D. W. R.; Coulibaly, S.; Balog, S.; Simon, Y. C.; Fiore, G. L.; Weder, C. Mechanochemistry with Metallosupramolecular Polymers. *J. Am. Chem. Soc.* **2014**, *136*, 10493–10498.

(7) Li, J.; Nagamani, C.; Moore, J. S.; Moore, S. Polymer Mechanochemistry: From Destructive to Productive. *Acc. Chem. Res.* **2015**, *48*, 2181–2190.

(8) Larsen, M. B.; Boydston, A. J. "Flex-Activated" Mechanophores: Using Polymer Mechanochemistry to Direct Bond Bending Activation. *J. Am. Chem. Soc.* **2013**, *135*, 8189–8192.

(9) Bowser, B. H.; Craig, S. L. Empowering Mechanochemistry with Multi-Mechanophore Polymer Architectures. *Polym. Chem.* **2018**, *9*, 3583–3593.

(10) Kryger, M. J.; Munaretto, A. M.; Moore, J. S. Structure-Mechanochemical Activity Relationships for Cyclobutane Mechanophores. *J. Am. Chem. Soc.* **2011**, *133*, 18992–18998.

(11) Ong, M. T.; Leiding, J.; Tao, H.; Virshup, A. M.; Martı, T. J. First Principles Dynamics and Minimum Energy Pathways for Mechanochemical Ring Opening of Cyclobutene. **2009**, *9* (1), 6377–6379.

(12) Kean, Z. S.; Gossweiler, G. R.; Kouznetsova, T. B.; Hewage, G. B.; Craig, S. L. A Coumarin Dimer Probe of Mechanochemical Scission Efficiency in the Sonochemical Activation of Chain-Centered Mechanophore Polymers. *Chem. Commun.* **2015**, *51*, 9157–9160.

(13) Lenhardt, J. M.; Black, A. L.; Craig, S. L. Gem-Dichlorocyclopropanes as Abundant and Efficient Mechanophores in Polybutadiene Copolymers under Mechanical Stress. *J. Am. Chem. Soc.* **2009**, *131*, 10818–10819.

(14) Lee, B.; Niu, Z.; Wang, J.; Slebodnick, C.; Craig, S. L. Relative Mechanical Strengths of Weak Bonds in Sonochemical Polymer Mechanochemistry. *J. Am. Chem. Soc.* **2015**, *137*, 10826–10832.

(15) Lenhardt, J. M.; Black Ramirez, A. L.; Lee, B.; Kouznetsova, T. B.; Craig, S. L. Mechanistic Insights into the Sonochemical Activation of Multimechanophore Cyclopropanated Polybutadiene Polymers. *Macromolecules* **2015**, *48*, 6396–6403.

(16) Chen, Z.; Mercer, J. A. M.; Zhu, X.; Romaniuk, J. A. H.; Pfattner, R.; Cegelski, L.;

Martinez, T. J.; Burns, N. Z.; Xia, Y. Mechanochemical Unzipping of Insulating Polyladderene to Semiconducting Polyacetylene. *Science (80-.).* **2017**, *357*, 475–479.
(17) Schleyer, P. V. R.; Wiliiams, J. E.; Blanchard, K. R. The Evaluation of Strain in Hydrocarbons. The Strain in Adamantane and Its Origin. *J. Am. Chem. Soc.* **1970**, *92*, 2377–2386.
(18) Etsuka, B. H. T.; Sobe, Ã. K. I.; Agiwara, M. H. Synthesis and Properties of Addition-Type Poly (Norbornene) s with Siloxane Substituents. *Polym. J.* **2009**, *41*, 643–649.
(19) Park, K. H.; Twieg, R. J.; Ravikiran, R.; Rhodes, L. F.; Shick, R. A.; Yankelevich, D.; Knoesen, A. Synthesis and Nonlinear-Optical Properties of Vinyl-Addition Poly(Norbornene)S. *Macromolecules* **2004**, *37*, 5163–5178.
(20) Liu, B.; Li, Y.; Mathews, A. S.; Wang, Y.; Yan, W.; Abraham, S.; Ha, C. S.; Park, D. W.; Kim, I. Synthesis of Vinyl-Type Functionalized Polynorbornenes with Cyclic Pendant Imide Side Groups by Using Palladium-Based Catalyst for Low Dielectric Constant Materials. *React. Funct. Polym.* **2008**, *68* (12), 1619–1624.
(21) Gmernicki, K. R.; Hong, E.; Maroon, C. R.; Mahurin, S. M.; Sokolov, A. P.; Saito, T.; Long, B. K. Accessing Siloxane Functionalized Polynorbornenes via Vinyl-Addition Polymerization for CO2 Separation Membranes. *ACS Macro Lett.* **2016**, *5*, 879–883.
(22) Belov, N.; Nikiforov, R.; Starannikova, L.; Gmernicki, K. R.; Maroon, C. R.; Long, B. K.; Shantarovich, V.; Yampolskii, Y. A Detailed Investigation into the Gas Permeation Properties of Addition-Type Poly(5-Triethoxysilyl-2-Norbornene). *Eur. Polym. J.* **2017**, *93*, 602–611.
(23) Lenhardt, J. M.; Ong, M. T.; Choe, R.; Evenhuis, C. R.; Martinez, T. J.; Craig, S. L. Trapping a Diradical Transition State by Mechanochemical Polymer Extension. *Science (80-.).* **2010**, *329*, 1057–1060.
(24) May, P. A.; Munaretto, N. F.; Hamoy, M. B.; Robb, M. J.; Moore, J. S. Is Molecular Weight or Degree of Polymerization a Better Descriptor of Ultrasound-Induced Mechanochemical Transduction? *ACS Macro Lett.* **2016**, *5*, 177–180.
(25) Kuijpers, M. W. A.; Iedema, P. D.; Kemmere, M. F.; Keurentjes, J. T. F. The Mechanism of Cavitation-Induced Polymer Scission; Experimental and Computational Verification. *Polymer (Guildf).* **2004**, *45*, 6461–6467.
(26) Lenhardt, J. M.; Ogle, J. W.; Ong, M. T.; Choe, R.; Martinez, T. J.; Craig, S. L. Reactive Cross-Talk between Adjacent Tension-Trapped Transition States. *J. Am. Chem. Soc.* **2011**, *133*, 3222–3225.
(27) Malhotra, S. L. Ultrasonic Modification of Polymers. II. Degradation of Polystyrene, Substituted Polystyrene, and Poly(n-Vinyl Carbazole) in the Presence of Flexible Chain Polymers. *J. Macromol. Sci. Part A - Chem.* **1982**, *18* (7–8), 1055–1085.
(28) Malhotra, S. L. Ultrasonic Solution Degradations of Poly(Alkyl Methacrylates). *J. Macromol. Sci. Part A - Chem.* **1986**, *23*, 729–748.
(29) Striegel, A. M. Influence of Chain Architecture on the Mechanochemical Degradation of Macromolecules. *J. Biochem. Biophys. Methods* **2003**, *56*, 117–139.
(30) Fox, T. G.; Flory, P. J. Second-Order Transition Temperatures and Related Properties of Polystyrene. I. Influence of Molecular Weight. *J. Appl. Phys.* **1950**, *21*, 581–591.
(31) Müller, K.; Kreiling, S.; Dehnicke, K.; Allgaier, J.; Richter, D.; Fetters, L. J.; Jung, Y.; Yoon, D. Y.; Greiner, A. Synthesis and Rheological Properties of Poly(5-n-Hexylnorbornene). *Macromol. Chem. Phys.* **2006**, *207*, 193–200.
(32) Potisek, S. L.; Davis, D. A.; Sottos, N. R.; White, S. R.; Moore, J. S. Mechanophore-

Linked Addition Polymers. **2007**, 13808–13809.

Chapter 5. Investigation of the dynamic nature of 1,2-oxazines derived from peralkyl cyclopentadiene and nitrosocarbonyl species[2]

5.1 INTRODUCTION

For decades, the hetero-Diels-Alder (HDA) reaction of nitrosocarbonyl species has been utilized as a versatile synthetic transformation for production of 1,2-oxazines (**Scheme 5.1**).[1–7] Attractive aspects include the potential for regio- and stereo controlled introduction of nitrogen and oxygen into carbon frameworks, and ample opportunities for downstream manipulation of the *N*-substituted oxazine. In a subset of examples of 1,2-oxazine applications, the ready reversibility of the HDA reaction was targeted as a means to control *in situ* generation of highly reactive nitrosocarbonyl moieties. For example, King, Miyata, and Toscano have highlighted the potential to use this cycloreversion for generation of HNO, a purported therapeutic, presumably following hydrolysis of the nitrosocarbonyl intermediate.[8–14]

Scheme 5.1 Generalized depiction of the reversible HDA reaction of nitrosocarbonyls.

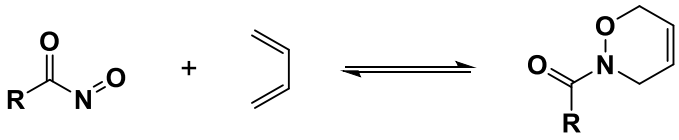

More recently, the dynamic HDA reaction of nitrosocarbonyls has been applied in the design of advanced polymeric architectures and functional materials. A key example from

[2] Reproduced with permission from Kensy, V. K.; Peterson, G. I.; Church, D. C.; Yakelis, N. A.; Boydston, A. J. "Investigation of the dynamic nature of 1,2-oxazines derived from peralkyl cyclopentadiene and nitrosocarbonyl species" *Org. Biomol. Chem.*, **2016**, 14, 5617-5621. Copyright 2016 The Royal Society of Chemistry.

Read de Alaniz and coworkers demonstrated application of nitrosocarbonyl HDA reactions to prepare block copolymers via highly efficient polymer chain end coupling.[15] In their report, reactive nitrosocarbonyl dienophiles were generated *in situ* at polymer chain ends either by oxidation of hydroxamic acids or cycloreversion of 9,10-dimethylanthracene-based adducts. In the presence of a complementary cyclopentadiene-terminated polymer, efficient chain end coupling was accomplished.

Inspired by this movement toward applications in the polymer field, we considered integration of polymer chain end coupling and nitrosocarbonyl hydrolysis to enable controlled *deconstruction* of block copolymers.[16] For this purpose, the 1,2-oxazine moiety was employed as a thermally labile trigger. Upon thermolysis, subsequent hydrolysis of the nitrosocarbonyl intermediate initiated a controlled depolymerization sequence leading to deconstruction of a self-immolative polymer block. Clearly, the "click-like" nature of the HDA reaction, tunable cycloreversion of oxazines, diverse reactivity of nitrosocarbonyl species, and overall structural modularity provide a powerful combination for advances in polymer and materials designs.

We became interested in the potential applications of polymers and network materials bearing high densities of oxazine moieties. One may envision, for example, taking advantage of robust dynamic covalency to access covalent adaptable networks as has been demonstrated for Diels-Alder and HDA adducts.[17–21] Such systems display broad tunability with regard to stimuli-responsiveness and overall materials properties, stemming largely from the modularity of the diene and dienophile building blocks. On the other hand,

controlled breakdown of oxazine-rich materials could enable controlled release of HNO. HNO generation has received a lot of attention in recent years due to its purported use as a treatment of cardiovascular diseases and as an anticancer agent.[22–26] Notably, the breadth of potential applications place disparate demands on the reactivity of the oxazine and constituent nitrosocarbonyl species (high fidelity cycloaddition/ cycloreversion versus hydrolytic instability) while maintaining a need for retro-HDA reactions to take place at moderate temperatures. To further explore the chemical space and potential applications of oxazine-based systems, we have investigated the reversibility and robustness of a series of oxazines relevant to polymer-oriented applications. Herein, we describe our investigations of the reactivity of oxazines derived from a series of nitrosocarbonyl dienophiles and a peralkylated cyclopentadiene. Particular focus is placed upon comparative analysis of the reversibility of the HDA reaction as a function of nitrosocarbonyl structure, and overall fidelity of the cycloaddition/cycloreversion equilibrium versus deleterious side reactions.

5.2 Results and Discussion

Motivated by potential downstream applications in the development of functional polymeric materials, we targeted oxazines that were based upon readily polymerizable norbornene frameworks.[27] Additionally, we centered upon cyclopentadiene-based oxazines to provide an attractive starting point for balance between stability and reversibility of the HDA adducts. Toward this end, coupling of carboxylic acid **1** and alcohol **2** in the presence of carbonyldiimidazole provided ester **3** in 70% isolated yield (**Figure 5.1**). This pivotal intermediate was then used to prepare a series of oxazines via HDA reaction with nitrosocarbonyl species generated *in situ*.[1,28–30]

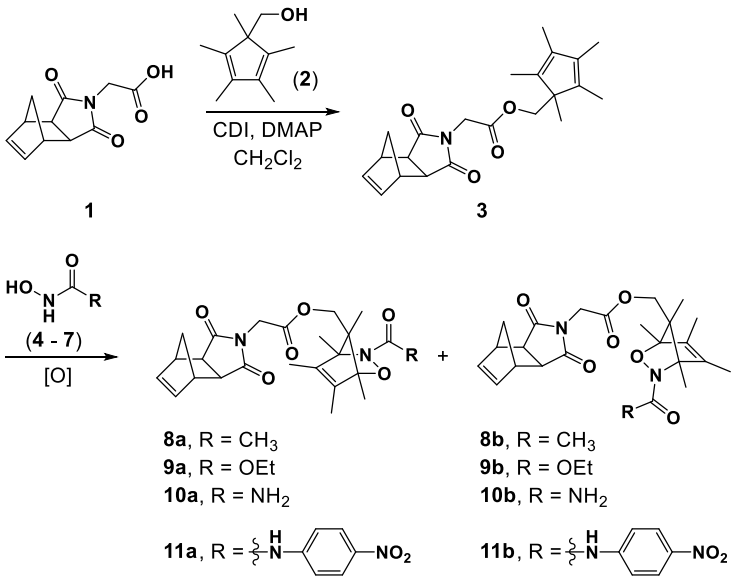

Oxidation Conditions

Oxazine	Oxidant	Time (h)	Isolated Yield
8	TBAP	2	64%
9	TBAP	2.5	97%
10	TBAP	3	88%
11	CuCl, pyridine	18	70%

Figure 5.1 Synthesis of norbornene-tethered oxazine isomers. In each case, reactions proceeded to 100% conversion as judged by TLC.

We initially evaluated the use of CuCl/pyridine to catalyze the nitrosocarbonyl formation. Although good yields of **11** were achieved via oxidation of **7** in the presence of **3**, analogous reactions with coupling partners **4** - **6** were met with limited success. Turning instead to

tetrabutylammonium periodate as a stoichiometric oxidant remedied the situation, providing the corresponding oxazines **8** - **10** in good to excellent yields. Notably, each oxazine was isolated as a mixture of what appeared to be a roughly 3:1 ratio of two diastereomers (each racemic).

Separation of the isomers by standard chromatographic techniques was unsuccessful. However, we found that slow vapour diffusion of diethyl ether into solutions of **10** in CH_2Cl_2 produced single crystals suitable for X-ray analysis. We were able to separate crystals that were ultimately found to be individual diastereomers **10a** and **10b** (**Figure 5.2**), which can be viewed as *anti* and *syn* isomers, respectively. With small quantities of each diastereomer of **10** at hand, we were able to obtain a discrete ^{1}H NMR spectrum for each. From these, we identified **10a** as the major diastereomer produced in the initial mixture of products. The CH_3 groups indicated in **Figure 5.2** proved to be useful diagnostic handles for ^{1}H NMR analyses and tracking of *anti* and *syn* isomers for oxazines **8**, **9**, and **11** by analogy to **10**.

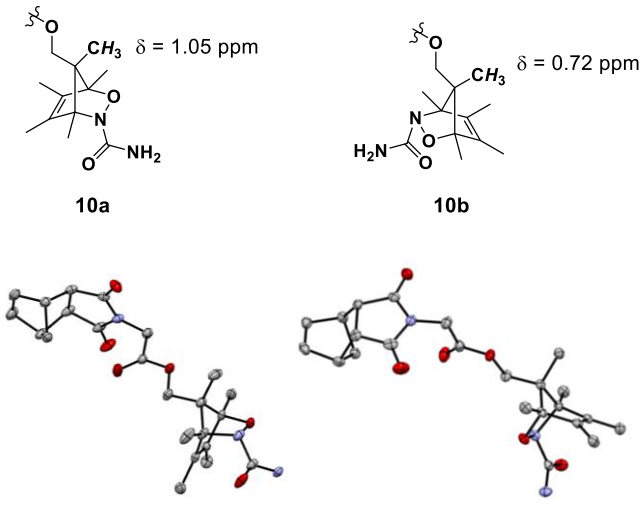

Figure 5.2 Molecular structures obtained via single crystal X-ray analysis of **(left) 10a**, and **(right) 10b**. Ellipsoids drawn at the 50% probability level, protons removed for clarity.

We next turned toward probing the dynamic nature of each oxazine. Specifically, each set of isomers was heated in DMSO-d_6 (15 mM) and monitored by ^{1}H NMR spectroscopy. In each case, the initial mixture contained a roughly 3:1 ratio of diastereomers, which equilibrated to a roughly 1:1 ratio over time. At ambient temperature, no observable isomerization took place for any of the oxazines over the course of several hours. When heated at 37 °C (**Figure 5.3**, **top**), we observed gradual equilibration of the diastereomers with strong dependence upon the nature of the nitrosocarbonyl component. For example, oxazine **8** did not appear to reach equilibrium even within 12 d at 37 °C, indicating much slower isomerization than oxazines bearing more electron donating substituents (cf. **9** - **11**). Oxazine **9** appeared to isomerize more rapidly than **8**, but also continued to show gradual change in the ratio of isomers up to 12 d. The hydroxyurea-derived systems (**10** and **11**) were found to approach equilibrium at the highest relative rates. The facile isomerization, particularly of **10** and **11**, at 37 °C suggests to us that these platforms may be suitable for incorporation into dynamic covalent networks or related materials that become active under biological conditions.

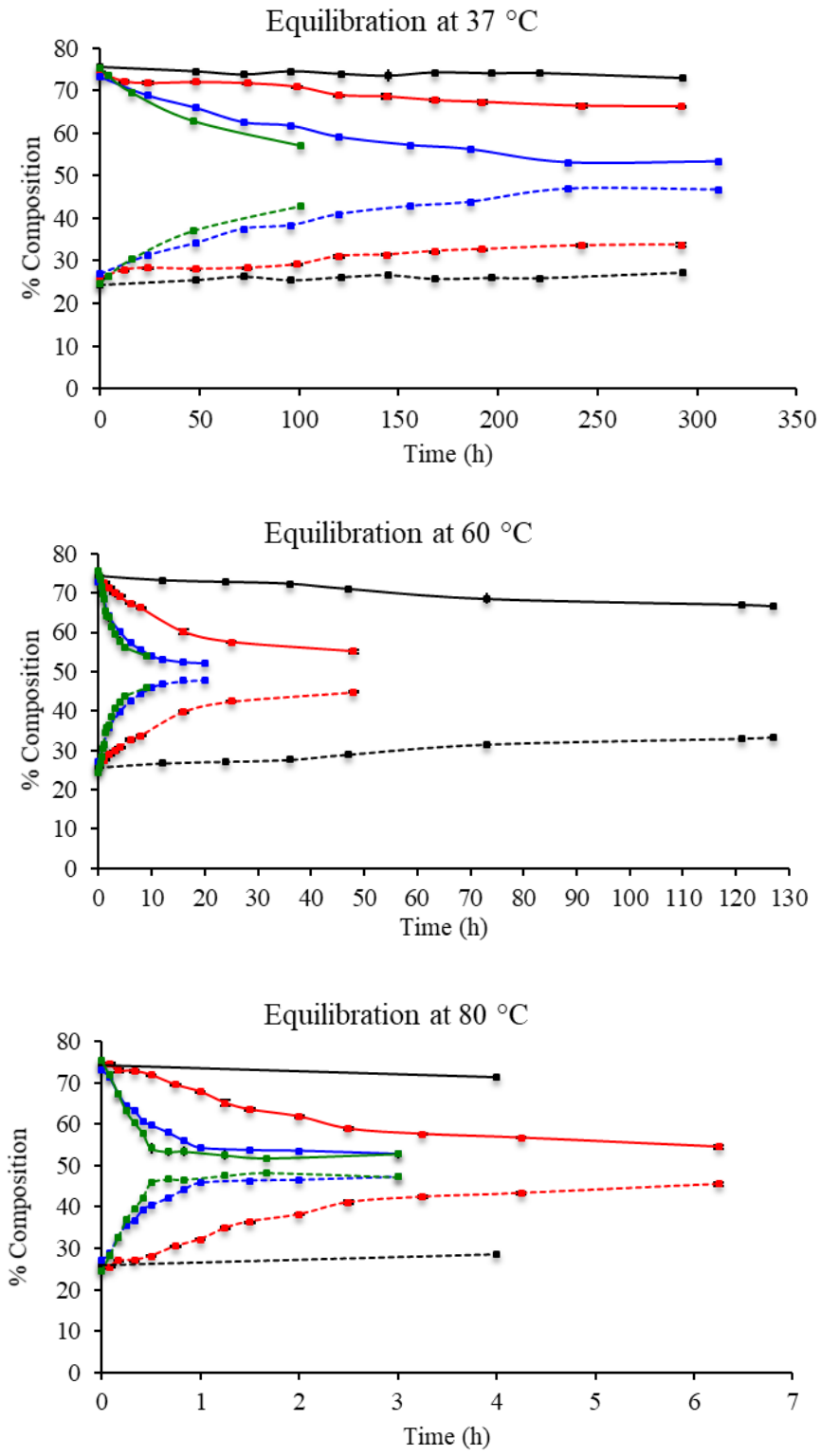

Figure 5.3 Equilibration of oxazines in DMSO-d_6. Solid line = isomer A, dashed line = isomer B. Black = **8**, red = **9**, blue = **10**, green = **11**. Data points are an average of three runs, errors bars = one standard deviation, lines are for visual aid only.[31] Percent composition refers to the ratio of isomers A and B.

The general trend in isomerization rate (**8** < **9** < **10** < **11**) was preserved at the higher temperatures as well (**Figure 5.3**). At 60 °C (**Figure 5.3**, **middle**), the least reactive oxazine (**8**) displayed discernible isomerization over the course of several days, whereas changes in the diastereomeric ratios for **10** and **11** appeared to have ceased after a few hours. Further increase in the temperature to 80 °C (**Figure 5.3**, **bottom**) resulted in full equilibration within minutes for **10** and **11** (50 and 25 min, respectively), whereas the composition of **8** continued to show gradual change over the course of several hours (see Experimental for extended plots).

As stated previously, the oxazine retro-HDA reaction releases nitrosocarbonyl species, which have the potential to undergo hydrolysis, dimerization, or ene reactions.[32] These deleterious reactions were not observed to any appreciable extent in the experiments represented in **Figure 5.3** despite prolonged reaction times and no special precautions being taken to dry the DMSO solvent. To explore the oxazine reactivity in aqueous environment, we examined each of the oxazines at 60 °C in a 30% D_2O/DMSO-d_6 mixture, which was the maximum D_2O content at which each of the oxazines remained soluble at room temperature. Each oxazine mixture was monitored by ^{1}H NMR spectroscopy for 156 h. Oxazines **8** and **9** showed no loss of oxazine content and isomerization rates similar to those observed in DMSO-d_6. In contrast, examination of oxazine **10** revealed a small amount of cyclopentadiene **3** (4.5%) developing over the course of the experiment (**Figure 5.4**, **top**). Presumably, the formation of **3** can be ascribed to hydrolysis of the intermediate nitrosocarbonyl species. When oxazine **11** was examined under the aqueous reaction conditions, we found nearly complete loss of both oxazine isomers and concomitant

formation of **3** (**Figure 5.4**, **bottom**). Collectively, these results confirm that the oxazine moiety can be structurally tuned toward either robust dynamic behaviour or controlled degradation.

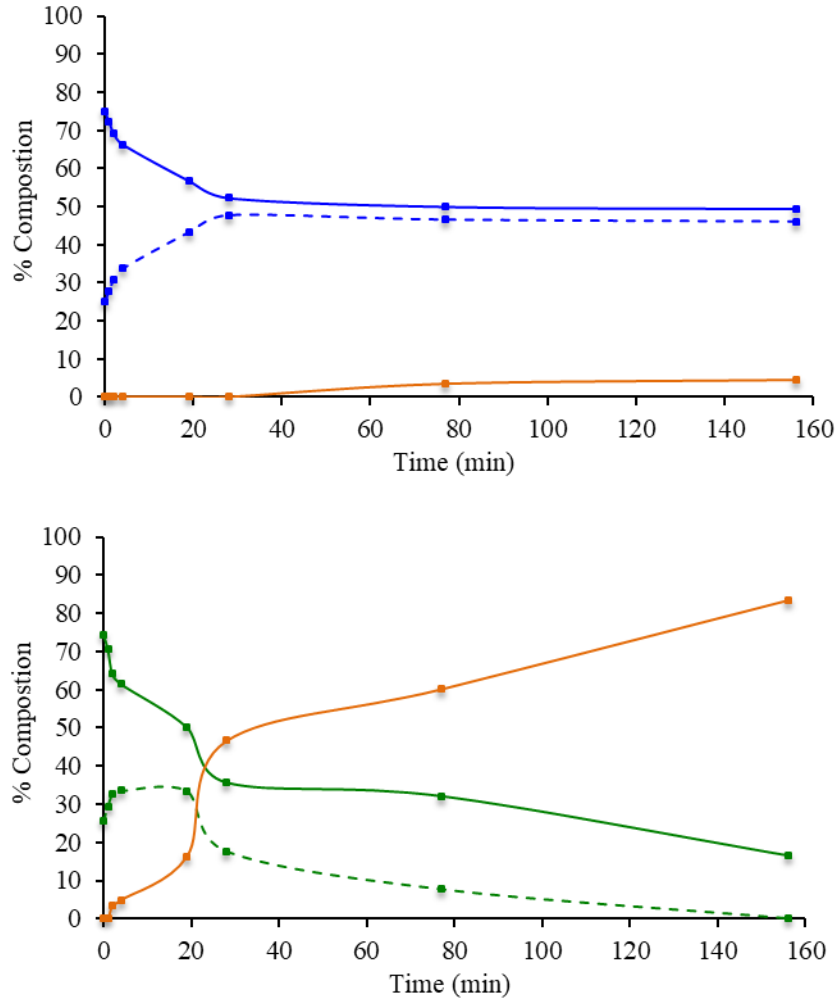

Figure 5.4 Equilibration and hydrolysis of oxazines in D_2O/DMSO-d_6 at 60 °C.[31] Solid line = isomer A, dashed line = isomer B. **(top)** Oxazine **10** in blue, cyclopentadiene **3** in orange. **(bottom)** Oxazine **11** in green, cyclopentadiene **3** in orange. Data points are an average of two runs, lines are for visual aid only. Percent composition refers to the fraction of each species relative to the total sum of isomer A, isomer B, and **3**.

Encouraged by the results from the small molecule oxazine studies, we next explored whether the dynamic nature would remain consistent within related polymeric systems. Toward this end, we synthesized **poly(11)** via ring-opening metathesis polymerization

(ROMP) using a third-generation Grubbs catalyst (**Scheme 5.2**).[33] Specifically, monomer **11** was reacted with the Ru-based initiator (35:1 initial monomer to initiator ratio) in CH_2Cl_2 at 0 °C for 3 h, at which point full consumption of monomer was confirmed by ^{1}H NMR analysis. Following termination of the polymerization with ethyl vinyl ether, filtration through alumina/Celite, and isolation by precipitation of the polymer into methanol, we obtained **poly(11)** in 20% isolated yield. Analysis of **poly(11)** by ^{1}H NMR spectroscopy and gel-permeation chromatography (GPC) indicated intact oxazines (3:1 ratio of isomers), a weight-average molecular weight (M_w) of 30.0 kDa, and a molecular weight dispersity ($Đ$) of 1.05.

Scheme 5.2 ROMP of **11** to produce **poly(11)**. Oxazines are a mixture of *anti* and *syn* isomers.

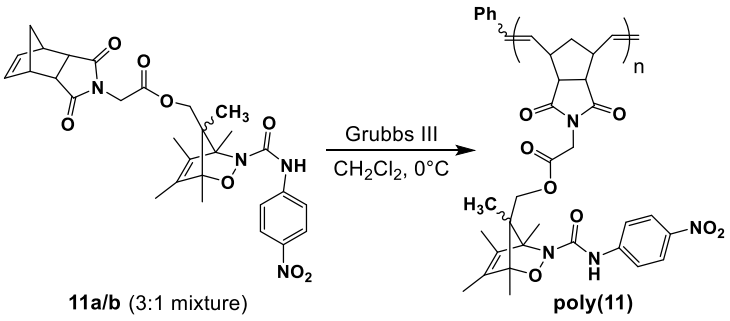

With **poly(11)** in hand, we then monitored the isomerization of the oxazine units using a solution of the polymer in DMSO-d_6 at 60 °C and variable-temperature ^{1}H NMR spectroscopy (VT-NMR). The alkene proton resonances within the polymer backbone were compared with the diagnostic methyl signals of the oxazine isomers over the course of the experiment. Under these conditions, **poly(11)** showed no signs of degradation of the

oxazine units and complete isomerization within 5 h, consistent with the equilibration time of monomer **11** (**Figure 5.5**).

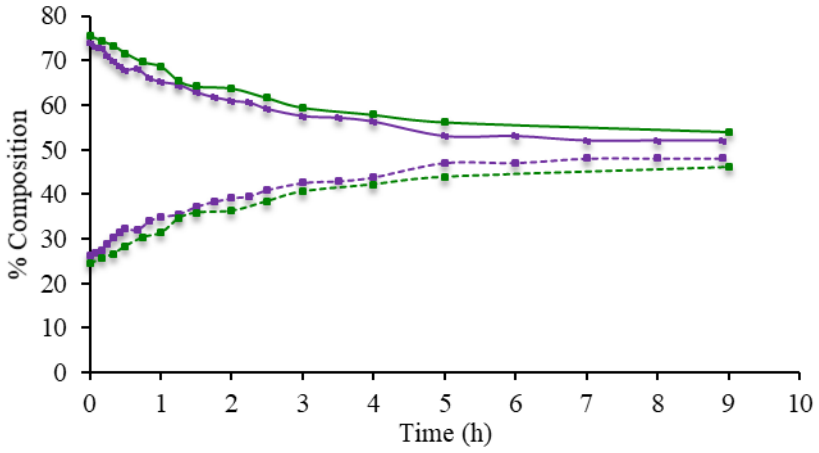

Figure 5.5 Equilibration of oxazine **11** (green) and **poly(11)** (purple) in DMSO-d_6 at 60 °C. Solid line = *anti* isomer, dashed line = *syn* isomer. Percent composition refers to the ratio of *anti* and *syn* isomers.

To investigate the potential for dynamic nitrosocarbonyl exchange from the polymeric system, **poly(11)** was heated at 60 °C in the presence of either oxazine **9** or **10**, each in a 2:1 ratio relative to oxazine repeat units in **poly(11)** (**Scheme 5.3**). After heating each mixture, the solution was added dropwise into an excess of cold methanol, causing selective precipitation of the polymeric species. In each case, ^{1}H NMR analysis of the final polymers revealed signals consistent with successful conversion of oxazine units, giving rise to **poly(9-*co*-11)** and **poly(10-*co*-11)** from the corresponding small molecule oxazines. Each copolymer was found to have a ca. 2:1 ratio of oxazine units consistent with the initial feed ratios. These experiments confirm the ability to successfully crossover oxazine functionality with a polymeric system and may provide opportunities for post-polymerization modifications and reversible crosslinking strategies.

Scheme 5.3 Dynamic oxazine crossover between **poly(11)** and small molecule oxazines **9** and **10**. Oxazines are a mixture of *anti* and *syn* isomers.

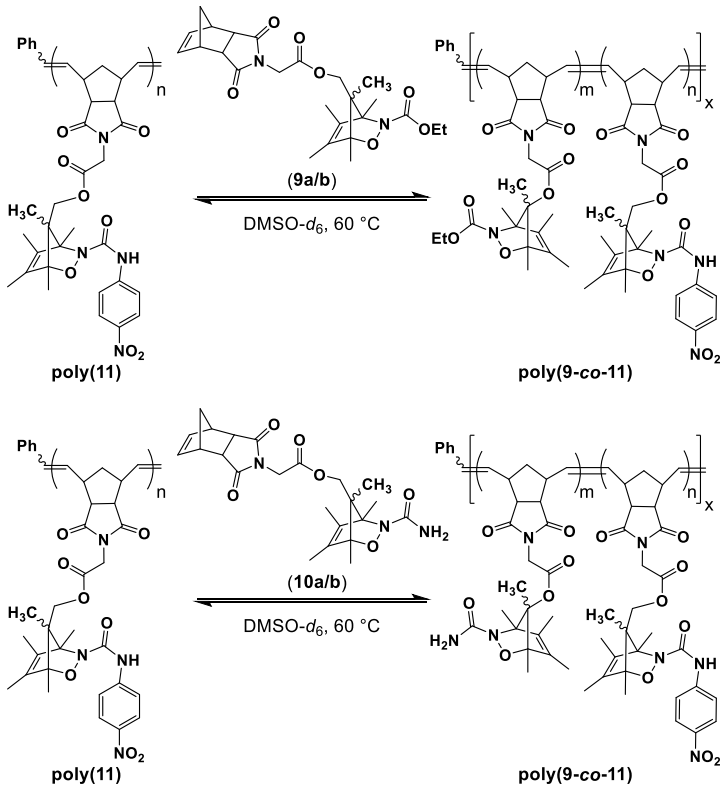

5.3 CONCLUSIONS

We have investigated a series of *N*-carbonyl-substituted oxazines that display readily reversible HDA reactivity. Coincidental production of a diastereomeric mixture of each oxazine provided a convenient method for comparative analysis of their dynamic nature as a function of structure and temperature. The systems appeared to be relatively well behaved, with dynamic equilibration and preservation of oxazine content persisting for several hours at elevated temperatures. Moreover, we found encouraging results toward incorporation of these oxazines into dynamic covalent networks and release platforms based upon polymer-oriented and hydrolysis studies. Collectively, this short series of

compounds displays a broad range of (retro)HDA rates and general robustness that may help to guide the design of adaptable network materials and functional polymers.

5.4 ACKNOWLEDGEMENTS

We gratefully acknowledge financial support from the National Science Foundation (DMR-1452726) and the University of Washington. We thank Professor Werner Kaminsky for X-ray crystallography.

5.5 EXPERIMENTAL

General Considerations. Dry THF, pyridine, DMSO, and CH_2Cl_2 were obtained from a Glass Contour solvent purification system. All other reagents and solvents were used as obtained from commercial sources. Grubbs 3rd generation catalyst, $(iMesH_2)(C_5H_5N)_2(Cl)_2Ru{=}CHPH$, was synthesized according to literature procedure.[33] ^{1}H and ^{13}C NMR spectra were recorded on a Bruker AVance 300 or 500 MHz spectrometer. Chemical shifts are reported in delta (δ) units, expressed in parts per million (ppm) downfield from tetramethylsilane using the residual protio-solvent as an internal standard ($CDCl_3$, ^{1}H: 7.26 ppm and ^{13}C: 77.16 ppm and DMSO-d_6, ^{1}H: 2.50 ppm). HRMS was performed on a Thermo LTQ Orbitrap with a resolution setting of 30,000. Gel permeation chromatography (GPC) was performed using a GPC setup consisting of: a Shimadzu pump, 3 in-line columns, and Wyatt light scattering and refractive index detectors THF as the mobile phase.

Scheme 5.4 Synthesis of **3**.

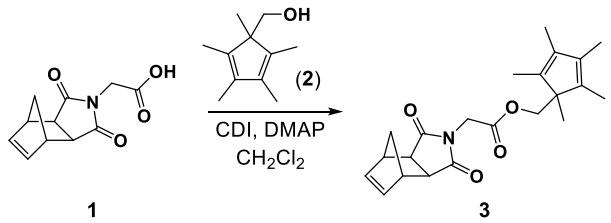

Compounds **1** and **2** were synthesized according to the literature.[16,27] Into a flame-dried, N_2-purged round bottom flask, *N*,*N*-carbonyldiimidazole (1.4 g, 8.7 mmol, 1.3 eq.), a stir bar, and 15 mL of CH_2Cl_2 were added. To this solution, **1** (1.9 g, 8.7 mmol, 1.3 eq.) was added portion-wise. The reaction mixture was then stirred at room temperature for 45 minutes. After this time, DMAP (81.8 mg, 0.7 mmol, 0.1 eq.) and **2** (1.1 g, 6.7 mmol, 1.0 eq.) in 15 mL of CH_2Cl_2 were added to the reaction mixture. The reaction mixture was then stirred at room temperature for 18 hours. The solution was then washed successively with 1 M HCl (2 × 30 mL), sat. $NaHCO_3$ (2 × 30 mL), and brine (2 × 30 mL). The organic layer was dried over Na_2SO_4 and then concentrated under reduced pressure. The resulting residue was purified by flash chromatography (10% EtOAc/Hex) on silica gel and the product was isolated as a white solid (70% yield). ^{1}H NMR (300 MHz, $CDCl_3$) δ 6.20 (t, *J*= 1.7 Hz, 2H), 4.03 (s, 2H), 3.91 (s, 2H), 3.19 (s, 2H), 2.62 (s, 2H), 1.65 (d, *J* = 9.0 Hz, 12H), 1.56 (d, *J* = 9.9 Hz, 1H), 1.41 (d, *J* = 9.6 Hz, 1H), 0.84 (s, 3H). ^{13}C NMR (125 MHz, $CDCl_3$) δ 176.7, 166.6, 138.0, 137.8, 135.1, 66.8, 55.2, 47.8, 45.2, 42.7, 39.1, 16.7, 10.9, 10.0. HRMS: $[M+H]^+$ calcd for $C_{22}H_{28}NO_4$, 370.2018; found, 370.20247.

Scheme 5.5 Synthesis of Oxazines **8-10**

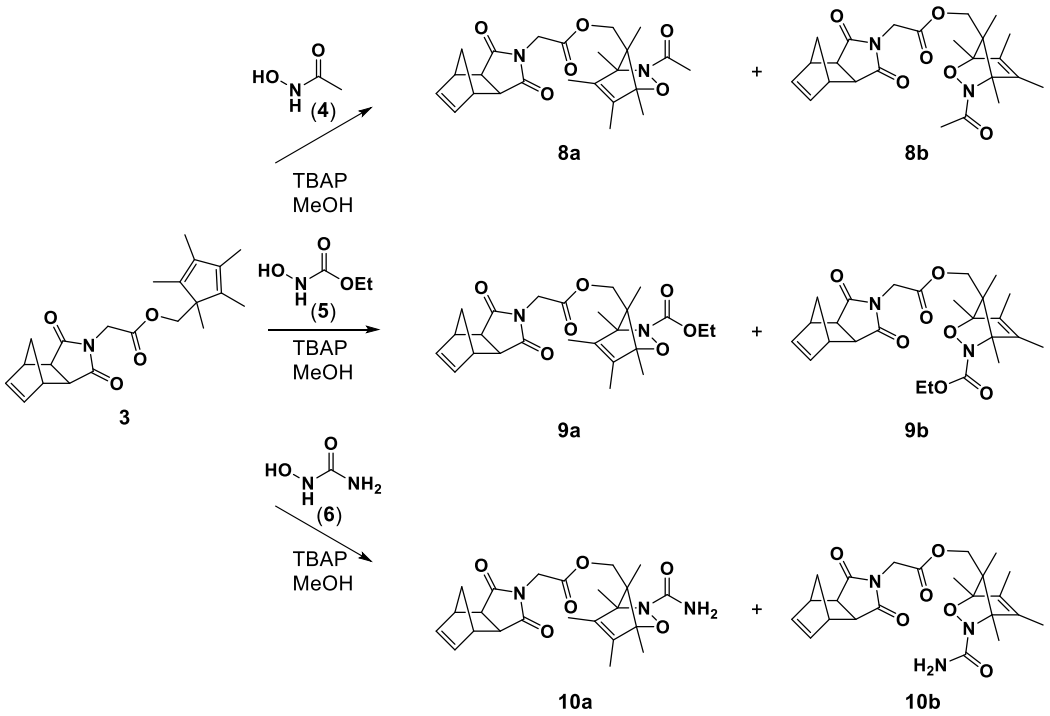

General Procedure for the Synthesis of Oxazines 8-10. A N_2-purged round bottom flask was charged with **3** (0.586 g, 1.6 mmol, 1.0 eq.), tetrabutylammonium periodate (0.8371 g, 1.9 mmol, 1.2 eq.), a stir bar, and MeOH (50 mL). To this solution, hydroxyurea (1.9 mmol, 1.2 eq.) in 30 mL of MeOH was added dropwise. The reaction mixture was stirred vigorously and monitored by TLC. Upon consumption of **3**, the organic layer was concentrated under reduced pressure and then taken up in EtOAc. The organic solutin was then washed successively with sat. aq. Na_2SO_3 (2 × 30 mL) and sat. aq. $NaHCO_3$ (2 × 30 mL). The organic layer was dried over Na_2SO_4 and then concentrated under reduced pressure. The crude material was purified by flash chromatography (50% EtOAc/Hex) on silica gel and the products were isolated as white solids.

8: Isolated yield = 64%. ^{1}H NMR (300 MHz, $CDCl_3$) δ 6.30 (t, *J*= 1.7 Hz, 2H), 4.30–4.12 (m, 2.5H), 3.90–3.81 (m, 1.5H), 3.31 (t, *J*= 1.6 Hz, 2H), 2.75 (s, 2H), 1.87–1.86 (m, 3H), 1.77–1.74 (m, 3H), 1.67–1.63 (m, 7H), 1.54–1.51 (m, 1H), 1.37 (s, .75H), 1.33 (s, 2.25H), 1.02 (s, 2.25H),

0.73 (s, 0.75H). ^{13}C NMR (125 MHz, $CDCl_3$) δ 178.2, 177.1, 166.9, 139.8, 138.1, 132.5, 94.6, 79.7, 68.2, 66.8, 61.4, 48.1, 45.5, 42.9, 39.3, 24.0, 12.4, 12.1, 10.9, 9.4, 1.1. HRMS: $[M+H]^+$ calcd for $C_{24}H_{31}N_2O_6$, 443.2182; found, 443.21971.

9: Isolated yield = 97%. ^{1}H NMR (300 MHz, $CDCl_3$) δ 6.30 (s, 2H), 4.31–4.20 (m, 2.5H), 4.13 (q, *J*= 7.08 Hz, 2H), 3.85 (s, 1.5H), 2.75 (s, 2H), 1.73 (m, 3H), 1.67–1.65 (m, 3H), 1.60–1.51 (m, 5H), 1.38–1.35 (m, 3H), 1.24 (t, *J*= 7.0 Hz, 3H), 1.04 (s, 2.25H), 0.73 (s, 0.75H). ^{13}C NMR (125 MHz, $CDCl_3$) δ 177.09, 177.07, 166.9, 160.2, 138.0, 133.8, 94.2, 80.1, 77.3, 77.1, 76.8, 68.4, 66.6, 62.0, 61.5, 48.1, 45.4, 42.9, 39.3, 14.5, 13.0, 12.4, 12.0, 11.6, 10.8, 9.5, 1.0. HRMS: $[M+H]^+$ calcd for $C_{25}H_{33}N_2O_7$, 473.2288; found, 473.23041.

10: Isolated yield = 88%. ^{1}H NMR (300 MHz, $CDCl_3$) δ 6.31 (t, *J*= 1.6 Hz, 2H), 4.36–4.14 (m, 2.5H), 3.89–3.81 (m, 1.5H), 3.31 (t, *J*= 1.6 Hz, 2H), 2.75 (s, 2H), 1.76–1.74 (m, 3H), 1.69–1.63 (m, 7H), 1.57–1.51 (m, 2H), 1.37 (s, .75H), 1.33 (s, 2.25H), 1.05 (s, 2.25H), 0.72 (s, 0.75H). ^{13}C NMR (125 MHz, $CDCl_3$) δ 177.2, 167.0, 164.7, 138.1, 132.2, 100.1, 95.0, 80.7, 68.6, 66.8, 61.7, 60.4, 48.2, 45.5, 43.0, 39.4, 12.7, 11.1, 9.3, 1.1 . HRMS: $[M+H]^+$ calcd for $C_{23}H_{30}N_3O_6$, 444.2135; found, 444.21479.

10a: ^{1}H NMR (300 MHz, $CDCl_3$) δ 6.31 (t, *J*= 1.7 Hz, 2H), 4.24 (d, *J*= 17.1 Hz, 1H), 4.17 (d, *J*=17.0 Hz, 1H), 3.87 (d, *J*= 10.9 Hz, 1H), 3.83 (d, *J*= 10.9 Hz, 1H), 3.32 (t, *J*= 1.7 Hz, 2H), 2.76 (s, 2H), 1.76 (d, *J*= 1.3 Hz, 3H), 1.69 (d, *J*= 1.3 Hz, 3H), 1.66–1.63 (m, 4H), 1.54 (d, *J*= 10.3 Hz, 1H) 1.33 (s, 3H), 1.05, (s, 3H).

10b: ^{1}H NMR (300 MHz, $CDCl_3$) δ 6.31 (t, *J*= 2.0 Hz, 2H), 4.35 (d, *J*= 11.8 Hz, 1H), 4.21 (d, *J*= 11.8 Hz, 1H), 3.32 (t, *J*= 1.6 Hz, 2H), 2.75 (s, 2H), 1.74 (d, *J*= 1.5 Hz, 3H), 1.66 (d, *J*= 1.1 Hz, 1H), 1.65–1.61 (m, 4H), 1.54 (d, 10.1 Hz, 1H), 1.37 (s, 3H), 0.73 (s, 3H).

Scheme 5.6 Synthesis of **S1** and **S2**

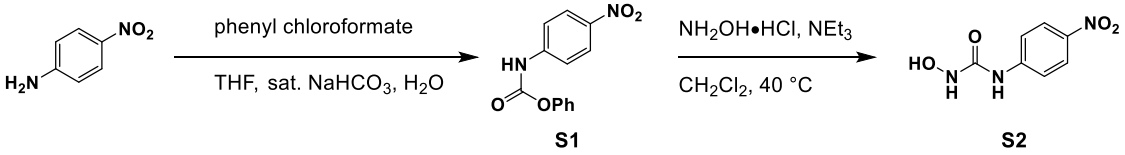

Synthesis of S1. Preparation of **S1** by an alternative method was previously reported.[34] A round bottom flask was charged with 4-nitroaniline (0.7001 g, 5.0 mmol, 1.0 eq.), a stir bar, 2 mL of THF, 0.6 mL of sat. $NaHCO_3$, and 0.4 mL of H_2O. Phenyl chloroformate (0.64 mL, 5.1 mmol, 1.02 eq.) was then added drop-wise via an addition funnel. The resulting mixture was stirred at room temperature for 3 hours. The reaction mixture was then diluted with EtOAc and then washed with sat. $NaHCO_3$ (2 × 10mL) followed by brine (1 × 10 mL). The organic layer was dried over Na_2SO_4 and then concentrated under reduced pressure. The resulting carbamate was used without further purification (97% crude yield). ^{1}H NMR (500 MHz, $CDCl_3$) δ 8.21 (d, J = 9.0 Hz, 2H), 7.60 (d, J = 9.0 Hz, 2H), 7.49 – 7.35 (m, 3H), 7.30 – 7.24 (m, 1H), 7.19 (d, J = 7.8 Hz, 2H). ^{13}C NMR (125 MHz, $CDCl_3$) δ 151.3, 150.2, 143.6, 143.5, 129.7, 126.4, 125.4, 121.6, 118.2.

Synthesis of S2. Preparation of **S2** by an alternative method was previously reported.[12] Into a flame-dried, N_2-purged round bottom flask was added carbamate **S1** (0.6 g, 2.32 mmol, 1.0 eq.), NEt_3 (0.32 mL, 2.32 mmol, 1.0 eq.), CH_2Cl_2 (2.32 mL) and a stir bar. Separately, hydroxylamine (0.559 g, 8 mmol) and potassium carbonate (2.222 g, 16 mmol) was free-based in dry DMSO (4 mL) for 12 hours. A solution of free-based hydroxylamine (2.32 mL in DMSO, 4.64 mmol, 2.0 eq.) was then added into the solution containing **S1**. The resulting mixture was then heated at 40 °C and stirred for 3 hours. After being removed from heat and returning to room temperature, the reaction mixture was added into 30 mL of H_2O and extracted with EtOAc (2 × 10 mL). The combined organic layers were dried over Na_2SO_4 and then concentrated under reduced pressure. The desired product was obtained as a yellow solid (83% yield). ^{1}H NMR (500 MHz, DMSO) δ

9.49 (s, 1H), 9.27 (s, 1H), 9.15 (s, 1H), 8.14 (d, J = 9.0 Hz, 2H), 7.92 (d, J = 8.9 Hz, 2H). ^{13}C NMR (125 MHz, DMSO-d_6) δ 157.8, 146.4, 141.4, 124.8, 118.5.

Scheme 5.7 Synthesis of **11**

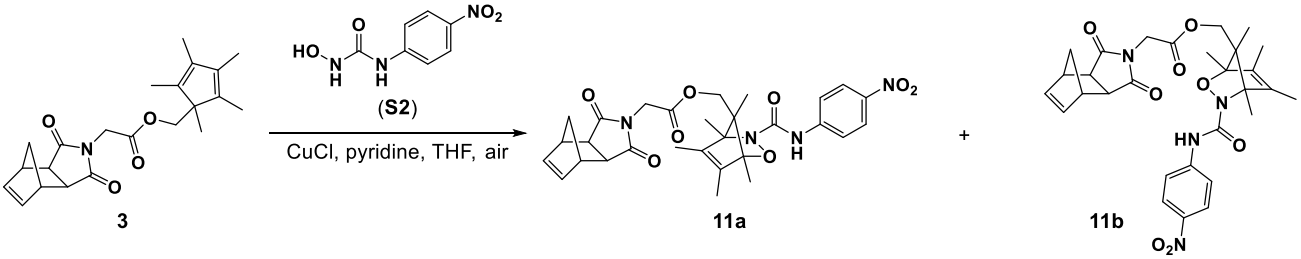

Synthesis of 11. A round bottom flask was charged with **3** (0.336 g, 0.9 mmol, 1.0 eq.), **2** (0.359 g, 1.8 mmol, 1.2 eq.), a stir bar, and THF (10 mL). CuCl (0.037 g, 0.36 mmol, 0.4 eq.) and pyridine (7.3 µL, 0.09 mmol, 0.1 eq.) were then added. The reaction mixture was vigorously stirred under ambient conditions for 18 hours. EtOAc (10 mL) and sat. aq. EDTA (10 mL) were then added to the reaction mixture. The organic layer was separated and then washed successively with sat. EDTA (2 × 10 mL) and brine (2 × 10 mL). The organic layer was dried over Na_2SO_4 and then concentrated under reduced pressure. The crude material was purified by flash chromatography (20% EtOAc/Hex) on silica gel and the product was isolated as a yellow solid (70% yield). ^{1}H NMR (300 MHz, $CDCl_3$) δ 8.10 (d, J= 8.9 Hz, 2H), 7.75 (s, 1H), 7.56 (d, *J*= 9.3 Hz, 2H), 6.27 (s, 2H), 4.39–4.16 (m, 2.5H), 3.92–3.84 (m, 1.5H), 3.32 (s, 2H), 2.77 (s, 2H), 1.77–1.75 (m, 3H), 1.71–1.65 (m, 6.5H), 1.56–1.53 (m, 1.5H), 1.46–1.43 (m, 3H), 1.10 (s, 2.25H), 0.78 (s, 0.75H). ^{13}C NMR (126 MHz, $CDCl_3$) δ 177.11, 177.07, 166.8, 159.7, 143.7, 143.1, 139.2, 138.01, 137.98, 132.5, 125.1, 118.5, 100.0, 96.8, 96.3, 81.3, 68.1, 65.9, 62.1, 60.8, 48.1, 45.5, 42.9, 39.2, 15.3, 13.0, 12.7, 12.6, 12.5, 12.0, 11.1, 10.9, 9.3. HRMS (ESI): $[M+H]^+$ calcd for $C_{29}H_{33}N_4O_8$, 565.2298; found, 565.23191.

Scheme 5.8 Synthesis of **poly(11)**

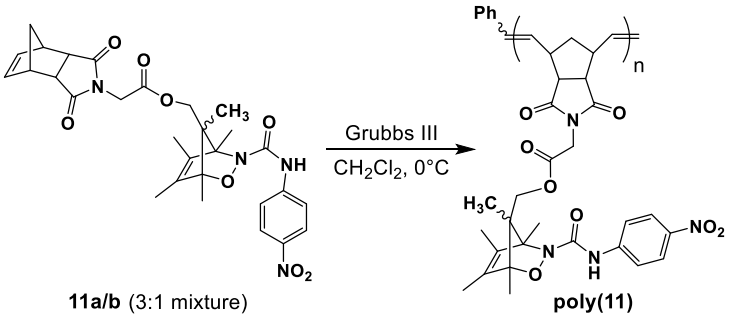

Synthesis of poly(11).

Into a flame-dried, N_2-purged round bottom flask, monomer **11** (733 mg, 1.3 mmol, 35 eq.), a stir bar, and 2.6 mL of CH_2Cl_2 were added. Once homogeneous, the solution was cooled in an ice bath at 0 °C and Grubbs 3rd generation catalyst (26.6 mg, 0.04 mmol, 1.0 eq.) in 4.6 mL of CH_2Cl_2 was quickly added. The reaction solution was stirred for 3 hours, during which time the ice bath expired. Ethyl vinyl ether (4.0 mL) was then added to the reaction mixture and the solution was stirred for an additional 10 minutes. The reaction mixture was then concentrated under reduced pressure and dissolved in a minimal amount of CH_2Cl_2. The polymer solution was then filtered through an alumina/Celite plug using CH_2Cl_2 as eluent. The solution volume was reduced under reduced pressure and then added dropwise into an excess of methanol, causing the polymer to precipitate from solution. The polymer was then collected by vacuum filtration, washed with additional methanol, and then dried under vacuum to provide a light-yellow powder (147 mg, 20% yield). M_w = 30.0 kDa, M_n = 25.7 kDa, Đ = 1.05.

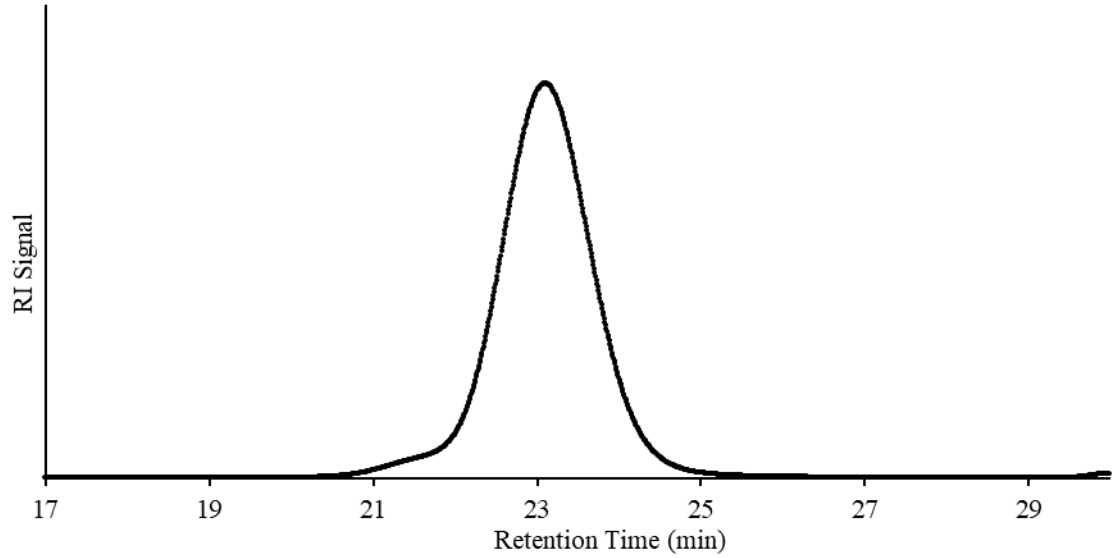

Figure 5.6 RI trace of **poly(11)**.

General method for monitoring the small-molecule isomerization

Into a 20 mL flame-dried, N_2-purged scintillation vial sealed with a rubber septum, oxazine (0.0298 g, 0.067 mmol, 1.0 eq.), 1,4-dicyanobenzene (0.0085 g, 0.066 mmol, 0.99 eq.), 4.5 mL DMSO-d_6, and a stir bar were added. The vials were then submerged into a pre-heated oil bath maintained at the designated temperature. At designated time points, 0.3 mL aliquots were removed by syringe and transferred into NMR tubes and then frozen in an ice bath until the NMR spectra were collected. Runs were done in triplicate.

Method for monitoring the isomerization of poly(11)

In an N_2-purged NMR tube, **poly(11)** (0.0051 g, 0.0002 mmol) was dissolved in anhydrous DMSO-d_6 (0.5 mL). The isomerization was monitored using a Bruker AVance 499 MHz spectrometer equipped with a variable temperature probe set to 60 °C, taking 8 scans every five minutes.

General Procedure for Nitrosocarbonyl Exchange between poly(11) and monomers 9 and 10

Into a 7 mL flame-dried, N_2-purged vial was charged with **poly(11)** (0.031 g, 0.0012 mmol, 1 eq.), 3.67 mL DMSO, and a stir bar. To this solution was also added either **9** (0.052 g, 0.110 mmol, 92 eq.) or **10** (0.050 g, 0.110 mmol, 92 eq.). The vial was then sealed with a rubber septum and submerged into an oil bath preheated to 60 °C where it was maintained for 27 hours in the case of **9** or 7 hours in the case of **10**. Each solution was added dropwise into an excess of cold methanol, causing precipitation of polymeric species [**poly(9-*co*-11)** and **poly(10-*co*-11)**]. The resulting mixtures were then centrifuged, decanted, and the resulting solids washed with methanol, and centrifuged twice more. The polymer residues were then collected and dried under vacuum.

General method for monitoring the small-molecule hydrolysis

Into a 20 mL scintillation vial sealed with a rubber septum, oxazine (0.0418 g, 0.074 mmol, 1.0 eq.), 1,4-dicyanobenzene (0.0101 g, 0.078 mmol, 1.05 eq.), 4.96 mL DMSO-d_6, 1.97 mL D_2O and a stir bar were added. The vials were then submerged into a pre-heated oil 60°C bath. At designated time points, 0.3 mL aliquots were removed by syringe into NMR tubes and frozen in an ice bath until the NMR spectra were collected. Runs were done in duplicate.

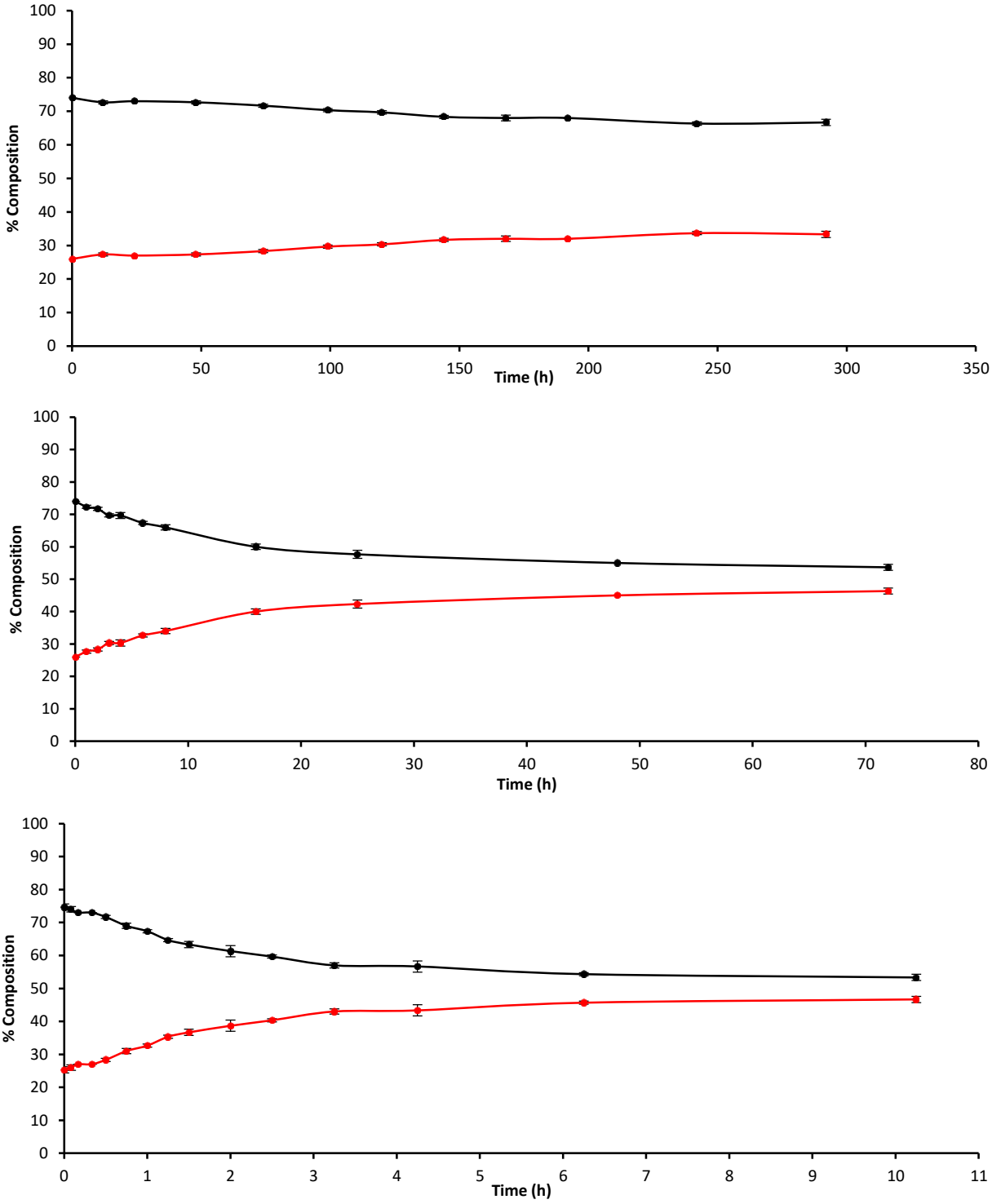

Figure 5.7 Extended time plots for isomerization of 8. Black = **8a**, red = **8b**. Top = 37 °C, middle = 60 °C, bottom = 80 °C. Average of three runs, error bars = one standard deviation, lines are visual aid.

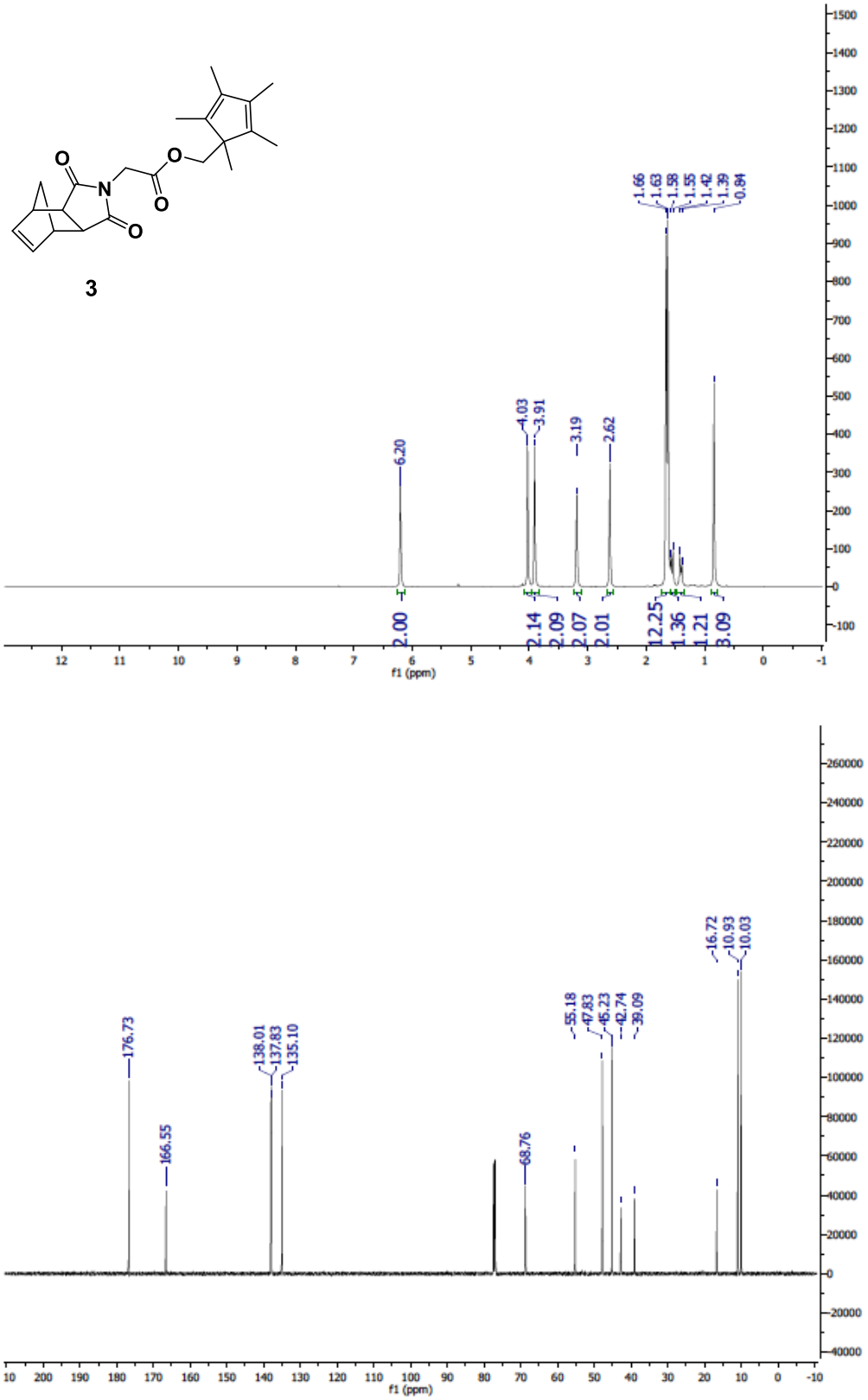

Figure 5.8 (top) ^{1}H and **(bottom)** ^{13}C NMR of **3**

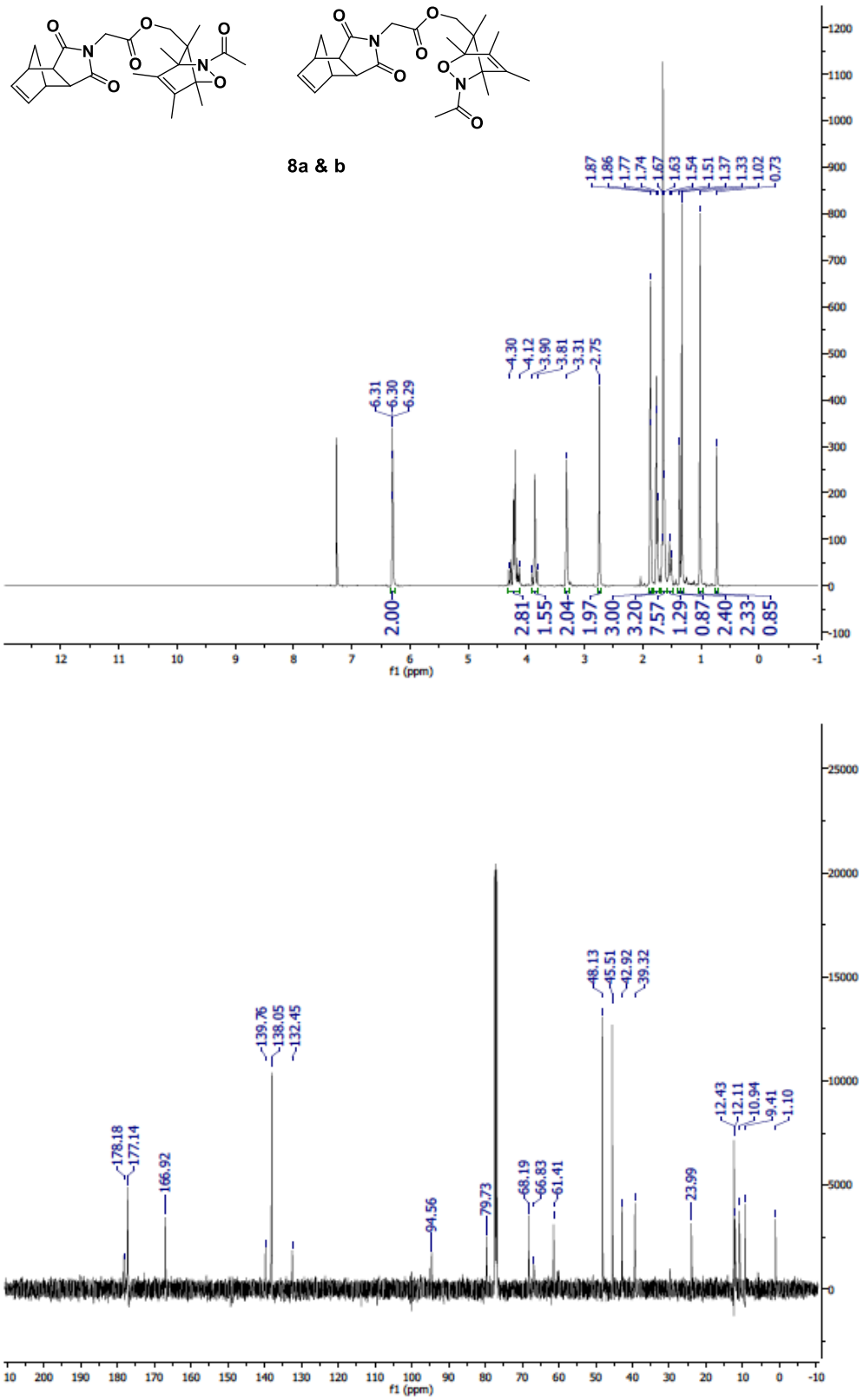

Figure 5.9 (top) ^{1}H and **(bottom)** ^{13}C NMR of **8a&b**

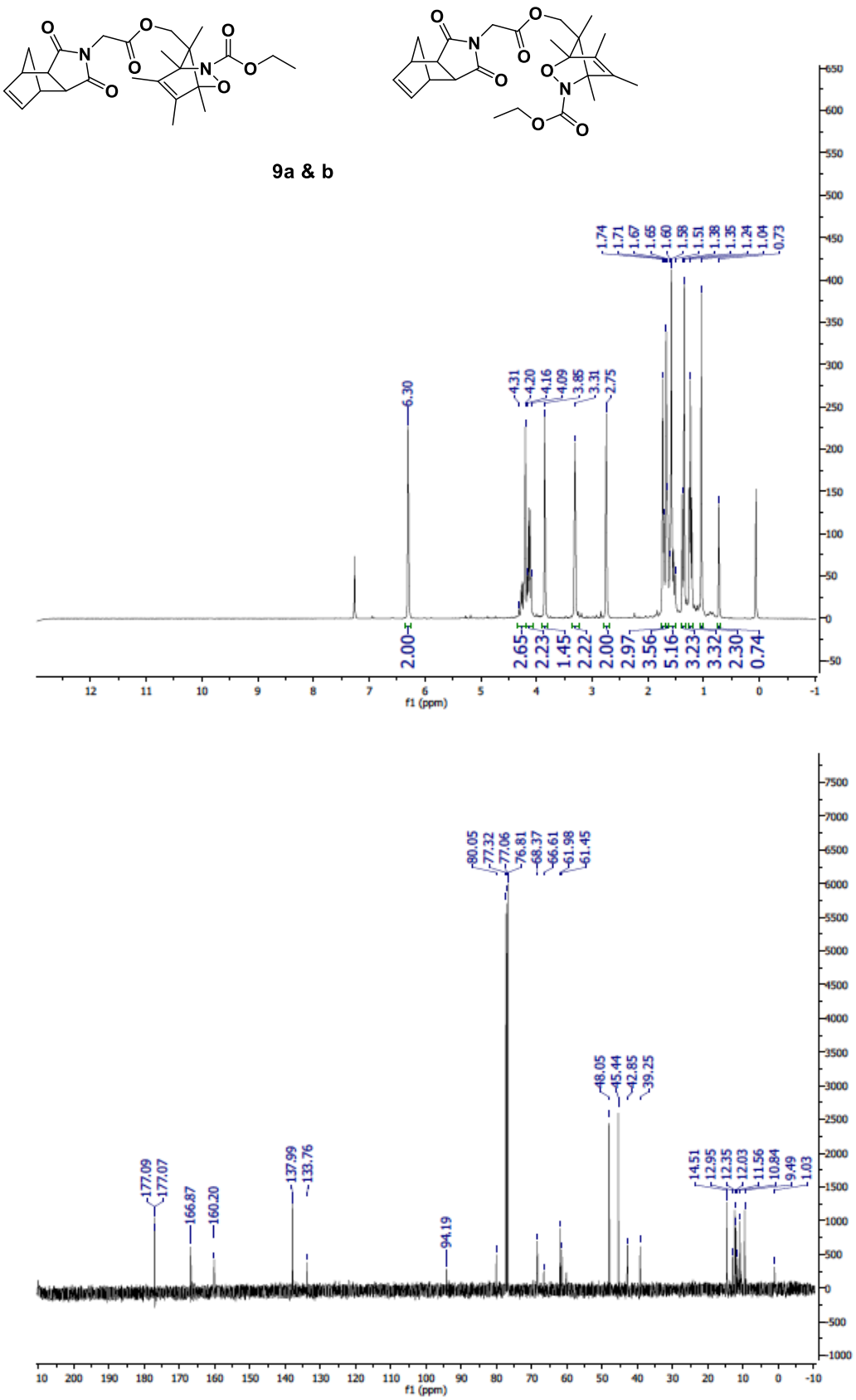

Figure 5.10 (top) ^{1}H and **(bottom)** ^{13}C NMR of **9a&b**

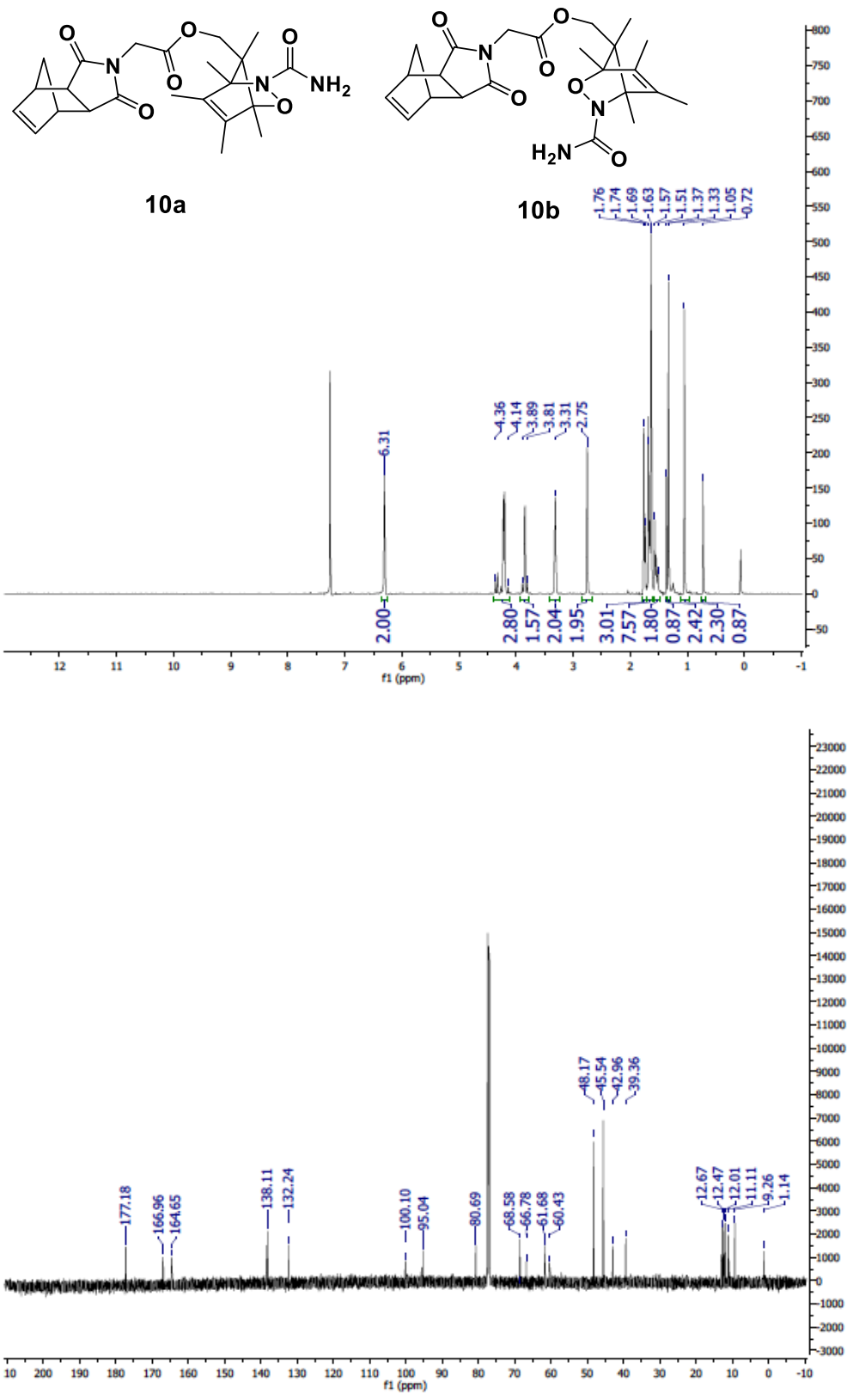

Figure 5.11 (top) ^{1}H and **(bottom)** ^{13}C NMR of **10a&b**

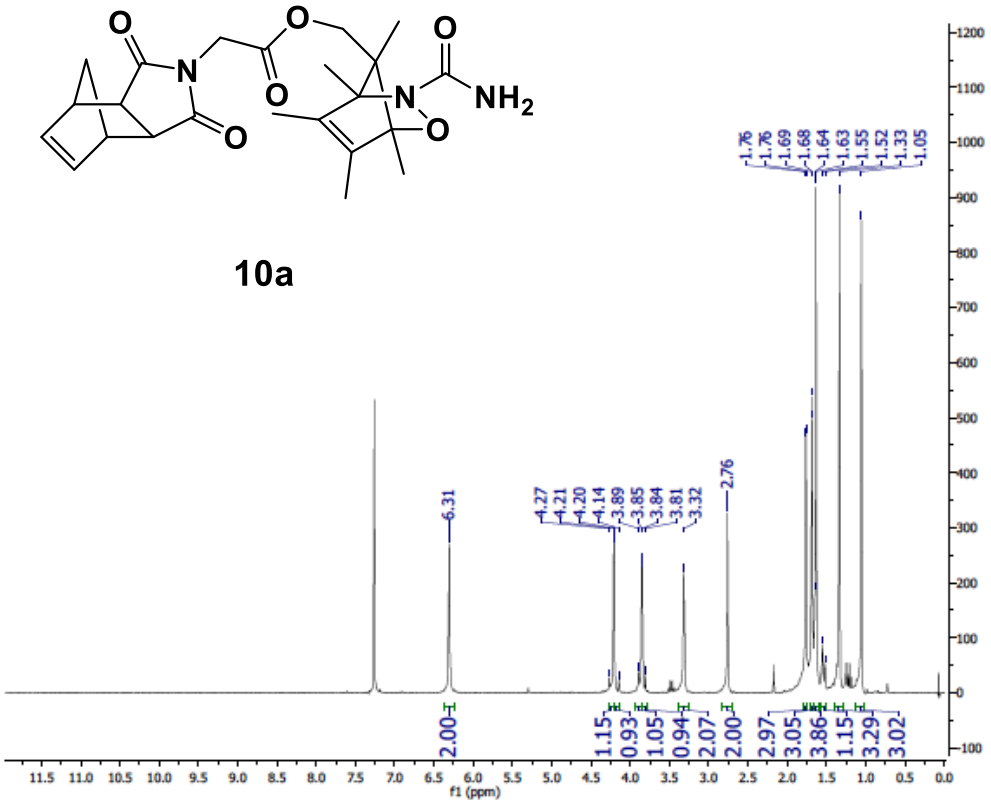

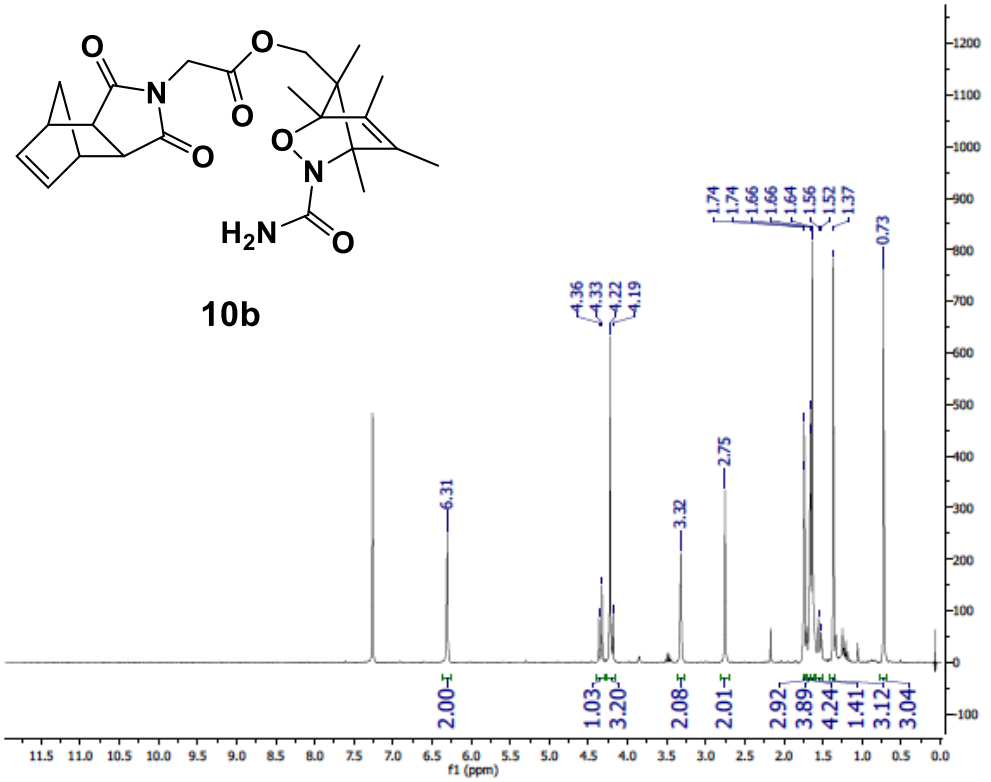

Figure 5.12 (top) ^{1}H NMR of isolated **10a** and **(bottom)** ^{1}H NMR of isolated **10b**

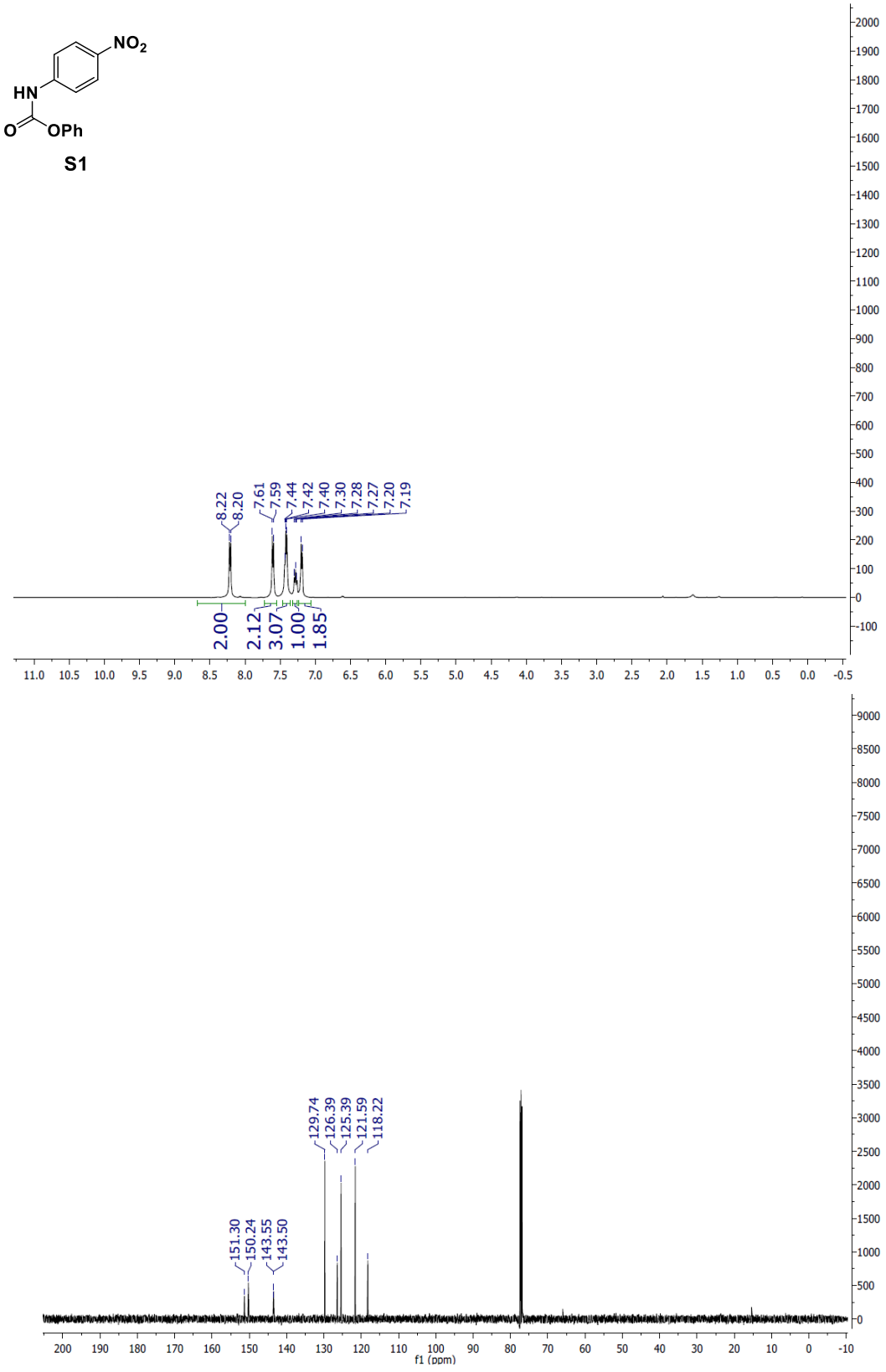

Figure 5.13 (top) ^{1}H and **(bottom)** ^{13}C NMR of **S1**

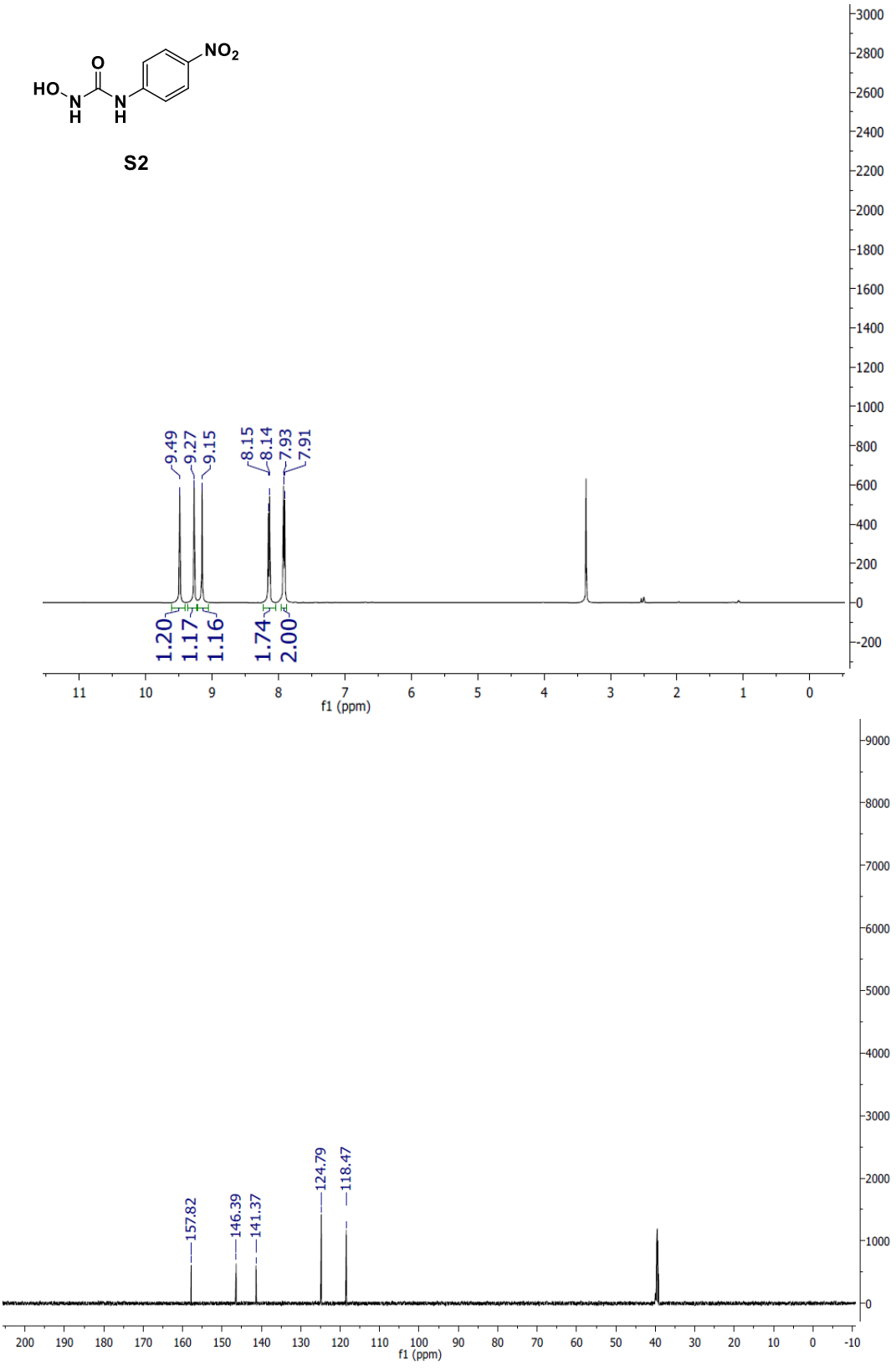

Figure 5.14 (top) ^{1}H and **(bottom)** ^{13}C NMR of **S2**

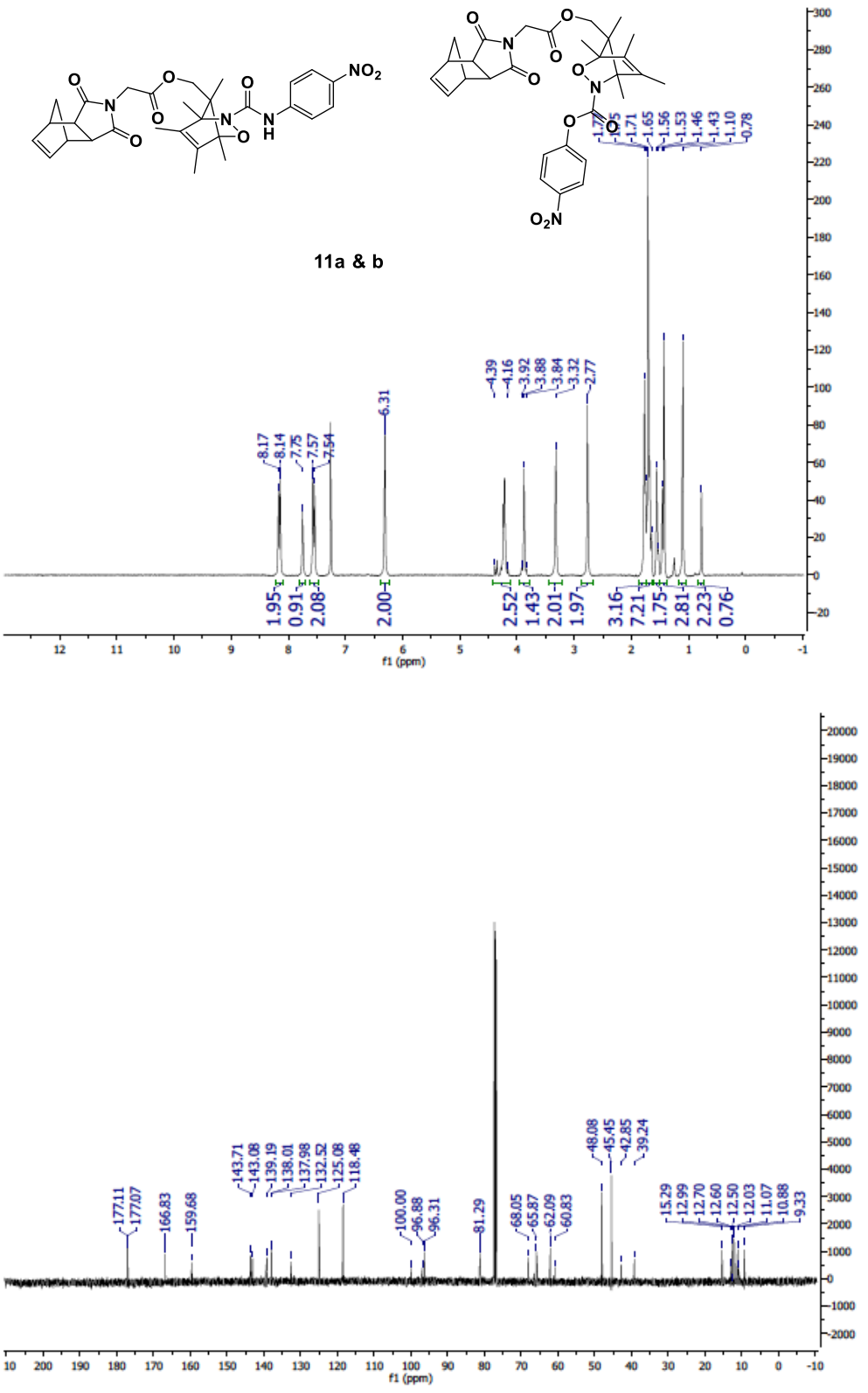

Figure 5.15 (top) ^{1}H and **(bottom)** ^{13}C NMR of **11a&b**

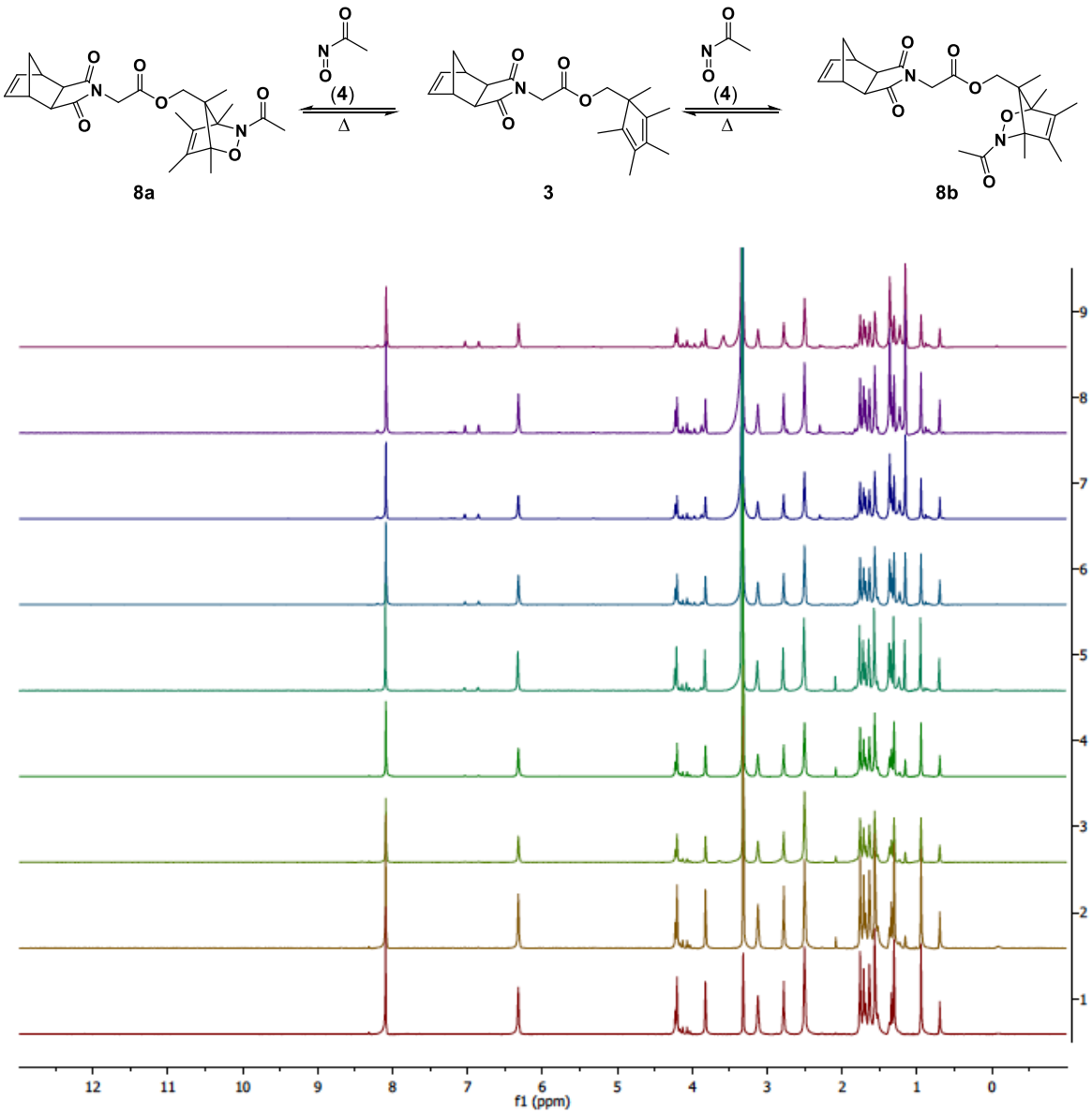

Figure 5.16 Representative NMR stacked plots of small molecule isomerization of **8** at 60°C

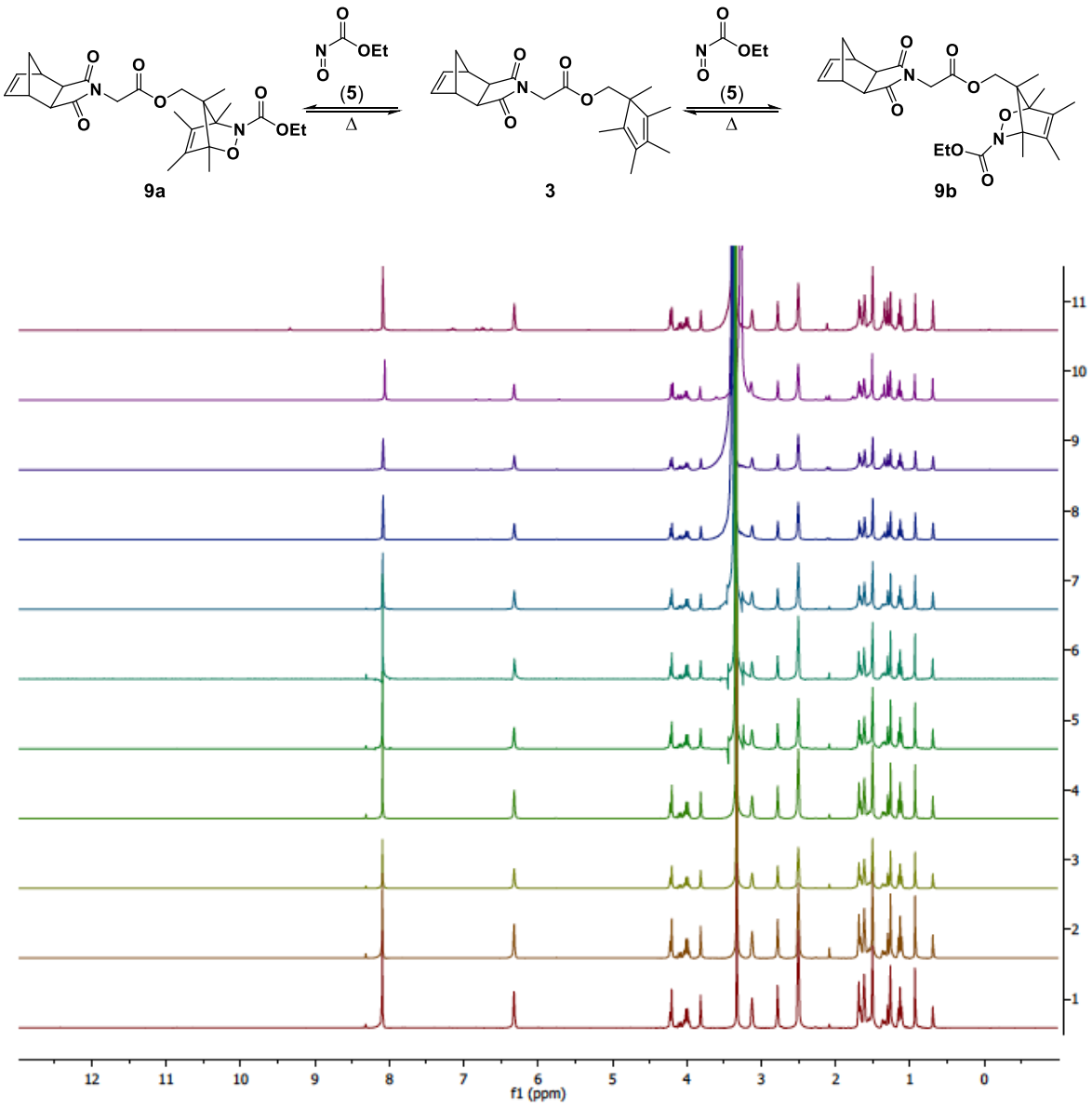

Figure 5.17 Representative NMR stacked plots of small molecule isomerization of **9** at 60°C

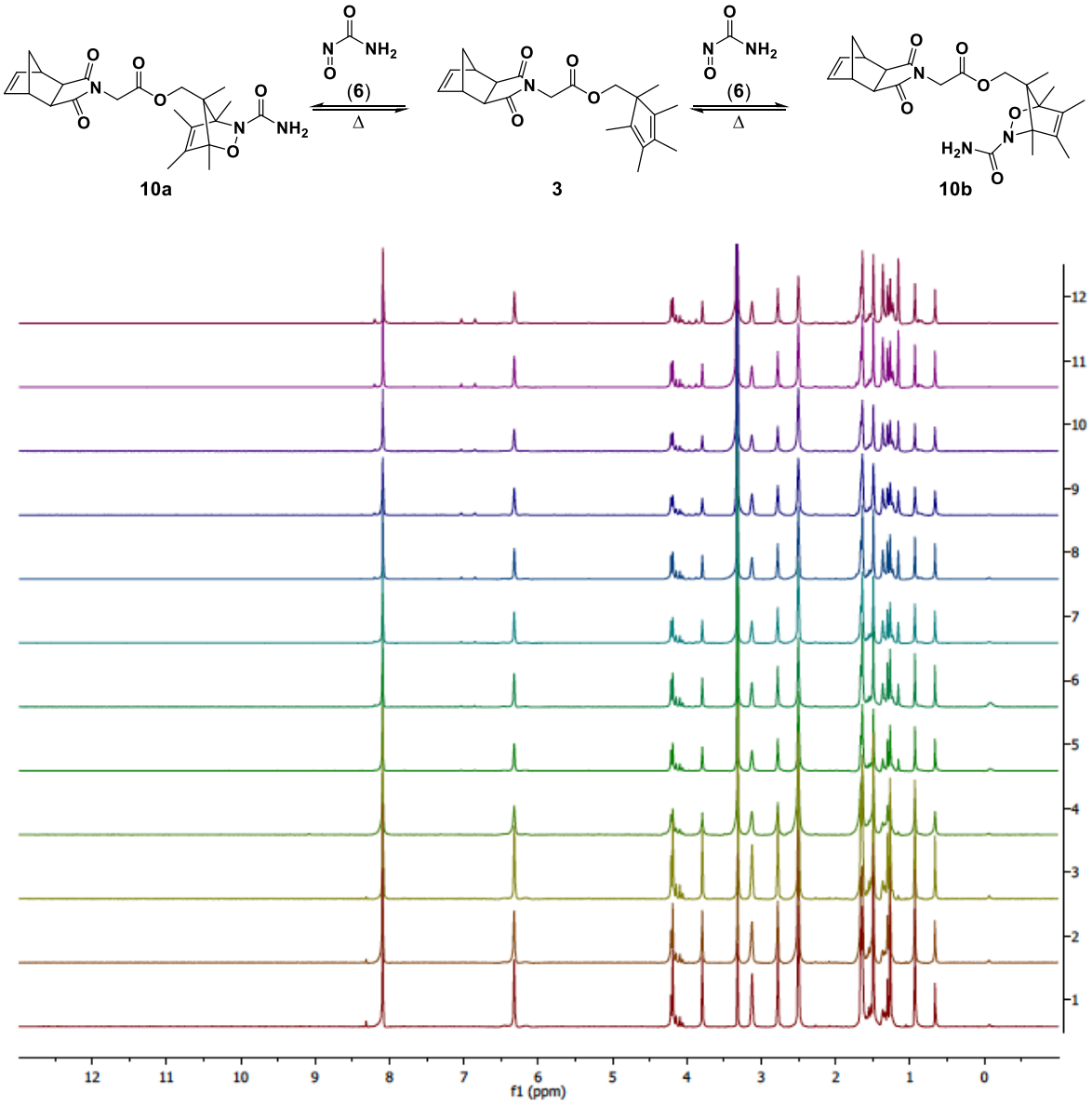

Figure 5.18 Representative NMR stacked plots of small molecule isomerization of **10** at 60°C

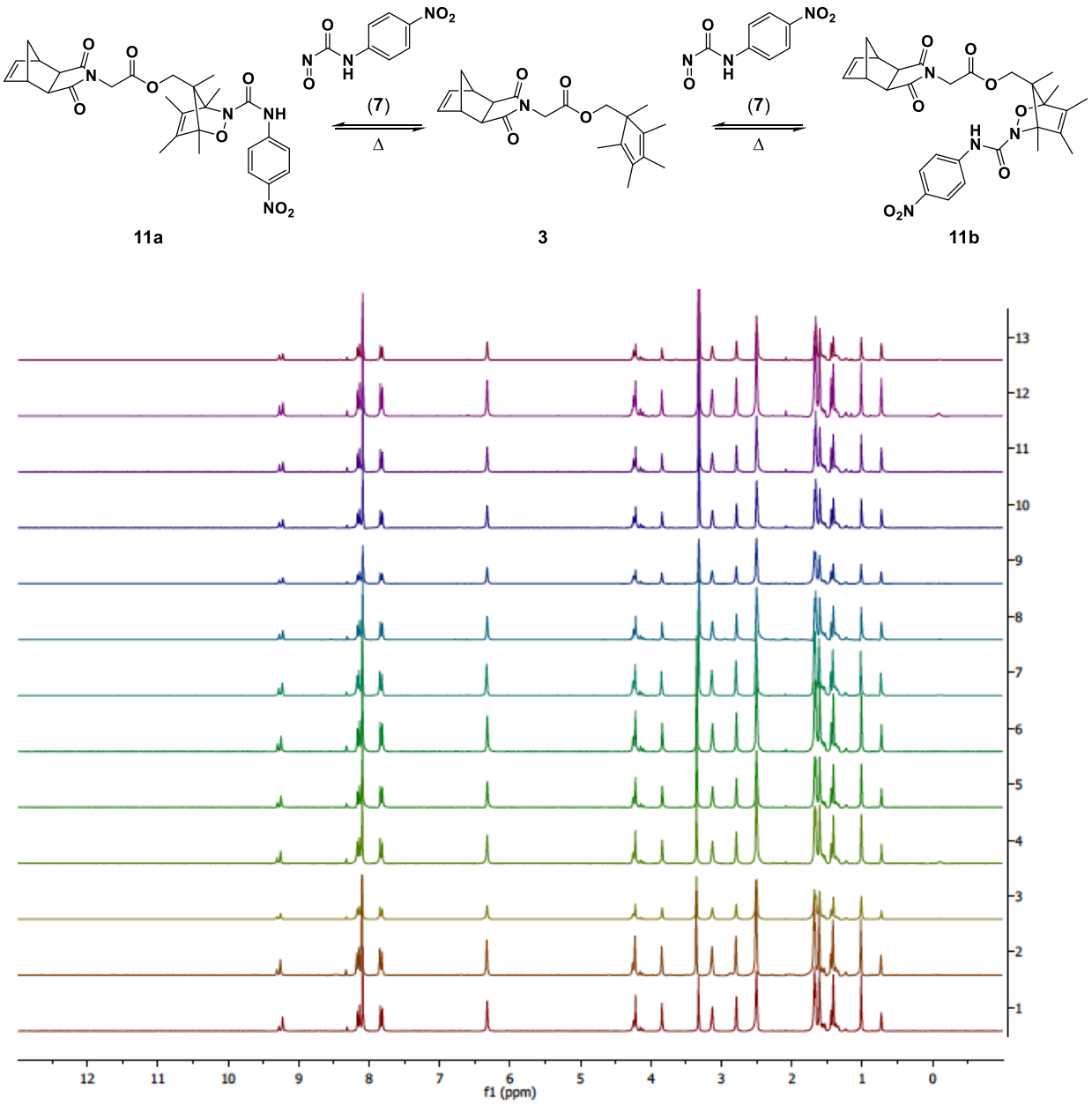

Figure 5.19 Representative NMR stacked plots of small molecule isomerization of **11** at 60°C

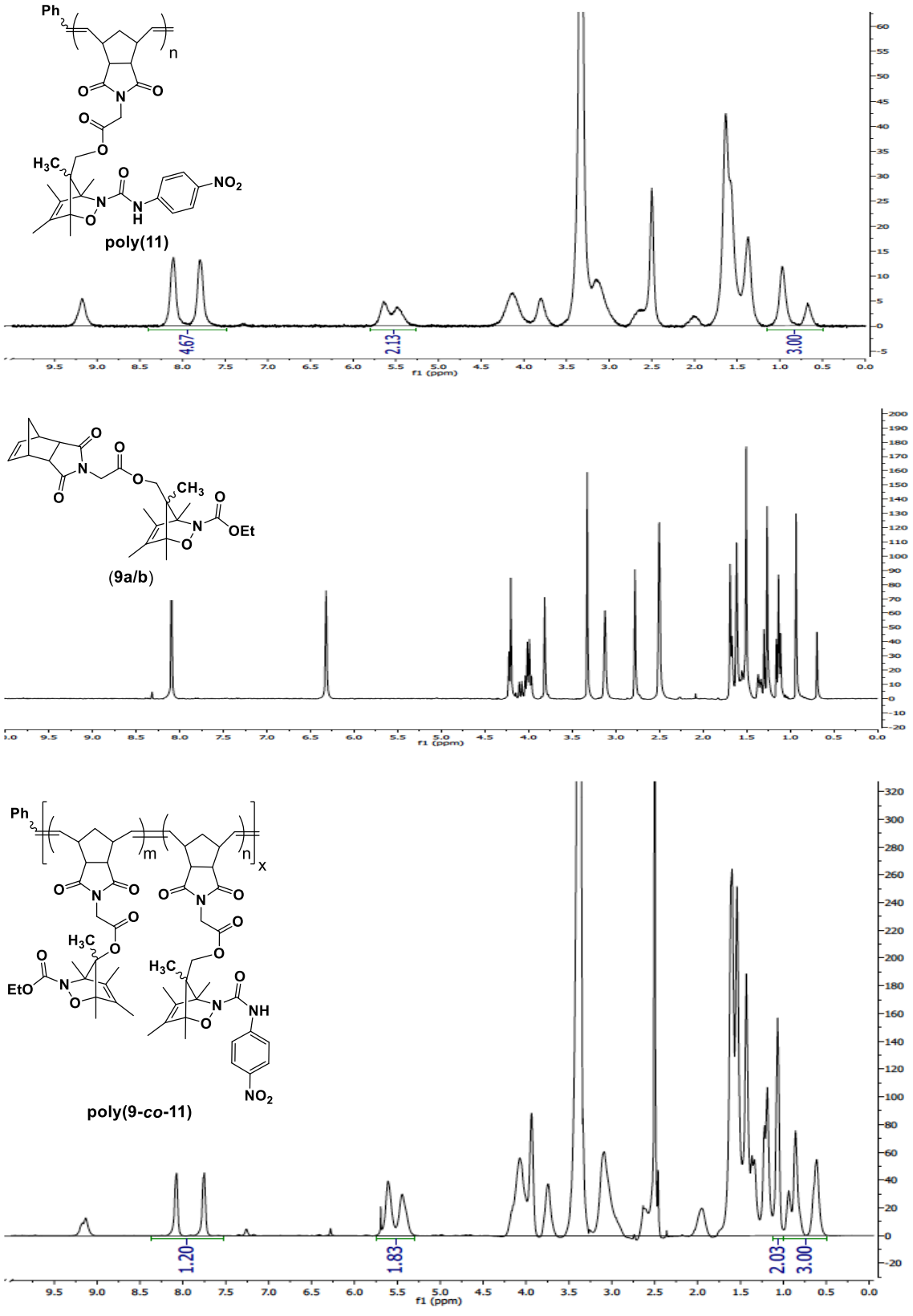

Figure 5.20 NMR analysis of nitrosocarbonyl exchange between **poly(11)** and monomer **9**

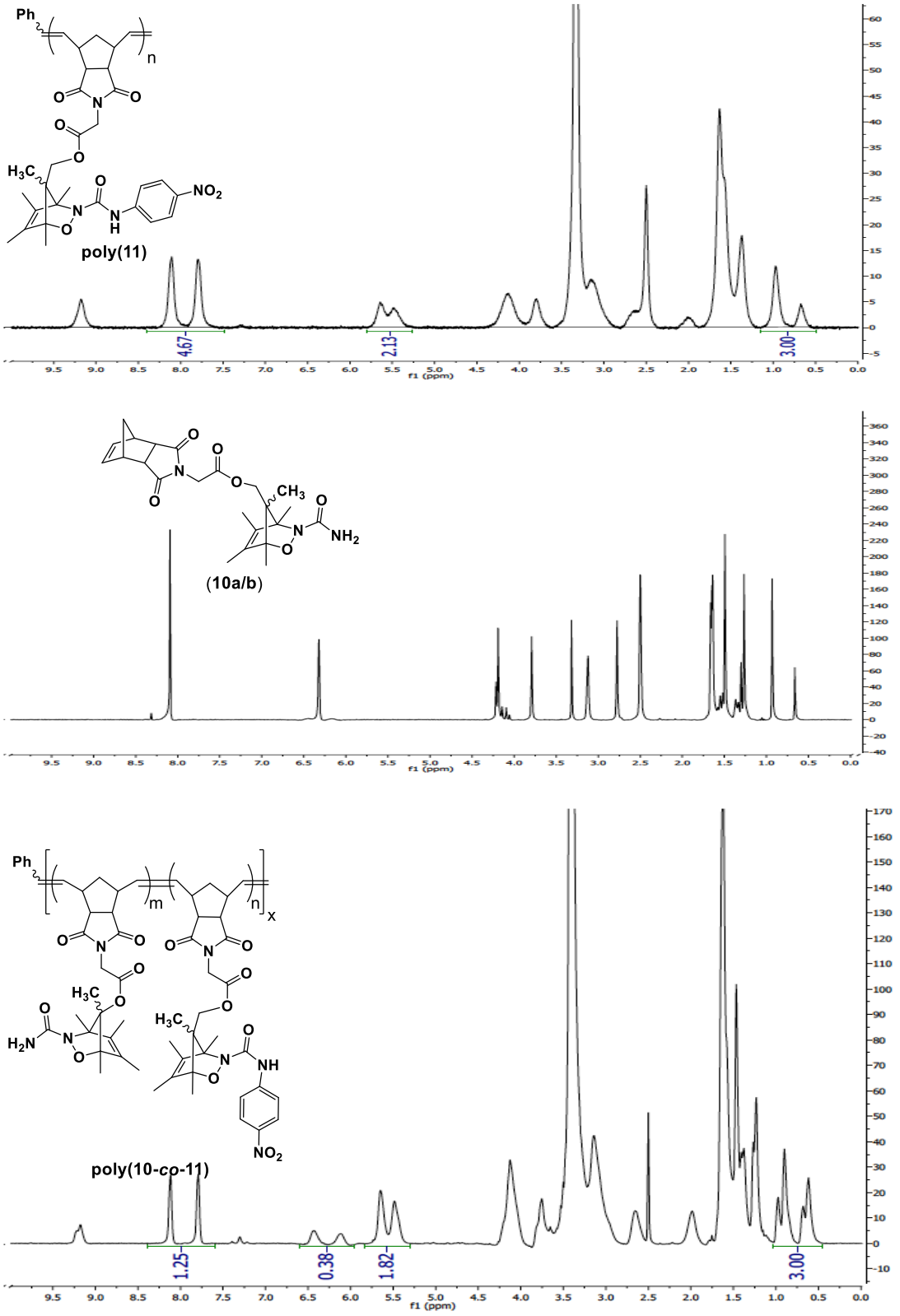

Figure 5.21 NMR analysis of nitrosocarbonyl exchange between **poly(11)** and monomer **10**

5.6 NOTES AND REFERENCES FOR CHAPTER 5

(1) Bodnar, B. S.; Miller, M. J. The Nitrosocarbonyl Hetero-Diels –Alder Reaction as a Useful Tool for Organic Syntheses Angewandte. *Angew. Chem. Int. Ed.* **2011**, *50*, 5630–5647.

(2) Palmer, L. I.; Frazier, C. P.; Alaniz, J. R. De. Developments in Nitrosocarbonyl Chemistry : Mild Oxidation of N-Substituted Hydroxylamines Leads to New Discoveries. *Synthesis (Stuttg).* **2013**, No. 46, 269–280.

(3) Kirby, G. W. Electrophilic C-Nitroso-Compounds. *Chem. Soc. Rev.* **1977**, *6*, 1–24.

(4) Kirby, G. W.; Sweeny, J. G. Formation and Dienophilic Reactions of Transient C-Nitrosocarbonyl Compounds. *J. Chem. Soc. Perkin Trans.* **1981**, *1*, 3250–3254.

(5) Corrie, J. E. T.; Kirby, G. W.; Mackinnon, J. W. M. Reactions of Transient C-Nitrosocarbonyl Compounds with Dienes, Mono- Olefins, and Nucleophiles. *J. Chem. Soc. Perkin Trans. 1* **1985**, 883–886.

(6) Kirby, G. W.; McGuigan, H.; Mackinnon, J. W. M.; McLean, D. Formation and Reactions of C-Nitrosoformate Esters, a New Class of Transient Dienophiles. *J. Chem. Soc. Perkin Trans.* **1985**, *1*, 1437–1442.

(7) Christie, C. C.; Kirby, G. W.; McGuigan, H.; Mackinnon, J. W. M. C-Nitrosoformamides, a New Class of Transient Dienophiles Formed by Oxidation of N-Hydroxyureas. *J. Am. Chem. Soc. Perkin Trans* **1985**, 2469–2473.

(8) Xu, Y.; Alavanja, M. M.; Johnson, V. L.; Yasaki, G.; King, S. B. Production of Nitroxyl (HNO) at Biologically Relevant Temperatures from the Retro-Diels-Alder Reaction of N-Hydroxyurea-Derived Acyl Nitroso-9,10-Dimethylanthracene Cycloadducts Dimethylanthracene Cycloadducts. *Tetrahedron Lett.* **2000**, *41*, 4265–4269.

(9) Zeng, B. B.; Huang, J.; Wright, M. W.; King, S. B. Nitroxyl (HNO) Release from New Functionalized N-Hydroxyurea-Derived Acyl Nitroso-9,10-Dimethylanthracene Cycloadducts. *Bioorganic Med. Chem. Lett.* **2004**, *14*, 5565–5568.

(10) Atkinson, R. N.; Storey, B. M.; King, S. B. Reactions of Acyl Nitroso Compounds with Amines: Production of Nitroxyl (HNO) with the Preparation of Amides. *Tetrahedron Lett.* **1996**, *37*, 9287–9290.

(11) Adachi, Y.; Nakagawa, H.; Matsuo, K.; Suzuki, T.; Miyata, N. Photoactivatable HNO-Releasing Compounds Using the Retro-Diels –Alder Reaction. *Chem. Commun.* **2008**, 5149–5151.

(12) Matsuo, K.; Nakagawa, H.; Adachi, Y.; Kameda, E.; Aizawa, K.; Tsumoto, H.; Suzuki, T.; Miyata, N. Photoinduced Upregulation of Calcitonin Gene-Related Peptide in A549 Cells through HNO Release from a Hydrophilic Photocontrollable HNO Donor. *Chem. Pharm. Bull.* **2012**, *60*, 1055–1062.

(13) Evans, A. S.; Cohen, A. D.; Gurard-Levin, Z. A.; Kebede, N.; Celius, T. C.; Miceli, A. P.; Toscano, J. P. Photogeneration and Reactivity of Acylnitroso Compounds. *Can. J. Chem.* **2011**, No. 89, 130.

(14) King, S. B. N-Hydroxyurea and Acyl Nitroso Commpounds as Nitroxy (HNO) and Nitric Oxide (NO) Donors. *Curr. Top. Med. Chem.* **2005**, *5*, 665–673.

(15) Samoshin, A. V; Hawker, C. J.; Alaniz, J. R. De. Nitrosocarbonyl Hetero-Diels−Alder Cycloaddition: A New Tool for Conjugation. *ACS Macro Lett.* **2014**, *3*, 753–757.

(16) Peterson, G. I.; Church, D. C.; Yakelis, N. A.; Boydston, A. J. 1,2-Oxazine Linker As a Thermal Trigger for Self-Immolative Polymers. *Polym. (United Kingdom)* **2014**, *55* (23),

5980–5985.
(17) Oehlenschlaeger, K. K.; Guimard, N. K.; Brandt, J.; Mueller, J. O.; Lin, C. Y.; Hilf, S.; Lederer, A.; Coote, M. L.; Schmidt, F. G.; Barner-Kowollik, C. Fast and Catalyst-Free Hetero-Diels-Alder Chemistry for on Demand Cyclable Bonding/Debonding Materials. *Polym. Chem.* **2013**, *4*, 4348–4355.
(18) Kloxin, C. J.; Scott, T. F.; Adzima, B. J.; Bowman, C. N. Covalent Adaptable Networks (CANs): A Unique Paradigm in Cross-Linked Polymers. *Macromolecules* **2010**, *43*, 2643–2653.
(19) Jin, Y.; Yu, C.; Denman, R. J.; Zhang, W. Recent Advances in Dynamic Covalent Chemistry. *Chem. Soc. Rev.* **2013**, *42*, 6634–6654.
(20) Rowan, S. J.; Cantrill, S. J.; Cousins, G. R. L.; Sanders, J. K. M.; Stoddart, J. F. Dynamic Covalent Chemistry. *Angew. Chem. Int. Ed.* **2002**, *41*, 898–952.
(21) Gandini, A. The Furan/Maleimide Diels– Alder Reaction : A Versatile Click–Unclick Tool in Macromolecular Synthesis. *Prog. Polym. Sci.* **2013**, *38*, 1–29.
(22) Miranda, K. M.; Nagasawa, H. T.; Toscano, J. P. Donors of HNO. *Curr. Top. Med. Chem.* **2005**, *5*, 649–664.
(23) Guthrie, D. A.; Ho, A.; Takahashi, C. G.; Collins, A.; Morris, M.; Toscano, J. P. "Catch-and-Release" of HNO with Pyrazolones. *J. Org. Chem.* **2015**, *80*, 1338–1348.
(24) Guthrie, D. A.; Nourian, S.; Takahashi, C. G.; Toscano, J. P. Curtailing the Hydroxylaminobarbituric Acid−Hydantoin Rearrangement To Favor HNO Generation. *J. Org. Chem.* **2015**, *80*, 1349–1356.
(25) Sutton, A. D.; Williamson, M.; Weismiller, H.; Toscano, J. P. Optimization of HNO Production from N , O-Bis-Acylated Hydroxylamine Derivatives. *Org. Lett.* **2012**, *14*, 472–475.
(26) Guthrie, D. A.; Kim, N. Y.; Siegler, M. A.; Moore, C. D.; Toscano, J. P. Development of N -Substituted Hydroxylamines as Efficient Nitroxyl (HNO) Donors. *J. Am. Chem. Soc.* **2012**, *134*, 1962–1965.
(27) Conrad, R. M.; Grubbs, R. H. Tunable , Temperature-Responsive Polynorbornenes with Side Chains Based on an Elastin Peptide Sequence. *Angew. Chem. Int. Ed.* **2009**, *48*, 8328–8330.
(28) Frazier, C. P.; Bugarin, A.; Engelking, J. R.; Read De Alaniz, J. Copper-Catalyzed Aerobic Oxidation of N-Substituted Hydroxylamines: Efficient and Practical Access to Nitroso Compounds. *Org. Lett.* **2012**, *14*, 3620–3623.
(29) Chaiyaveij, D.; Cleary, L.; Batsanov, A. S.; Marder, T. B.; Shea, K. J.; Whiting, A. Copper (II)-Catalyzed Room Temperature Aerobic Oxidation of Hydroxamic Acids and Hydrazides to Acyl-Nitroso and Azo Intermediates , and Their Diels-Alder Trapping. *Org. Lett.* **2011**, *13*, 3442–3445.
(30) Frazier, C. P.; Palmer, L. I.; Samoshin, A. V; Alaniz, J. R. De. Accessing Nitrosocarbonyl Compounds with Temporal and Spatial Control via the Photoredox Oxidation of N -Substituted Hydroxylamines. *Tetrahedron Lett.* **2015**, *56*, 3353–3357.
(31) 1,4-Dicyanobenzene Was Used as an Internal NMR Standard in the Trials.
(32) Keck, G. E.; Webb, R. R.; Yates, J. B. A Versatile Method for Carbon-Nitrogen Bond Formation via Ene Reactions of Acylnitroso Compounds. *Tetrahedron* **1981**, *37*, 4007–4016.
(33) Love, J. A.; Morgan, J. P.; Trnka, T. M.; Grubbs, R. H. A Practical and Highly Active Ruthenium- Based Catalyst That Effects the Cross Metathesis of Acrylonitrile. *Angew.*

Chem. Int. Ed. **2002**, *41*, 4035–4037.
(34) Jiang, Y.; Zhang, J.; Cao, Y.; Chai, X.; Zou, Y.; Wu, Q.; Zhang, D.; Jiang, Y.; Sun, Q. Synthesis, In Vitro Evaluation and Molecular Docking Studies of New Triazole Derivatives as Antifungal Agents. *Bioorg. Med. Chem. Lett.* **2011**, *21*, 4471–4475.